UNIVERSITÀ DEGLI STUDI DI TRIESTE

XXVIII CICLO DEL DOTTORATO DI RICERCA IN

NANOTECNOLOGIE

QUANTITATIVE ANALYSIS OF TUMOR BIOMARKERS IN MICRO-SAMPLES WITH DNA BASED NANODEVICES

Settore scientifico-disciplinare: CHIM/01

DOTTORANDO
ALESSIA AMODIO

COORDINATORE
PROF. LUCIA PASQUATO

SUPERVISORE DI TESI
DR. MATTEO CASTRONOVO

TUTORE
PROF. FRANCESCO RICCI

ANNO ACCADEMICO 2014 / 2015

“Sono alquanto scettico nei confronti di quei settori nei quali le persone mostrano precocità, come la musica e la matematica. La precocità evidenzia il talento. Questo non mi piace. Mi piace di più l'idea che gli esseri umani possano fare qualunque cosa aggrada loro anche se qualche volta hanno bisogno di imparare. Hanno bisogno di un insegnante che risvegli la loro intelligenza. Non occorre un talento speciale per essere un chimico. Chiunque può esserlo a condizione che lavori sodo.”

R. Hoffmann

Abstract

The field of DNA nanotechnology aims to create molecular structures and devices by using DNA as an engineering material. The specificity of Watson-Crick base pairing, combined with a dramatic decrease in the cost of synthesis, has made DNA a widely used material for the assembly of molecular structures and dynamic molecular devices for a wide range of applications including smart drug release, cell biology and imaging.

The major objective of my PhD work has been to develop novel DNA-based nanodevices for diagnostic applications using non-canonical DNA/DNA interactions (Hoogsteen interactions) that are able to form triplex DNA structures. More specifically, I rationally designed, developed and characterized signal-on electrochemical DNA sensors, based on triplex-forming DNA probes, with improved affinity and specificity of recognition compared to classic electrochemical DNA sensors, based on simple Watson-Crick interactions. Moreover, since such Hoogsteen interactions are strongly pH dependent, I also demonstrated the possibility to control with pH changes DNA strand displacement reaction, an important class of DNA-based reactions, and the self-assembly of DNA nanostructures.

The results that I have achieved during my PhD can have implication for the development of DNA nanodevices whose assembly and functionality can be triggered in the presence of specific biological targets, thus offering promising applications in different fields such as diagnosis, synthetic biology, drug release, imaging, smart-nanomaterials and nanoscale components.

Abstract

L'obiettivo delle nanotecnologie a DNA è sviluppare strutture molecolari e dispositivi usando il DNA come materiale. La specificità dell'appaiamento delle basi di tipo Watson-Crick e la diminuzione dei costi di sintesi hanno reso il DNA un materiale ampiamente utilizzato per l'assemblaggio di nanostrutture e dispositivi molecolari dinamici che possono essere impiegati in numerose applicazioni: rilascio di farmaci, terapie intelligenti, *imaging*.

L'obiettivo principale del mio lavoro di Dottorato è stato lo sviluppo di nanodispositivi innovativi per applicazioni diagnostiche che sfruttano interazioni DNA/DNA (interazioni di tipo Hoogsteen), capaci di formare strutture di DNA a tripla elica. In particolare, ho progettato, sviluppato e caratterizzato sensori elettrochimici a DNA di tipo *signal-on*, basati su una sonda che porta alla formazione di una struttura a tripla elica. Tali sonde permettono di migliorare l'affinità e la specificità del riconoscimento molecolare rispetto ai classici sensori basati solo sull'appaiamento di tipo Watson-Crick. Inoltre, essendo le interazioni di tipo Hoogsteen fortemente dipendenti dal pH, ho sviluppato un approccio razionale per ottenere il controllo, mediante una semplice variazione del pH della soluzione, di una classe importante di reazioni basate sul DNA: le reazioni di *strand displacement* di DNA e l'autoassemblaggio di nanostrutture basate sul DNA.

I risultati ottenuti durante il mio Dottorato rappresentano un punto di partenza per lo sviluppo di nanodispositivi il cui assemblaggio e la cui funzionalità sono attivati in presenza di uno specifico target biologico, offrendo così promettenti applicazioni in campi come la diagnostica, la biologia sintetica, il rilascio di farmaci, lo sviluppo di nano componenti e l'*imaging*.

Thesis outline

The thesis is organized into 5 main chapters. The first chapter is a brief introduction on DNA nanotechnology and it contains an overview of the state of the art, with a focus on the use of non B-DNA structures, stabilized by Hoogsteen interactions. The experimental work conducted in the course of my PhD is described in the next three chapters of the thesis (chapter 2-4). Each chapter is organized as a scientific paper and consists of different sections, a general introduction and motivation of the work described, followed by a presentation of the results, followed by discussions and conclusions. A description of relevant experimental details for each chapter is placed at the end of each chapter, as well as the references. The last chapter of the thesis provides a brief summary for the reader and a contextual frame and perspective for the results obtained in each project.

A brief summary of each chapter is provided here to facilitate the reader's effort.

Chapter 1 represents a brief overview of the field of DNA nanotechnology. It shows how structural DNA nanotechnology and functional DNA based nanodevices have been independently coevolving in the last 34 years. At the end of the chapter the attention is focused on the development of DNA based nanodevices by exploiting non B-DNA structure, in particular those stabilized by Hoogsteen interactions. The chapter also dissects the possibility to couple these nanodevices with passive and rigid scaffold to expand the range of applications of DNA nanotechnology.

Chapter 2 describes the development of a novel signal-on electrochemical DNA sensor based on the use of a clamp-like DNA probe that binds a complementary target sequence through two distinct and sequential events, which lead to the formation of a triplex DNA structure. It shows how this target-binding mechanism can improve both the affinity and specificity of recognition as opposed to classic probes solely based on Watson-Crick recognition. The chapter ends with the possible application of such DNA biosensor in the field of DNA nanotechnology.

Chapter 3 describes a rational approach to achieve control, through a simple change of the solution's pH, over an important class of DNA association-based reactions. It

explains how I took advantage of the pH dependence of parallel Hoogsteen interactions to rationally designed two triplex-based DNA strand displacement strategies that can be triggered and finely regulated at either basic or acidic pHs. Because pH change represents an important input both in healthy and pathological biological pathways, the chapter ends with possible implication of my strategies for the development of DNA nanostructures whose assembly and functionality can be triggered in the presence of specific biological targets.

Chapter 4 describes how to integrate a pH-modulated strand displacement circuitry with DNA tile self-assembly as to introduce another reliable control variable to regulate or trigger the formation of molecular structures. The chapter ends with the possible applications of the obtained results.

Finally, in a short chapter, the conclusions are drawn. The major findings are highlighted and future applications of them are presented.

List of Publications

1. Ranallo, S.; Amodio, A.; Idili, A.; Porchetta, A.; Ricci, F. Electronic control of DNA-based Nanoswitches and Nanodevices. *Chem Science* 2016, 7, 66.
2. Idili, A.; Porchetta, A.; Amodio, A.; Vallée-Bélisle, A.; Ricci, F. Controlling Hybridization Chain Reactions with pH. *Nano Lett.* 2015, 15, 5539.
3. Amodio, A.*; Zhao, B.*; Porchetta, A.*; Idili, A.; Castronovo, M.; Fan, C.; Ricci, F. Rational design of pH-controlled DNA Strand Displacement. *J. Am. Chem. Soc.* 2014, 136, 16469.
4. Idili, A.*; Amodio, A.*; Vidonis, M.; Feinberg-Somerson, J.; Castronovo, M.; Ricci, F. Folding-Upon-Binding and Signal-On Electrochemical DNA Sensor with High Affinity and Specificity. *Anal. Chem.* 2014, 86, 9013.

Contents

Chapter 1 - Introduction

1.1 B-DNA and non-B DNA: from living cells to test tubes

The life has selected DNA as best material to store genetic information. The two pyrimidine bases, cytosine (C) and thymine (T), and the two purine bases, adenine (A) and guanine (G), constitute the building blocks of DNA biopolymers (Figure 1.1). As first proven by Watson and Crick in 1953, DNA has a right-handed, helical, duplex structure, termed B-DNA.[1] In living cells, DNA, which acts as the carrier of the genetic information, does not usually exist as a single-stranded sequence, but only as a pair of molecules that are tightly held together by non-covalent interactions. Under certain conditions, DNA in living cells can form unique structures rather than double helix of B-DNA. Specifically, repetitive DNA sequences have the potential to fold into non-B DNA structures such as hairpin, triplex, cruciform, left-handed Z-form, tetraplex, poly(dA) duplex (A-motif).[2-7] These unusual secondary structures may affect the gene metabolism process and also participate in several biologically important processes.

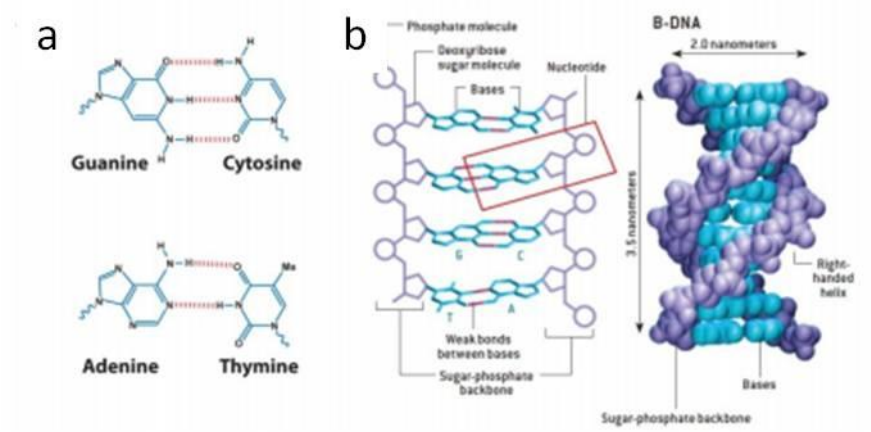

Figure 1.1 DNA has an intrinsically nanoscale structure. (a) Purine bases are connected to pyrimidine bases by weak interactions. Adenine can bind only to thymine through two hydrogen bonds, while cytosine can bind only to guanine through three hydrogen bonds. This arrangement of two nucleotides binding together across the double helix is called, base pair. (b) The complementary between the bases allow the formation of double helix. DNA most common conformation is B-DNA. In its B form, double stranded DNA is a right-handed, helical

molecule with a diameter of approx. 2 nm and a distance of 0.34 nm between adjacent base pairs. The rise of the helix is around 10.5 base pairs (bp) per turn.[8] (Adapted from reference 3).

To date, more than 10 different types of non-B structures have been reported, such as cruciform, left-handed, Z-DNA. In order to form these structures, DNA strand should be folded in a different manner from B-DNA or make non-canonical interactions, such as Hoogsteen interactions. Hoogsteen interactions play an important role in stabilizing several non B-DNA conformations, such as G-quadruplex, i-motif, triplex and A-motif. These kind of structures are characterized by a different relative content of purines or pyrimidynes in the sequence, thus inducing the folding of multistranded secondary structures based on Hoogsteen interactions.[9] Among all the non-B structures, I will focus my attention on these four particular structures.

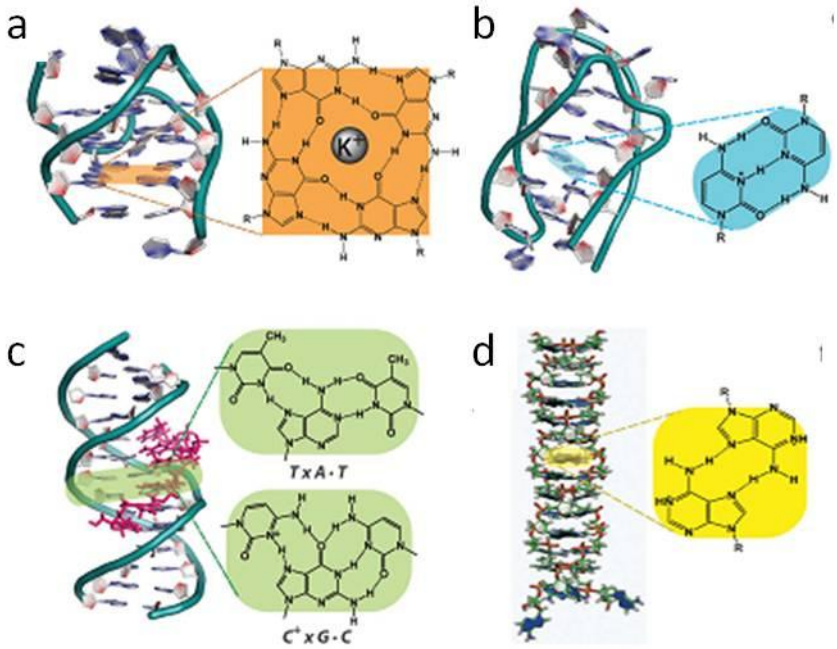

Figure 1.2. Non-B DNA structures stabilized by Hoogsteen interactions. (a) G-quadruplex and G-tetrads composed of four guanine bases. (b) i-motif and hemiprotonated C:C$^+$ base pairs. (c) parallel triplex which consists of TxA•T and CxG•C$^+$ triplets. (d) A-motif and A:A base pair (Adapted from references 2).

G-rich strands may self-assemble into intramolecular or intermolecular G-quadruplex. The building blocks of G-quadruplexes are G-quartets that arise from the formation of Hoogsteen hydrogen-bonding between four guanines (Figure 1.2a). The planar G-quartets stack on top of each other, giving rise to four-stranded helical structures. The

formation of this structure is strongly dependent on monovalent cations such as K^+ and Na^+ and, hence, physiological buffer conditions favour their formation. G-rich sequences are observed frequently in the promoter region of oncogene and human telomeric DNA.[10-12]

DNA sequences containing stretches of cytosines can form intercalated, quadruple-helical structures, under acidic conditions. [13,14] The tetrameric structures, called i-motif, consists of two, parallel duplexes combined in an antiparallel fashion by forming intercalated hemiprotonated cytosine-cytosine(+) base pairs (Figure 1.2b). [15] It is known that C-rich sequences are present within or near the regulatory regions of less than 40% of all genes, especially in the promoter region of oncogene and human telomeric DNA.[10,16]

DNA sequences are also capable of adopting three-stranded structure called triplex. Triplex-formation requires a double-stranded duplex in Watson-Crick configuration and a single-stranded nucleotide sequence that acts as the third strand (Figure 1.2c). The third strand binds in the major groove of the duplex forming Hoogesteen or *reverse* Hoogsteen hydrogen bonds with the purines of the duplex. This also determines the orientation of the third strand with respect to the purines in the duplex. There are six different nucleotide triplets that allow the formation of two hydrogen bonds between the purines in the duplex and the nucleotides binding in the major groove. These nucleotide triplets are used to classify the triplex structures in different motifs. [17] The mirror repeats of the hompurine-homopyrimidine stretch in the upstream regulatory regions of several genes are known to form an intramolecular triplex structure, called "H-DNA". [18-20]

A-Rich DNA has been shown to form parallel duplexes called A-motifs. A-motif exhibits a single-stranded right-handed helical structure stabilized by the - stacking of adenine bases at alkaline and neutral pH, whereas poly(dA) (or poly(A)) at acidic pH forms a right-handed helical duplex with parallel-mannered chains and tilted protonated bases (Figure 1.2d). Poly(A) is a tail component of mRNA in all eukaryotic cells and it plays a key role in the stability of mRNA and translation initiation.[21]

B-DNA, as well as the structures mentioned above, is not only interesting because it stores and imparts genetic instructions but also because it can be used as engineering material. Therefore the predictability of base pairing, the large structural polymorphism, the high reactivity toward different molecular inputs, the availability of automated

synthetic methods and dropping costs, make DNA the ideal material to design and engineering smart nanodevices.

After a brief introduction on DNA nanotechnology, I will present how these secondary structures stabilized by Hoogsteen interactions became a valuable tool in the toolbox of this field, used for a wide range of applications such as, building new sensors, releasing payloads, or transforming static, complex DNA nanostructures into functional devices.

1.2 DNA Nanotechnology: breakthroughs and "cross-fertilizations"

In the early 1980s, the crystallographer Ned Seeman proposed a revolutionary idea, to exploit the unique recognition properties of DNA in a completely non-biological context, to use DNA as scaffold to hold biological macromolecules in regular latexes, in order to controllably orient macromolecules for crystallography experiments. [8] This objective was achieved by Seeman's group in 2009. [22] In 1994, another non-biological application was described for DNA in the field of computing. In fact, Adleman published the "wet-lab" solution for a computational problem by using DNA and standard molecular biology techniques.[23] At the end of the 20th century, the field of DNA nanotechnology was further extended by the first experimental demonstrations of switchable molecular structures made from DNA,[24,25] often called DNA "nanomachines" or DNA "nanodevices".[26] In 1996, the extremely fruitful biosensing concept of "molecular beacons" (MBs) was introduced. [27,28] Finally, in 2006 Rothemund proposed a way to fold a >7000-nt-long DNA molecule to create nanoscale shapes with locally regular patterns, termed "DNA origami". [29] Figure 1.3 shows a timeline of the major developments in the field of DNA nanotechnology. [26]

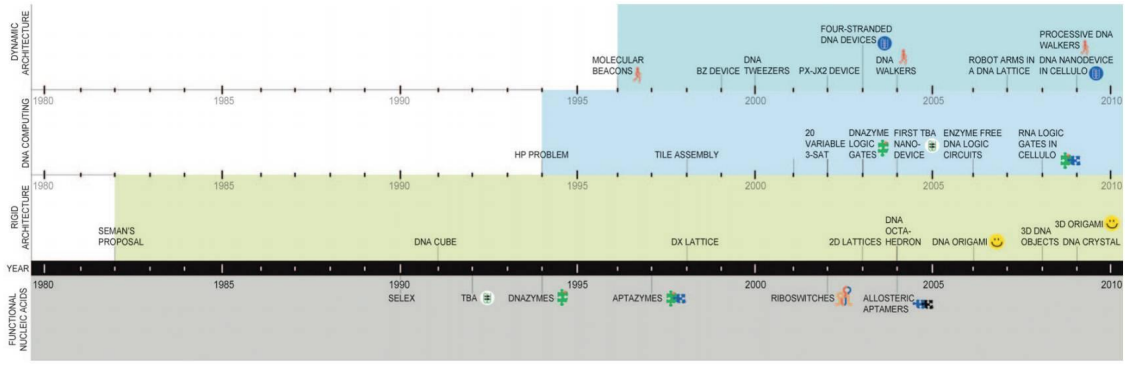

Figure 1.3. Timeline of the key developments in DNA nanotechnology. The devices from structural DNA nanotechnology are grouped into three main classes: rigid architectures, dynamic or movable architectures, and DNA computing. Development in structural DNA nanotechnology and related functional modules or concepts are indicated by similar symbols. [26] For completeness, at the bottom in light grey is shown the independent evolution of functional nucleic acids, although this topic will not be discussed in this thesis.

The aforementioned achievements represent some of the major breakthroughs in the field of DNA nanotechnology. These events further inspired and stimulated the work of many research groups, thus giving rise to many interdependencies and "cross-fertilizations".

By exploiting DNA's structural features and powerful base-pairing rules, the field of structural DNA nanotechnology aims at generating nanopatterned materials and to control molecular motion at the nanoscale. [30] The first successful attempt to construct a specific molecular architecture relies on the use of a double crossover motif in 1993. [31] This method is based on branched DNA molecules, called tiles that present single stranded overhangs, also called sticky ends. The sticky ends provide a consistent and convenient method for inter-structure association. Since 1993 different tiles have been developed and many discrete, periodic and aperiodic structures, as well as nanotubes have been constructed. In the attempt of showing the variety of tiles developed for building DNA nanostructures with this powerful approach, Figure 1.4 (from reference 32) shows a number of DNA nanotubes formed by the association of different types of tile (this topic will be further examined in chapter 4).

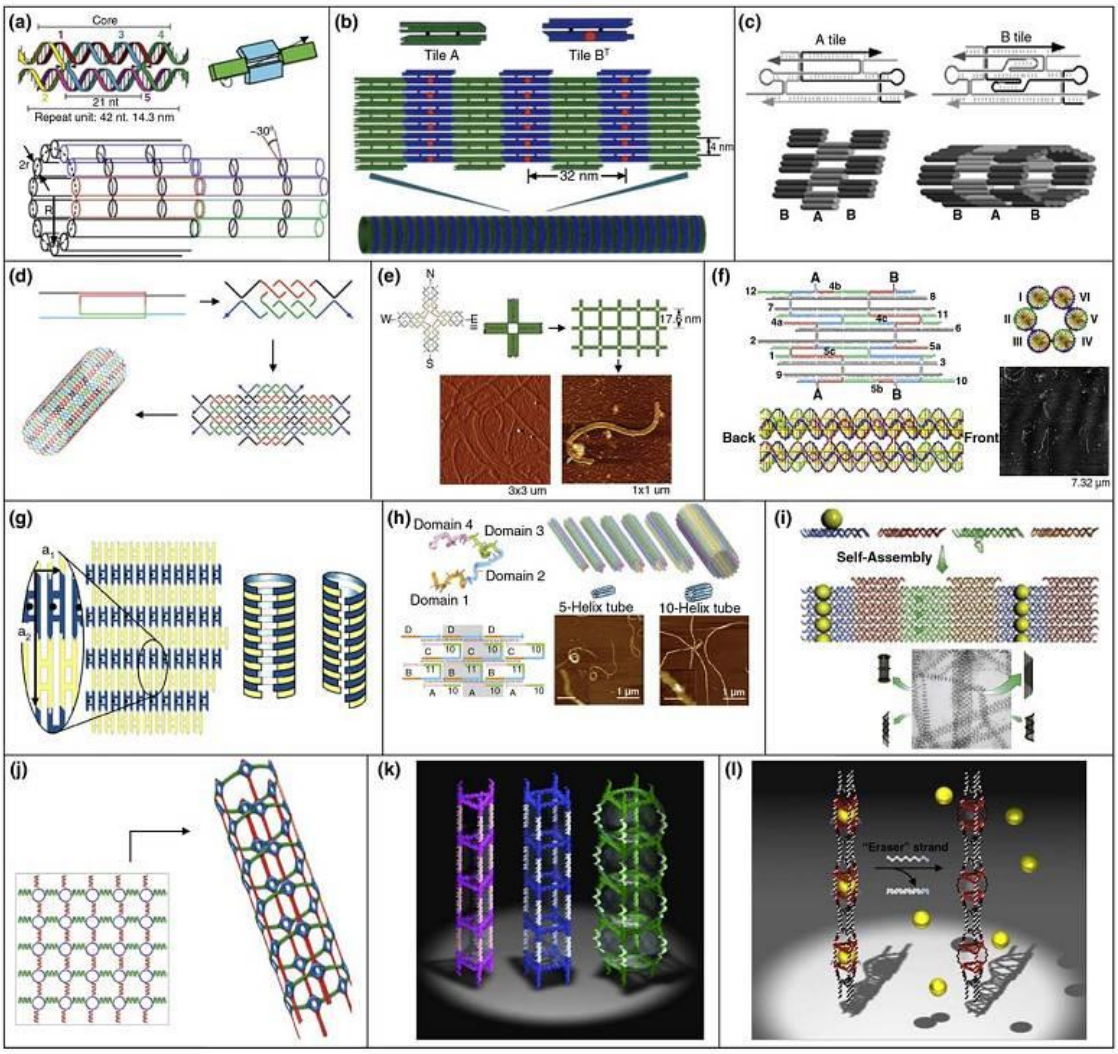

Figure 1.5. Examples of 3D-DNA nanotubes, built by using different tile. (a) A DNA tile is assembled from five single strands with sticky ends at the edges and then further hybridized to a nanotube with curvature between tiles. [33] (b) Two-dimensional DNA arrays prepared from two double-crossover tiles which have an extra DNA strand (orange dot), and a three-dimensional DNA tube structure formed in the presence of porphyrin connector. [34] (c) Two triple-crossover tiles (top) were employed to form a flat lattice (bottom left), which further assembled to nanotubes using disulfide linkages (bottom right). [35] (d) Two identical DNA strands associate with each other to form two-dimensional sheets and finally fold into nanotubes. [36] (e) Self-assembly of DNA nanoribbons using 4x4 DNA tile. [37] (f) Six-helix bundle motif with 14-nucleotide pairs between crossovers and sticky ends formed self-assembled nanotubes. [38] (g) Double-crossover tiles tessellate to form extended 2D arrays that then can fold and close upon themselves to form tubes either in rings or nested helices of the tiles. [39] (h) Self-assembly of long tubes with monodisperse circumferences of 4, 5, 6, 7, 8, 10, or 20 DNA helices. [40] (i) Self-assembly of 2D array with parallel lines of AuNPs results in the formation of tubes displaying patterns of AuNPs in stacked rings, single spirals, double spirals, and nested spiral tubes. [41] (j)

Covalently linked DNA nanotubes were generated from orthogonal stepwise crosslinking of bis-thiolated/bisaminated circular DNAs.[42] (k) Geometrically well-defined triangular and square-shaped DNA nanotubes that can exist in double-stranded and single-stranded forms with significantly different stiffness.[43] (l) DNA nanotubes, with longitudinal variation by alternating larger and smaller capsules along the tube length, exhibit size-selective encapsulation of gold nanoparticles into the large capsules of these tubes. The cargo can be spontaneously released by adding the specific DNA strands to open the nanotubes.[44] (From reference 32).

As mentioned above, one of the most significant advances to structural DNA nanotechnology was developed by Rothemund,[29] inspired by a work reported by the group of Joyce.[45] In DNA origami, a single continuous strand of DNA, the scaffold, is shaped and folded by using a large number of small DNA strands that act as staples. Even if other methods to build 1D, 2D and 3D, nanostructures have been reported,[46-49] DNA tile and DNA origami still remain the most applied approaches.

Figure 1.5 shows few examples of DNA nanostructures obtained applying these two approaches. Furthermore, in order to simplify the design process, user-friendly, open access software such as CADnano[50] and NUPACK[51] have been developed.

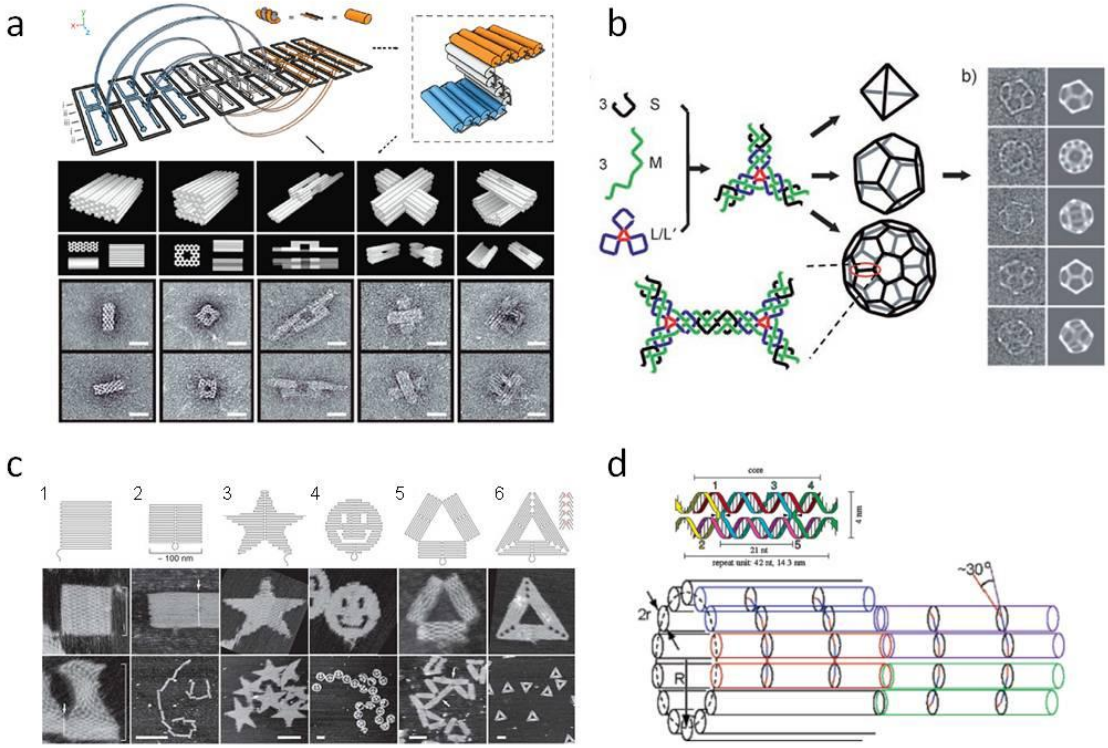

Figure 1.5. Example of DNA nanostructures obtained by using DNA origami or DNA tile technologies. (a) 3D DNA origami (*top panel*): a long strand of DNA (shown in grey) is first folded into a 2D sheet using staple strands (orange and blue). Selected portions of the 2D sheet

can then be joined together in space using other sequences of DNA that protrude from the plane of the DNA sheet (blue and white on the left), folding the sheet up into a 3D object (on the right). (*Middle panel*) perspective representation and planar projections of desired 3D objects, in which each DNA double helix is represented with a cylinder. (*Bottom panel*) EM images detecting relevant projections of the of 3D DNA origami. [52] (b) Hierarchical assembly of DNA-based 3D objects. (*left*) A sequence-symmetric three-point-star unit was assembled from three copies of strand M, three copies of strand S, and one central strand L. The central strand contains a single-stranded loop (red) of length 3 nt or 5 nt, which provides flexibility. Depending on loop length and total DNA concentration, the formation of tetrahedra, dodecahedra, or bucky balls is favored. (*right*) Cryoelectron microscopic images of DNA dodecahedra and corresponding projections expected from this structure.[53] (c) DNA origami shapes. (*Top row*) 1. square; 2. Rectangle; 3. Star; 4. Smiling face; 4. Triangle with rectangular domains, 5. Sharpe triangle with trapezoidal domains and bridges between them (red line inset). (*Bottom two rows*) A set of AFM images demonstrating the flexibility of the DNA Origami technology.[29] (d) A DNA nanotube assembled from a DNA tile. The tile characterized by five single strands with sticky ends at the edges and then further hybridized to a nanotube with curvature between tiles.[33] (Adapted from references 29, 33, 54, 55).

Besides the field of structural DNA nanotechnology a variety of DNA molecular devices have been engineered. A meaningful example in this field is represented by the seminal work of Yurke *et al.* in 2000. They reported "DNA tweezers", the first example of a nanomechanical device that was not only made from DNA but also driven by DNA as a fuel. [25] The nanomachine has the form of a pair of tweezers (Figure 1.6a), and is formed by the hybridization of three oligonucleotide strands called A, B and C. The reversible opening and closing of the molecular tweezers is achieved by the action of a fuel strand (F) followed by another strand that is fully complementary to the fuel, and thus termed anti-fuel (Ḟ). Specifically, strand F hybridizes with the dangling ends of strands B and C (shown in blue and green) to pull the tweezers in the closed state. Hybridization with the overhang section of F (red) allows Ḟ strand to displace F from the tweezers, by forming a double-stranded waste product FḞ, and thus it brings the tweezers in the initial, open state. The use of strand displacement reaction (for further details on this reaction see chapter 3), allow the cyclical repetition of the molecular tweezers motion until the poisoning of the system.

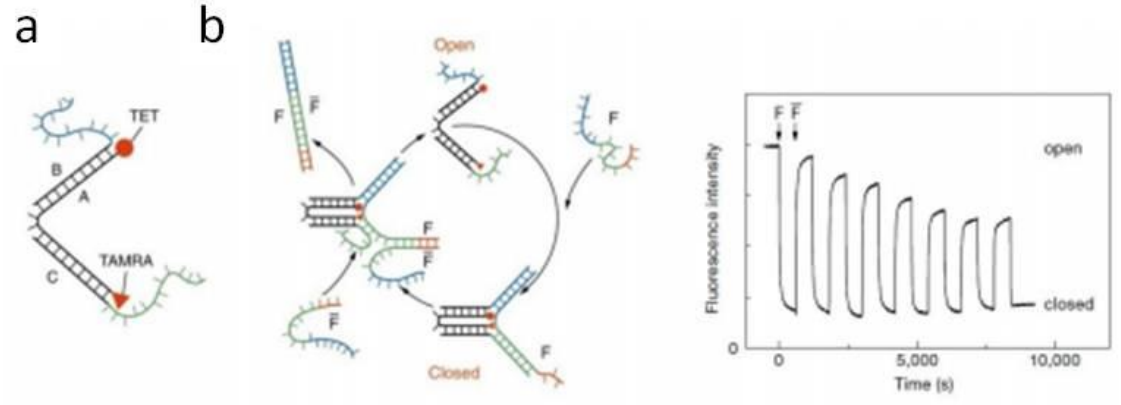

Figure 1.6. Design and cycle work of DNA molecular tweezer. (a) Structure of the molecular tweezers as formed by the self-assembly of three single strands. The motion of such nanodevice can be monitored thanks to a FRET pair. (b) Work cycle of the nanomachine. The mechanical motion of the nanomachine is triggered by F and Ḟ, that act as fuel and anti-fuel. For each work cycle a double stranded is produced as waste product. (Adapted from reference 25).

Many variations of the tweezers system have since been developed.[56-58] Furthermore, the development of DNA based nanodevices is not limited to DNA tweezers.

Among the first and simplest, yet most successful DNA-based molecular devices constructed so far are the MBs. [27,28] Molecular beacons are single-stranded hairpin stem structures doubly labelled with a fluorophore and a quencher. In the hairpin conformation, the fluorophore and the quencher are in proximity and the fluorescence of the beacon is low. In the presence of a strand complementary to the loop sequence, the hairpin stem unfolds to accommodate the longer double-stranded structure in the centre. MBs have seen a extensively applications in biosensing platforms. Other kind of DNA-based molecular switches have been reported. They have a common feature as they can flip reversibly between two or more state in a controllable manner, triggered by external stimuli such as temperature, [59] photoisomerization,[60-63] presence or depletion of various ions,[64] and protein binding.[65,66]

An unanticipated example of DNA based nanodevice is a molecular motor comprising a DNA walker that moves over a DNA-based breadboard. The first DNA-walker entirely of DNA was achieved by Shin and Pierce. [67] The walker component was a DNA duplex with two single-stranded extensions. After this first work, more complex arrangement and different approaches were adopted. [68,69] A common drawback in all these approach is that each move is step-by-step triggered by a distinct, external input, i.e. the manual addition of a DNA strand in solution. In turn, a second generation of DNA-walkers was

designed and developed by Pierce, Tuberfield, as well as Seeman and co-workers, to implement a DNA-walker with autonomous motion capability. The self-actuated motion was typically achieved by incorporating a catalytic reaction directly in the walker.
DNA tweezers and walkers are based on the same kind of reaction, DNA strand displacement reaction (this topic will be dissected in chapter 3). Due to its simplicity, this reaction has been widely used for molecular engineering, as well as to develop mechanisms able to drive many different dynamic devices. [70] Using DNA hybridization as an energy source, the Winfree and Pierce groups designed and engineered multiple strand displacement reactions to create complex reaction cascades and fuel DNA motors, including walking motors that autonomously move along track,[71-74] or DNA catalytic amplifiers that can sense and amplify signals.[75,76] Another remarkable application of displacement reaction is represented by Hybridization Chain Reaction (HCR) (Figure 1.7). [76] HCR is a process through which two metastable DNA hairpins, with identical necks and complementary loops, react with each other to form concatemer-like nanowires in the presence of a single strand DNA, that acts as initiator. HCR, introduced by Dirks and Pierce, [76] was applied by Venkataraman [77] to demonstrate an artificial "DNA comet", that represents the first attempt to use DNA polymerization reactions to drive molecular motion.

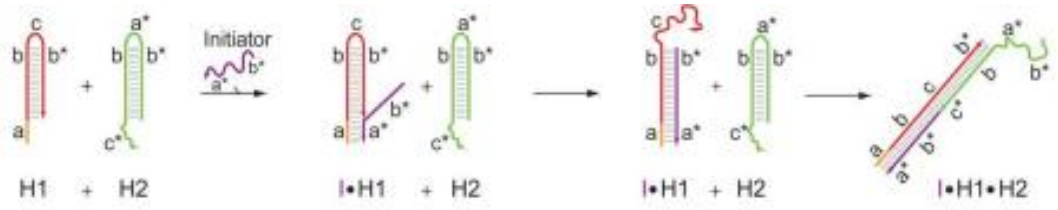

Figure 1.7. HCR mechanism. Two metastable tail-hairpins (H1 and H2) polymerise between each other to form a long chain-like duplex, only in the presence of an initiator strand (I). The reaction starts when I binds to the toehold portion (a) of H1, thus opening the hairpin through a strand displacement reaction. The newly exposed portion (c) of H1 then binds to the toehold portion (c*) of H2 and opens this latter hairpin to expose the portions (a*) and (b*) on H2 that are identical in sequence to I. Hence, a single copy of I can propagate an HCR event using both H1 and H2 hairpins to form a concatemer-like nanowire. (Adapted from reference 78).

The two complementary fields of structural DNA nanotechnology and DNA based nanodevices have been independently coevolving in the past 34 years. A most important achievement is the development of a number of strategies to precisely control and

organize complex DNA nanostructures, whereas there is still a lack of approaches to permit the dynamic transformation of such complex, static nanostructures towards enabling the implementation of complex, functional tools for a wider of applications in life sciences. DNA based nanodevices hold great promise for allowing achieving such a goal.

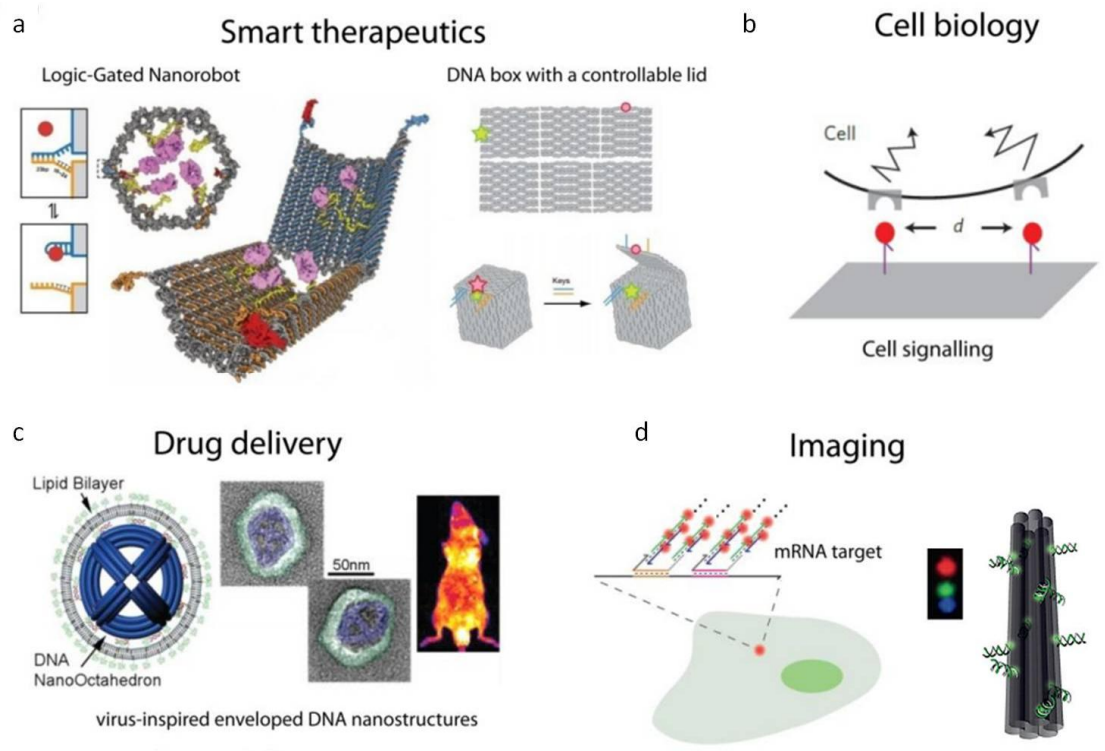

Figure 1.8. Applications of functional DNA nanostructures. (a) By combining nanostructures with functional units it is possible to create dynamic devices able to perform therapeutic actions targeting specific cells or tissues. (*left*) Design of a logic-gated DNA nanorobot with a DNA lock for its activation.[50] (*right*) Design of a DNA origami box and its opening/closing mechanism triggered by a DNA single strand. [51] (b) DNA origami can provide precise control over spatial organization of functional biomolecules, thus producing intriguing tools for quantitative measurements of biological processes. [79] (c) DNA nanostructures can be designed and engineered in order to attach drugs, target ligands and other modifications, such as lipid bilayers.[80] (d) (*left*) By using programmed multiple strand displacement reactions it is possible to engineer a novel class of sensitive and specific imaging probes to detect cellular RNA.[81] (*right*) DNA origami-based fluorescent barcodes as *in situ* imaging probes for fluorescence microscopy.[82] (Adapted from references 50, 51, 79-84).

In Figure 1.8 are reported some example that show some of the applications that can be obtained by coupling structural DNA nanotechnology and functional DNA nanodevices, such as smart therapeutic, drug delivery, imaging and cell biology. [50,51,79-82]

1.3 Not only Watson-Crick base pairs in the toolbox: Hoogsteen interactions

As described in the previous paragraphs, the first tool in the toolbox was obviously the stable B-DNA form, whereas one of the challenges in the field has been the construction of modular DNA architectures that can respond to external stimuli. [85] For this reason it is essential to add new tools in the toolbox that overcome the inherent limitation of B-DNA. Thanks to a breakthrough in 2002, Hoogsteen interactions entered the arena: two research groups, leaded by Mergny and Tan, [86,87] respectively, independently conceptualized and validated the transition of B-DNA to G-quadruplex implementing a nanoswitch. They started from B-DNA sequences incorporating a G-rich strand with quadruplex-forming capability along with a C-rich strand with i-motif-forming capability. [88] Shortly after, the Balasubramanian group introduced the first DNA nanomachines, in which the switch is triggered by pH change. [89] This latter system is based on two DNA single strands: one strand is a C-rich strand, containing four stretches of CCC in the sequence, while the other has a complementary sequence (G-rich) (Figure 1.9a). At acidic pH (pH 5) the C-rich strand folds into a closed i-motif structure, while, in turn, the G-rich strand adopts a random-coil conformation. When instead the pH value is raised to pH 8 the i-motif structure is inhibited, and in turn the hybridization between the two strands is observed. Interconversion of the closed and open state of the machinelike is thus achieved by cycling pH changes by adding H^+ or OH^-. The conformational change is detected with fluorescence spectrometry since a fluorophore and a quencher are located on the C-rich strand and reversibly change their FRET-based emission during the cycles.

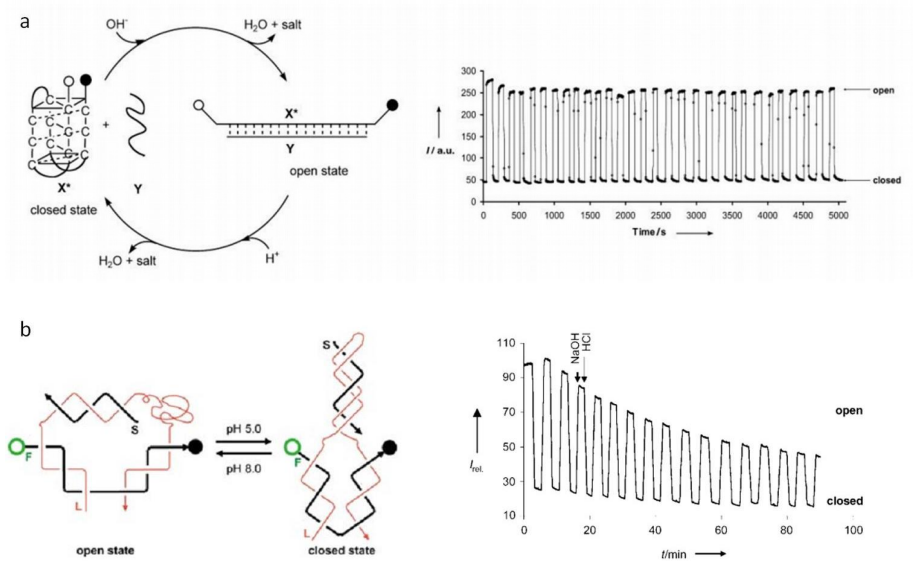

Figure 1.9. i-motif and triplex based nanoswitches, design and cycle work. (a) The system is composed of two DNA single strands: the first is a C-rich strand containing four stretches of CCC in the sequence, able to form at acidic pH an i-motif, while the second strand contains a complementary sequence. The pH acts as a chemical fuel. [89] (b) This molecular switch utilizes the triplex forming ability of a C-rich sequence (light red) that gets protonates under acidic conditions and forms CxG•C^+ triplex strand.[90] (Adapted from references 89,90).

The i-motif based nanoswitch can be triggered by using other stimuli such as light [91,92] or electrochemical stimuli. [93] Furthermore, Liedl *et al.* used a chemical oscillator to drive proton concentration changes, thus activating the i-motif based switch.[94,95]

Mao and co-workers designed a duplex triplex transition controlled with the pH, by using a ternary complex with a CG-rich duplex and a C-rich domain (shown in light red in Figure 1.9b).[90] Upon acidification, the C-rich domain is protonated, thus it can binds the duplex in the major groove. In this case the transition has been followed through a FRET pair. Other molecular switches based on the use of triplex DNA have been reported.[96,97]

After these first works, the research activities in this field expanded the use of these non-merely B-DNA-based structures to a wide range of applications. For example, both pH-controlled i-motif[98] and triplex [99,100] nanoswitches have been exploited to assemble gold nanoparticles together. Another interesting application is related to the possibility of performing controllable release of payloads, and in this regard G-quadruplex[101], i-motif,[93,101-103] and triplex,[104] have been applied.

Moreover, the association and dissociation of i-motifs have been used to reversibly align collections of i-motif-functionalized, carbon nanotubes (CNTs), whose electrochemical properties switched between their aligned and monomeric forms.[105] Remarkably, a solid-state device comprised of a solid-state, conical nanopore with its inner surface functionalized with i-motif-forming sequences, has been shown to mimic the opening and closing of ion channels. Here, when the DNA strands are in the unstructured state at a neutral pH value, the solid-state nanopore remains open and an ionic current can pass through it. At acidic pH values, the formation of i-motifs by these sequences blocks the nanopore, and this is reflected in a reduction of the ionic current.[106]

A-motif has been described for the first time in 2009 by the Krishnan group,[107] it consists of a parallel-stranded A-rich duplex held together by $^{+}$A-H^{+}A base pairs at acidic pH, that dissociates into two single helices at neutral pH. Recently, the same group used the A-motif to build a reversible, self-assembled, rigid 1D DNA architecture. This unprecedented architecture is capable of reversible and complete assembly and disassembly into its building block through pH changes.[108]

1.4 B-DNA and non-B DNA: from test tubes to living cells

As already highlighted above (Figure 1.7), because of the small size and the biocompatibility and the programmability of DNA-based systems, the most intriguing applications of DNA nanotechnology lie at the interface with biology. Although several major challenges still remain to be solved, DNA nanotechnology has been used to achieve some goals in this field (Figure 1.7).

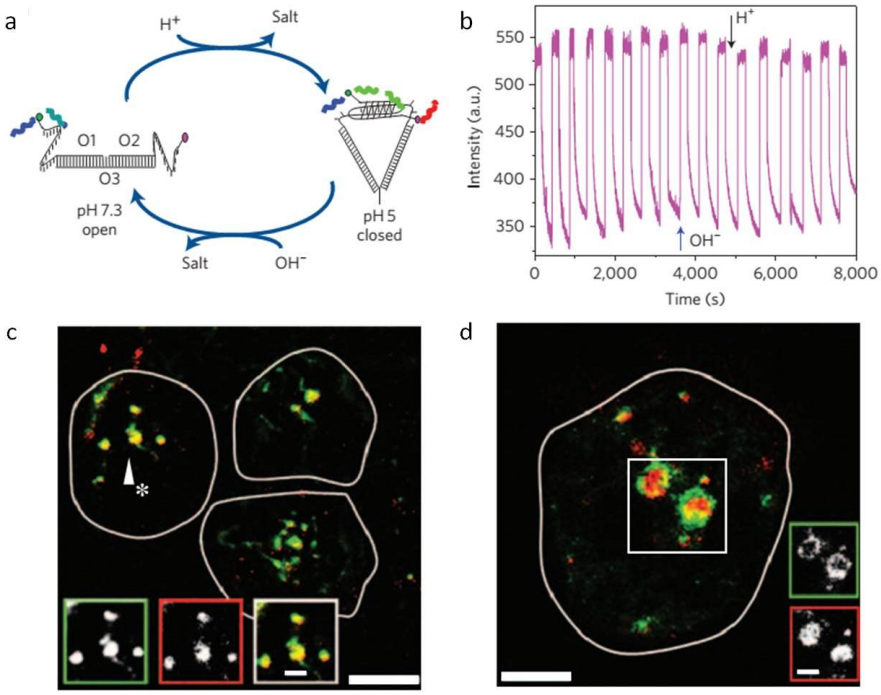

Figure 1.11.i-motif nanomachine able to map spatial and temporal pH changes inside living cells. (a) Schematic of the working principle of the I-switch in the "open" state (low FRET) at high pH, and in the "closed" state (high FRET) at low pH. (b) *In vitro* characterization of the I-switch through cycling pH change. The donor fluorescence intensity has cyclic peaks that occur upon alternate addition of acid (clack arrow) and base (blue arrow). (c) Co-localization of the I-switch (red) with endocytic vesicle marker FITC-dextran (green). (d) Co-localization of endocytosed I-switch (red) with Rab-5-GFP (green) positive endosome. (Adapted from reference 109).

Also in this case we can find some applications that rely on the use of non-B DNA structure stabilized by Hoogsteen interactions.

Inspired by the work of Yurke, [25] the Krishnan group exploited the pH sensitivity of i-motif structures to design a nanomachine able to map spatiotemporal pH changes inside living cells, through the endocytosis pathway.[109] The nanomachine, called "I-switch", contains two flexible strands of DNA that are rich in cytosine, with a third strand that holds them together (Figure 1.11a). Under acidic conditions, the two flexible strands form an i-motif, transforming the molecule from a linear or open conformation to a triangular or closed conformation. To quantify the conformational change directly, a FRET pair has been used. Thanks to this FRET pair they were able to map pH changes inside living cells, the fruit-fly haemocytes. The pH sensors have been engulfed through

endocytosis, they were encapsulated in endosomes and the endosomes maturation was followed. During this process a pH change is observe, due to proton pumps embedded within the membranes of the endosomes that change the environment inside from neutral (pH ~7) to acidic (pH ~5), at which point the endosomes fuse with organelles known as a lysosomes. In a follow-up study, the same group showed that pH-sensitive nanodevices can simultaneously track multiple pathways in the same cell.[110]

1.5 References

(1) Watson, J. D.; Crick, F. H. *Nature* 1953, 171, 737.

(2) Jungkweon, C.; Tetsuro, M. *Chem. Soc. Rev.* 2011, 40, 5893.

(3) Seeman, N. C. *Scientific American* 2004, 290, 64.

(4) Zhao, J.; Bacolla, A.; Wang, G.; Vasquez, K. M. *Cell. Mol. Life Sci.* 2010, 67, 43.

(5) Wang, G., Vasquez, K. M. *Mutat. Res.* 2006, 598, 103.

(6) Bacolla, A.; Wells, R. D. *Mol. Carcinog.* 2009, 48, 273.

(7) Wells, R. D.; Dere, R.; Hebert, M. L.; Napierala, M. Son, L. S. *Nucleic Acids Res.* 2005, 33, 3785.

(8) Seeman, N. C. *J. Theor. Biol.* 1982, 99, 237.

(9) Gilbert, D. E.; Feigon J. *Curr. Opin. Struct. Biol.* 1999, 9, 305.

(10) Brooks, T. A.; Kendrick, S.; Hurley, L. *FEBS J.* 2010, 277, 3459.

(11) Brooks, T. A.; Hurley, L. H. *Nat. Rev. Cancer* 2009, 9, 849.

(12) Hanahan, D.; Weinberg, R. A. *Cell* 2000, 100, 57.

(13) Guéron, M.; Leroy, J.-L. *Curr. Opin. Struct. Biol.* 2000, 10, 326.

(14) Mata, G.; Luedtke, N. W. *J. Am. Chem. Soc.* 2015, 137, 699.

(15) Lieblein, A. L.; Kramer, M.; Dreuw, A; Furtig, B.; Schwalbe, H. *Angew. Chem. Int. Ed.* 2012, 51, 4067.

(16) Huppert, J. L.; Balasubramanian S. *Nucleic Acid Res.* 2007, 35, 326.

(17) Frank-Kamenetskii, M. D.; Mirkin, S. M. *Annu. Rev. Biochem.* 1995, 64, 65.

(18) Frank-Kamenetskii, M. D. *Methods Enzymol.* 1992, 211, 180.

(19) Vasquez, K. M.; Glazer, P. M. *Q. Rev. Biophys.* 2002, 35, 89.

(20) Mukherjee, A.; Vasquez, K. M. *Biochimie* 2011, 93, 1197.

(21) Alberts, B. *Molecular biology of the cell. Garland Science*, New York, 4th edn. 2002

(22) Zheng, J.; Birktoft J. J.; Chen, Y.; Wang, T.; Sha, R.; Constantinou, P. E.; Ginell, S. L.; Mao, C.; Seeman, N. C. *Nature* 2009, 461, 74.

(23) Adleman, L. M. *Science* 1994, 266, 1021.

(24) Mao, C. D.; Sun, W. Q.; Shen Z. Y.; Seeman, N. C. *Nature* 1999, 397, 144.

(25) Yurke, B.; Tuberfield, A. J.; Mills, A. P.; Simmel, F. C.; Neumann, J. L. *Nature* 2000, 406, 605.

(26) Krishnan, Y.; Simmel, F. C. *Angew. Chem. Int. Ed.* 2011, 50, 3124.

(27) Tyagi, S.; Kramer, F. R. *Nature Biotechnol.* 1996, 14, 303.

(28) Wang, K.; *et al. Agew. Chem. Int. Ed.* 2009, 48, 856.

(29) Rothemund, P. W. K. *Nature* 2006, 440, 297.

(30) Aldaye, F. A.; Palemer, A. L.; Sleiman, H. F. *Science* 2008, 321, 1795.

(31) Fu, T. J.; Seeman, N. C. *Biochemistry* 1993, 32, 3211.

(32) Kwan Lo, P.; Metera, K. L.; Sleiman, H. F. *Curr Opin Chem Biol.* 2010, 14, 597.

(33) Rothemund, P. W. K.; Ekani-Nkodo, A.; Papadakis, N.; Kumar, A.; Fygenson, D. K.; Winfree, E. *J. Am. Chem. Soc.* 2004, 126, 16344.

(34) Endo, M.; Seeman, C.; Majima, T. *Angew. Chem. Int. Ed.* 2005, 44, 6074.

(35) Liu, D.; Park, S. H.; Reif, J. H.; LaBean, T. H. *Proc. Natl. Acad. Sci. U.S.A.* 2004, 101, 717.

(36) Liu, H.; Chen, Y.; He, Y.; Ribbe, A. E.; Mao, C. *Angew. Chem. Int. Ed.* 2006, 45, 1942.

(37) Yan, H.; Park, S. H.; Finkelstein, G.; Reif, J. H.; LaBean, T. H. *Science* 2003, 301, 1882.

(38) Mathieu, F.; Liao, S.; Kopatsch, J.; Wang, T.; Mao, C.; Seeman, N. C. *Nano Lett.* 2005, 5, 661.

(39) Mitchell, J. C.; Harris, J. R.; Malo, J.; Bath, J.; Turberfield, A. J. *J. Am. Chem. Soc.* 2004, 126, 16342.

(40) Yin, P.; Hariadi, R. F.; Sahu, S.; Choi, H. M. T.; Park, S. H.; LaBean, T. H.; Reif, J. H. *Science* 2008, 321, 824.

(41) Sharma, J.; Chhabra, R.; Cheng, A.; Brownell, J.; Liu, Y.; Yan, H. *Science* 2009, 323, 112.

(42) Wilner, O. I.; Henning, A.; Shlyahovsky, B.; Willner, I. *Nano Lett.* 2010, 10, 1458.

(43) Aldaye, F. A.; Lo, P. K.; Karam, P.; McLaughlin, C. K.; Cosa, G.; Sleiman, H. F. *Nature Nanotechnol.* 2009, 4, 349.

(44) Lo, P. K.; Karam, P.; Aldaye, F. A.; McLaughlin, C. K.; Hamblin, G. D.; Cosa, G.; Sleiman, H. F. *Nature Chem.* 2010, 2, 319.

(45) Shih, W. M.; Quispe, J. D.; Joyce, G. F. *Nature* 2004, 427, 618.

(46) Zhao, Z.; Yan, H.; Liu, Y. *Angew. Chem. Int. Ed.* 2010, 49, 1414.

(47) Zhao, Z.; Liu, Y.; Yan, H. *Nano Lett.* 2011, 11, 2997.

(48) Wei, B.; Dai, M.; Yin, P. *Nature* 2012, 485, 623.

(49) Ke, Y.; Ong, L. L.; Shih, W. M; Yin, P. *Science* 2012, 338, 1177.

(50) Douglas, S. M.; Bachelet, I.; Church, G. M. *Science* 2012, 335, 831.

(51) Andersen, E. S.; *et al.* *Nature* 2009, 459, 73.

(52) Douglas, S. M.; Dietz, H.; Liedl, T.; Hogberg, B.; Graf, F.; Shih, W. M. *Nature* 2009, 459, 414.

(53) He, Y.; Ye, T.; Su, M.; Zhang, C.; Ribbe, A. E.; Jiang, W.; Mao, C. D. *Nature* 2008, 452, 198.

(54) Modi, D.; Bhatia, D.; Simmel, F. C.; Krishnan, Y. *J. Phys. Chem. Lett.* 2010, 1, 1994.

(55) Simmel, F. C. *Angew. Chem. Int. Ed.* 2008, 47, 5884.

(56) Simmel, F. C.; Yurke, B.; *Phys. Rev. E* 2001, 63, 041913.

(57) Simmel, F. C.; Yurke, B.; Sanyal, R. J. *Nanosci. Nanotechnol.* 2002, 2, 383.

(58) Choi, S. W.; Makita, N.; Inoue, S.; Lesoil, C.; Yamayoshi, A.; Kano, A.; Akaike, T.; Maruyama, A. *Nano Lett.* 2007, 7, 172.

(59) Viasnoff, V.; Meller, A.; Isambert, H. Nano Lett. 2006, 6, 101; Tashiro, R.; Sugiyama, H. *Angew. Chem. Int. Ed.* 2003, 42, 6018.

(60) Liang, X.; Nishioka, H.; Takenaka, N.; Asanuma, H.; *ChemBio-Chem* 2008, 9, 702.

(61) Uno, S.-n.; Dohno, C.; Bittermann, H.; Malinovskii, V. L.; Haener, R.; Nakatani, K. *Angew. Chem. Int. Ed.* 2009, 48, 7362.

(62) Kang, H.; Liu, H.; Phillips, J. A.; Cao, Z.; Kim, Y.; Chen, Y.; Yang, Z.; Li, J.; Tan, W. *Nano Lett.* 2009, 9, 2690.

(63) White, S. S.; Li, H. T.; Marsh, R. J.; Piper, J. D.; Leonczek, N. D.; Nicolaou, N.; Bain, A. J.; Ying, L. M.; Klenerman, D. *J. Am. Chem. Soc.* 2006, 128, 11423.

(64) Ogura, Y.; Nishimura, T.; Tanida, J. *Appl. Phys. Express* 2009, 2, 025004.

(65) Shen, W.; Bruist, M. F.; Goodman, S. D.; Seeman, N. C. *Angew. Chem. Int. Ed.* 2004, 43, 4750.

(66) Gu, H.; Yang, W.; Seeman, N. C. *J. Am. Chem. Soc.* 2010, 132,4352.

(67) Shin, J. S.; Pierce, N. A. *J. Am. Chem. Soc.* 2004, 126, 10834.

(68) Sherman, W. B.; Seeman, N. C. *Nano Lett.* 2004, 4, 1203.

(69) Tian, Y.; Mao, C. D. *J. Am. Chem. Soc.* 2004, 126, 11410.

(70) Ditter, W. U.; Reuter, A.; Simmel, F. C. *Angew. Chem. Int. Ed.* 2004, 43, 3550.

(71) Omabegho, T.; Sha, R.; Seeman, N. C. *Science* 2009, 324, 67.

(72) Lund, K.; *et. al. Nature* 2010, 465, 206.

(73) Muscat, R.A.; Bath, J.; Tuberfield, A. J. *Nano Lett.* 2011, 11, 982.

(74) Wickham, S. F. J.; *et al. Nature Nanotech.* 2012, 7, 169.

(75) Condon, A. *Nat. Rev. Genet.* 2006, 7, 565.

(76) Dirks, R. M.; Pierce, N. A. *Proc. Natl. Acad. Sci. U.S.A.* 2004, 101, 15275.

(77) Venkataraman, S.; Dirks, R. M.; Rothemund, P. W. K.; Winfree, E.; Pierce, N. A. *Nature Nanotechnol.* 2007, 2, 490.

(78) Idili, A.; Porchetta, A.; Amodio, A.; Vallée-Bélisle, A.; Ricci, F. *Nano Lett.* 2015, 15, 5539.

(79) Shaw, A.; *et al. Nature Methods* 2014, 11, 841.

(80) Perrault, S. D.; Shih, W. M. *ACS Nano* 2014, 8, 5132.

(81) Choi, H. M. T.; Beck, V. A.; Pierce, N. A. *ACS Nano* 2014, 8, 4284.

(82) Lin, C.; Jungmann, R.; Leifer, A. M.; Li, C.; Levern, D.; Church, G. M.; Shih, W. M.; Yin, P. *Nature Chem.* 2012, 4, 832.

(83) Linko, V.; Dietz, H. *Curr Opin Biotech.* 2013, 24, 555.

(84) Chen, Y.-J.; Groves, B.; Muscat, R. A.; Seelig, G. *Nature Nanotechnol.* 2015, 10, 748.

(85) Liang, F.; Mochizuki, H.; Asanuma, H. *Small* 2009, 5, 1761.

(86) Li, J. J.; Tan, W. *Nano Lett.* 2002, 2, 315.

(87) Alberti, P.; Mergny, J. L. *Proc. Natl. Acad. Sci. U.S.A.* 2003, 100, 1569.

(88) Phan, A. T.; Mergny, J. L. *Nucleic Acids Res.* 2002, 30, 4618.

(89) Liu, D.; Balasubramanian, S. *Angew. Chem. Int. Ed.* 2003, 115, 5912.

(90) Chen, Y.; Lee, S. H.; Mao, C. D. *Angew. Chem. Int. Ed.* 2004, 43, 5335.

(91) Liu, H.; *et al. Phys. Chem. B* 2008, 112, 6893.

(92) Liu, H. J.; Xu, Y.; Li, F. Y.; Yang, Y.; Wang, W. X.; Song, Y. L.; Liu, D. S. *Angew. Chem. Int. Ed.* 2007, 46, 2515.

(93) Mao, Y.; Liu, D.; Wang, S.; Luo, S.; Wang, W.; Yang, Y.; Quyang, Q.; Jiang, L. *Nucleic Acids Res.* 2007, 35, e33.

(94) Liedl et al. *Angew. Chem. Int. Ed.* 2004, 43, 6469,

(95) Liedl, T.; Simmel, F. C. *Nano Lett.* 2005, 5, 1894.

(96) Brucale, M.; Zuccheri, G.; Samori, B. *Org. Biomol. Chem.* 2005, 3, 575.

(97) Idili, A.; Vallée-Bélisle, A.; Ricci, F. *J. Am. Chem. Soc.* 2014, 136, 5836.

(98) Seela, F; Budow, S. *Helv. Chim. Acta* 2006, 89, 1978.

(99) Jung, Y. H.; Lee, K.-B.; Kim, Y.-G.; Choi, I. S. *Angew. Chem. Int. Ed.* 2006 , 45, 5960.

(100) Chen, Y.; Mao, C. *Small* 2008, 4, 2191.

(101) Dittmer, W. U.; Reuter, A.; Simmel, F. C. *Angew. Chem. Int. Ed.* 2004, 43, 3550.

(102) Song, L.; Ho, V. H.; Chen, C.; Yang, Z.; Liu, D.; Chen, R.; Zhou, D. *Adv. Healthcare Mater.* 2013, 2, 275.

(103) Chen, C.; Pu, F.; Huang, Z.; Liu, Z.; Ren, J.; Qu, X. *Nucleic Acids Res.* 2011, 39, 1638.

(104) Porchetta, A.; Idili, A.; Vallée-Bélisle, A.; Ricci, F. *Nano Lett.* 2015, 15, 4467.

(105) Shin, S. R.; *et al. Chem. Commun.* 2009, 1240.

(106) Xia, F.; *et al. J. Am. Chem. Soc.* 2008, 130, 8345.

(107) Chakraborty, S.; Sharma, S.; Maiti, P. K.; Krishnan, Y. *Nucleic Acids Res.* 2009, 37, 2810.

(108) Saha, S.; Bhatia, D.; Krishnan, Y. *Small* 2010, 6, 1288.

(109) Modi, S.; Goswani, D.; Gupta, G. D.; Mayor, S.; Krishnan, Y. *Nature Nanotech.* 2009, 4, 325.

(110) Modi, S; Nizak, C.; Surana, S.; Halder, S.; Krishnan, Y. *Nature Nanotech.* 2013, 8, 459.

Chapter 2 - Folding-upon-binding and signal-on electrochemical DNA sensor with high affinity and specificity

2.1 Introduction

Biomolecular receptors such as proteins or nucleic acids that shift between two or more conformations upon binding to a specific target can be used to build robust, sensitive and specific sensors.[1,2] Since signal transduction is linked to the conformational change that occurs only upon binding, these receptors allow for detection of a specific target even within the incredibly complex media that exist within biological system. To create robust, rapid sensors that similarly link specificity and sensitivity, a number of structure-switching optical and electrochemical sensors have been reported in recent years for applications in the areas of diagnostics and imaging, and several different strategies have been employed in the design of binding-induced molecular switches.[1-3] Among the various structure-switching strategies employed by naturally occurring receptors, the use of a clamp-like mechanism where the receptor comprises two recognition elements that both bind and recognize the target, remains one of the most effective.[3] Inspired by this mechanism, A. Idili and co-workers have recently explored the thermodynamics by which a DNA clamp-like molecular receptor, that recognizes a specific complementary oligonucleotide target through both Watson-Crick and triplex-forming Hoogsteen interactions, can improve both the affinity and specificity of recognition.[4]

In the present work, I fully realize and exploit the advantages of such molecular "double-check" mechanism, by adapting this clamp-like sensing strategy to a DNA-based electrochemical biosensor (hereafter named E-DNA). The classic E-DNA sensor, first proposed by Plaxco et al. in 2003, [5,6] comprises a redox-label stem-loop or linear DNA probe immobilized on the surface of a gold electrode that, upon hybridization with its complementary target, leads to a rigid, duplex complex that brings the redox reporter far away from the electrode surface and thus suppresses the observed electrochemical signal (signal-off E-DNA sensor) [5,6]. Such strategy provides impressive advantages that include the reagentless nature of the platform, the adaptability to point-of devices, and the possibility to use it in complex real samples. [5-9] In this work I have used a clamp-switch probe to develop a signal-on E-DNA sensor, a type of structure-switching DNA probe that enables the single-step detection of specific oligonucleotides

in a reagentless fashion (i.e. without the need of adding exogenous reagents). We also demonstrate that this strategy results in significantly improved affinity and specificity relative to previously published E-DNA sensors.[5-9]

2.1 Results and discussion

The signaling element I have used for my signal-on E-DNA sensor is a redox reporter (MB) conjugated at the 3' end of my DNA-based clamp-switch probe. The probe is also labeled at the 5' end with a thiol group to support stable attachment to an interrogating gold electrode. My clamp-switch probe is composed of two recognition elements separated by an unstructured, 10-base loop (Figure 2.1a, black portion). The first recognition element, a 15-base polypyrimidine portion (Figure 2.1a, green portion), binds the target, a complementary polypurine sequence, via Watson-Crick base pairing. The second recognition element, a polypyrimidine sequence (Figure 1a, red portion), then binds the so-formed duplex via sequence-specific Hoogsteen base pairing.[4,11,12] The formation of this triplex structure occurs through a conformational switch that leads to its closure (Figure 2.1a).[4,13-20]

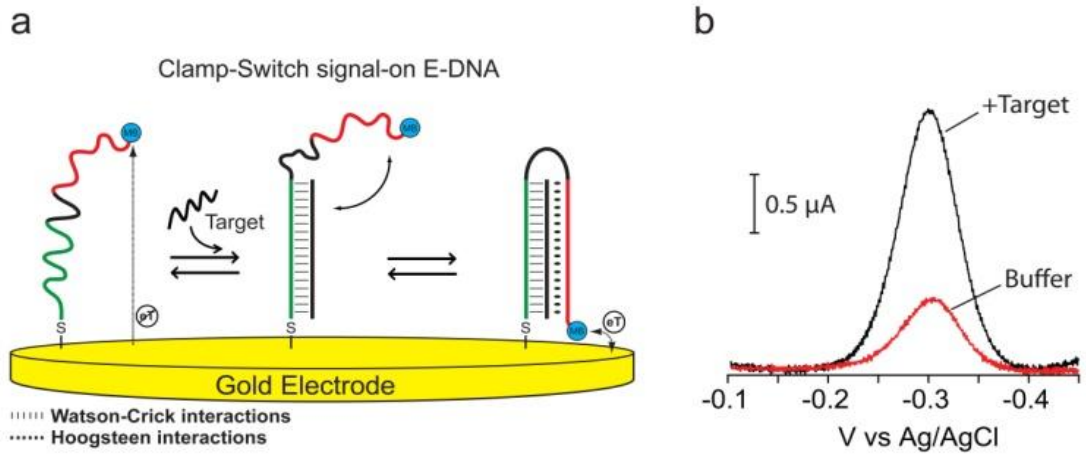

Figure 2.1. (a) The clamp-switch E-DNA sensor is comprised of a DNA probe modified at its 3'-terminus with a methylene blue redox tag and at its 5'-terminus with a thiohexyl moiety for attachment on a gold electrode. The probe is designed with a first recognition element, a 15-base polypyrimidine portion (green portion) that can recognize a complementary target sequence via Watson-Crick base pairing. The second recognition element, a polypyrimidine sequence (red portion) can then fold back to form a triplex structure through Hoogsteen base

pairing.[4,11,12] This brings the redox label into close proximity with the electrode surface, increasing electron transfer efficiency and resulting in an increase in the observed current (b).

In the absence of the oligonucleotide sequence complementary to the first recognition element, the probe, in its linear conformation, is flexible enough that the attached methylene blue maintains its mechanical freedom to remains, on average, very distant from the electrode surface, and thus exchanges electrons at a relatively low rate. Upon the addition of its specific DNA target, the E-DNA clamp probe folds into a triplex structure that confines the methylene blue near the electrode, thus increasing the electron transfer rate and the observed electrochemical voltammetric response (signal-on behavior) (Figure 2.1b).

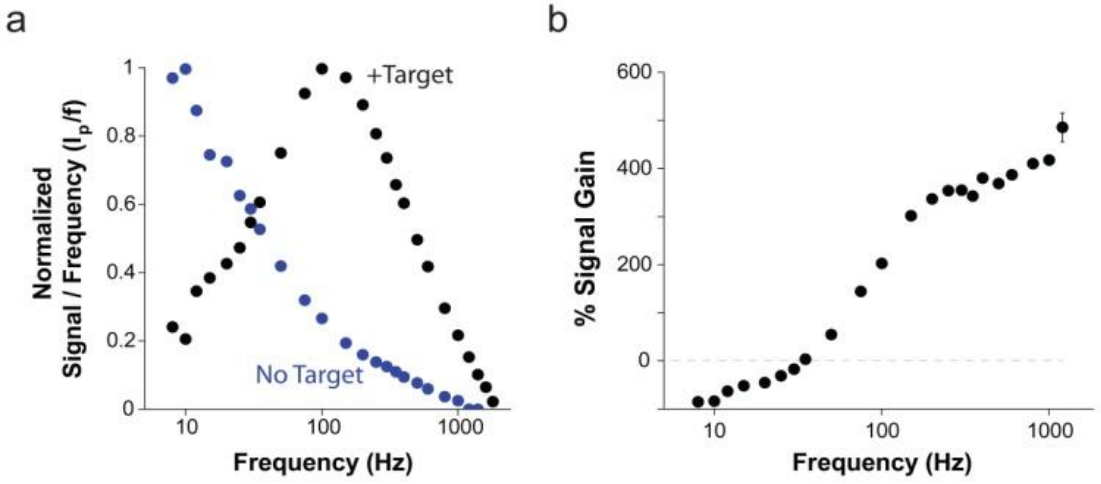

Figure 2.2. The change in electron transfer characteristics upon target binding provides a mechanism for tuning the signal gain of the E-DNA clamp-switch probe. Following target binding, the clamp-switch probe folds back to form a triplex structure and the methylene blue reporter is held in close proximity to the electrode surface, providing faster electron transfer than the unbound probe, which has more freedom to occupy positions distant from the electrode surface. (a) The ratio of the measured peak current to SWV frequency (I_p/f) as a function of frequency provides a way to measure the apparent electron transfer rate of the methylene blue reporter.[20] The bound E-DNA triplex (black) has a critical frequency around 100 Hz, for an apparent electron transfer rate of ~ 85 s^{-1}.The unbound free probe (blue) has a critical frequency $\leq$10 Hz, showing much slower electron transfer. (b) By varying the SWV frequency used to measure the probe, the ratio of signal between bound and unbound states is variable, providing highly tunable signaling characteristics. For most measurement frequencies, the signal current increases upon target binding with signal gain of up to 400% for measured frequencies. Only when the frequency falls below 25 Hz, a time scale in which the rapid electron transfer of the

bound state rapidly exhausts the signaling current, the observed signal of the unbound probe is higher than that in the presence of the target (signal-off behavior). For a matter of clarity in these binding curves and in those in the following figures, error bars have been depicted for only one point on each curve and represent the average and standard deviations of measurements performed on at least three independent sensors.

The signaling behavior of my E-DNA clamp-switch is directly linked to the closure of the clamp, which brings the methylene blue closer to the electrode and thus increases the electron transfer rate of the methylene blue redox reaction. To demonstrate this I have measured the apparent electron transfer rates using SWV. The electron transfer rate is directly proportional to the "critical frequency" - the maximum frequency-corrected peak current in the i_p/f vs. f curve, where i_p is the net peak current and f is the SWV frequency.[21,22] My E-DNA clamp-switch leads to a significant decrease in the critical frequency upon target binding, demonstrating a much faster electron transfer rate (Figure 2.2a). Crucially, this difference in electron transfer rate allows me to optimize measurement frequency to maximize signal gain.

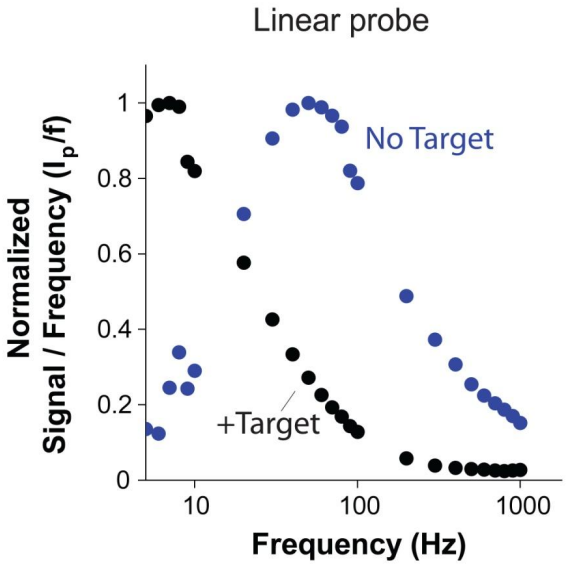

Figure 2.3. The ratio of peak current to SWV frequency (i_p/f) as a function of the inverse of the SWV frequency (1/f) exhibits a maxima at a critical frequency related to the apparent electron transfer rate. Target binding causes a shift in this critical frequency to lower frequencies. This kind of behavior is typical of the signal-off sensors.[23] By courtesy of Prof. K.W. Plaxco.

Despite the normally signal-on behavior of my clamp-switch sensor, I note that, similarly to other DNA-based architectures,[23] at very low SWV frequencies (below ~25 Hz) the behavior of the sensor is inverted, and the target-free state produces a signal

higher than that of the target-bound clamp state (Figure 2.2a). This is probably due to the fact that at low-enough measurement time scales, the target-bound redox reaction proceeds faster than the unbound redox reaction. This leads to exhausting electron transfer from the faster reaction and, thus allowing the slower reaction to dominate current measurements.

The behavior of the E-DNA clamp-switch sensor differs significantly from that of a classic E-DNA sensor based on a Watson-Crick linear hybridization probe[23]. For the latter, the presence of the target leads to a reduction of the apparent electron transfer rate (Figure 2.3) because target binding produces a more rigid duplex DNA, in which the methylene blue approaches the surface less frequently than in the target-free, linear probe. In turn, a linear E-DNA sensor displays a signal-off behavior at frequencies for which the E-DNA clamp-switch sensor leads, in contrast, to signal increase upon target binding. The percentage signal increase observed upon target binding varies with the SWV frequency used to measure the probe. At high-enough frequencies (>50 Hz), the signal current increases upon target binding with a signal gain that reached a maximum of 400% at the highest frequencies we have investigated (Figure 2.2b).

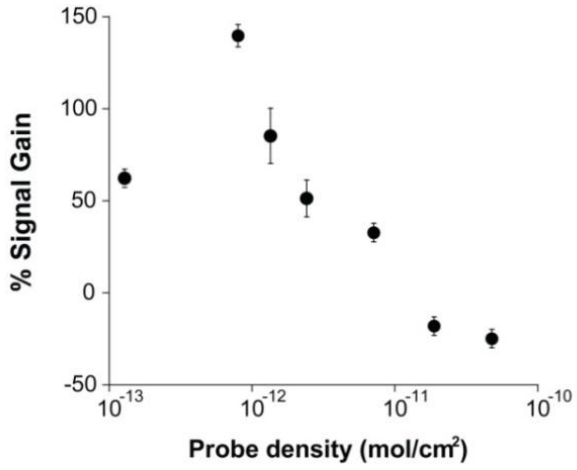

Figure 2.4. Since the E-DNA clamp-switch mechanism is based on the possibility of the probe to fold-back and form a triplex structure, its signal is strongly dependent on the probe surface density. We demonstrate this by fabricating E-DNA clamp-switch sensors of different probe densities by varying the concentration of the DNA clamp-switch probe employed during sensor fabrication and interrogating these sensors with saturating amount of a complementary target (13-mer, 300 nM). At high probe densities the triplex formation is so unfavored that we only observe a signal decrease (consistent with formation of the sole duplex DNA). As the probe

surface density decreases below a critical value of 10^{-11} mol/cm^2 the spacing between the probes increases enough to allow them to fold-back and form the triplex structure (signal-on behavior).

The signal of the E-DNA clamp-switch sensor strongly depends on probe density (Figure 2.4). Specifically, the signal-on behavior of the sensor is exclusively found at relatively low densities. At higher densities (>10^{-11} mol/cm^2) target binding leads to a signal decrease (signal-off). Presumably, at higher densities, steric hindrance and/or electrostatic effects inhibit the formation of a compact triplex structure, and favor the formation of the intermediate duplex-containing structure. I also note that the signal-to-noise ratio maximizes at intermediate probe densities, as it depends on absolute current intensity, which intrinsically depends on probe density.

The E-DNA clamp-switch sensor supports the signal-on detection of oligonucleotide targets with high affinity (Figure 2.5a). Binding curves with targets of different lengths show nanomolar affinity for complementary targets as short as 10 bases. Targets longer than 12 bases show similar affinities (Figure 2.5a). This is due to the fact that with longer targets we reach the ligand-depletion regime (i.e., the true K_D for the target is lower than the e ffective probe concentration in the working solution) and the observed K_D is not related anymore to the "true" probe-target K_D.[24]

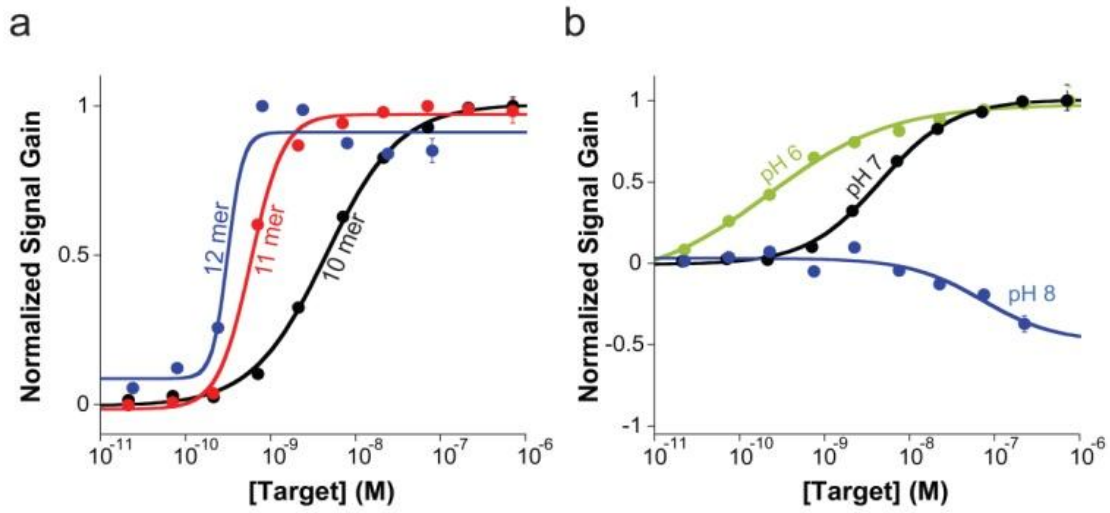

Figure 2.5. (a) The E-DNA clamp-switch sensor can detect specific complementary targets with high affinity. Here are shown binding curves of targets of different lengths (10, 11 and 12 bases). As expected, the affinity observed with longer targets is improved until we reach the ligand-depletion regime in which occupancy is no longer defined by the true affinity of the probe or the concentration of the target in solution, but by the total number of ligand (target) molecules in the sample relative to the total number of probes on the sensor surface. [24] In this

latter case, a bilinear binding curve is observed with a midpoint at a target concentration half of the effective probe concentration ($[P]_{eff}/2$). These binding curves were obtained by adding increasing concentration of perfectly matched targets of different length in a 2 mL 10 mM Tris buffer, 10 mM $MgCl_2$, 100 mM NaCl pH 7.0. (b) The sensing mechanism of the E-DNA clamp-switch sensor is based on the formation of a triplex structure upon target binding. Consistent with this and considering that triplex formation is unfavored at basic pH,[4,13-16] the affinity of our clamp-switch sensor becomes poorer as we increase the pH at which we interrogate the sensor. Interestingly, since a basic pH (here pH 8.0, blue curve) greatly inhibits triplex formation, we only observe duplex formation. These binding curves were obtained by adding increasing concentration of a perfectly matched target (10-mer) in a 2 mL 10 mM Tris buffer, 10 mM $MgCl_2$, 100 mM NaCl (pH 6, 7 and 8).

The evidenced sensing mechanism based on triplex formation is also supported by results obtained on the behavior of sensor's affinity as a function of pH (Figure 2.5b). As anticipated, the sensor's affinity for a 10-base target gets gradually poorer with increasing pH because Hoogsteen interactions are less stable at basic pHs (Figure 2.5b).[13,15] Interestingly, at pH 8 target binding does not lead anymore to signal increase, and a signal-off behavior is instead observed. My interpretation is that at this pH triplex formation is inhibited and the target binding only leads to the intermediate duplex-containing structure,[25,26] which in turn increases, on average, the distance between electrode surface and methylene blue leading to a signal-off behavior. The results obtained at pH 6 and pH 8 gives a direct comparison of the performance of an E-DNA clamp-switch probe with that of a simple hybridization probe, which is solely based on Watson-Crick interactions. Remarkably, the clamp-switch probe shows for the same 10-base target (K_D= 0.39 nM at pH 6) a 180-fold improved affinity compared to a simple hybridization probe (K_D = 72 nM, results obtained at pH 8).
To further investigate the behavior of the E-DNA clamp-switch sensor at pH 6 and 8, and provide direct evidence of the related structural motifs and of my above interpretation, I used AFM and an AFM-based nano-lithographic technique termed nanografting.[27] Using nanografting, I formed squared patches of monolayer of TOEG6. Such features provided with a reference monolayer for the quantification, by means of side-by-side topographic AFM imaging, of the height of the surrounding self-assembled monolayers (SAM) of DNA clamp molecules over an ultra-flat gold surface (Figure 2.6a-b, d-e).

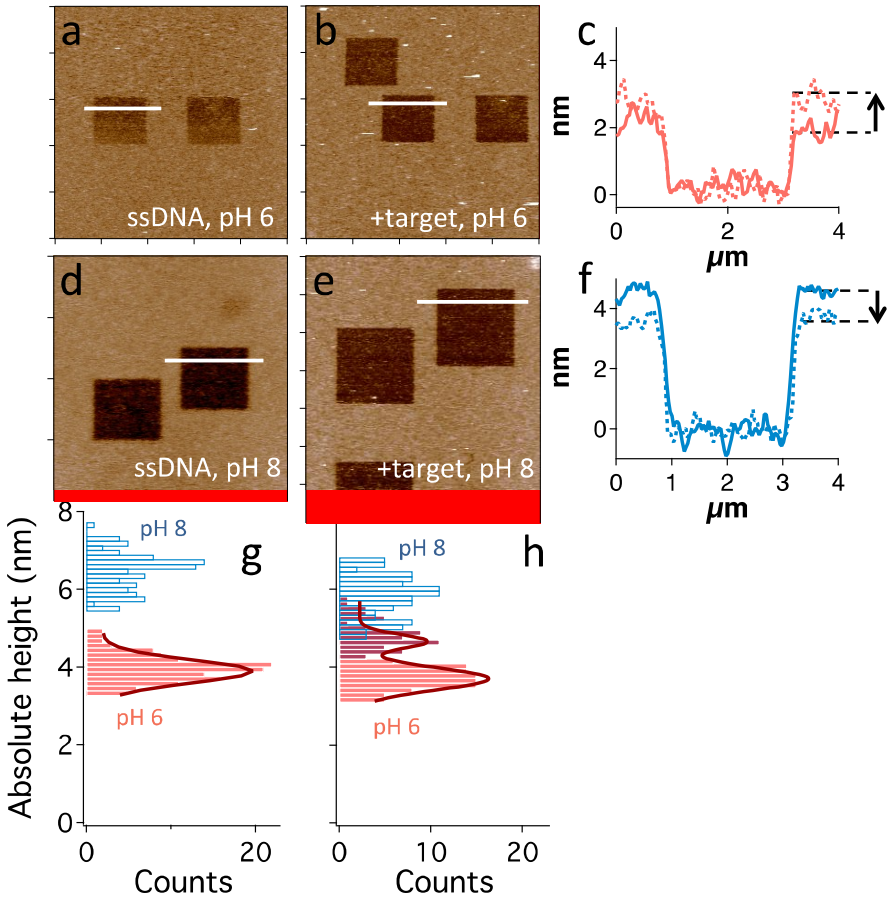

Figure 2.6. (a-f) Analysis of a representative sample that showcases the monolayer height change related to target binding at different pH values. a, b, d, e) AFM topography images showing the DNA monolayer (light brown) and the nanografted 2×2 μm^2 TOEG6 features (dark brown), produced for samples analyzed at pH 6 (a, b) and pH 8 (d, e), before and after target incubation (a, d and b, e, respectively). Images are color-coded in a brighter-is-higher fashion with a scale range of 10 nm. Bars, 4 μm. c, f) Overlapped height profiles (relative to the TOEG6 layer) obtained for the samples analyzed at pH 6 (a, b, c, red profile) and pH 8 (d, e, f, blue profile). Solid and dashed lines represent SAM height profiles before and after target incubation, respectively. An arrow marks the height increase observed at pH 6 and the decrease at pH 8. (g, h) Absolute DNA height distributions obtained from each nanografted patch at pH 6 and pH 8 are represented in red and blue, respectively. The former are fitted with Gaussian functions (dark red curves). ssDNA SAM height at pH 8 is ~ 3 nm higher than at pH 6 (g) and there is no overlapping between the two distributions. Height distribution at pH 6 can be well fitted by a single Gaussian curve. After hybridization with a 10-mer target (h), height distribution at pH 6 changes significantly, and a ~ 25% higher component (dark red bars) appears from the background, which is centered at a height slightly lower than 4 nm. This distribution was fitted with a double Gaussian curve. pH 8 height distribution shows a less

remarkable change, height values becoming ~ 10% lower after hybridization. The two height distributions after target incubation clearly overlap for values around 5 nm.

Whereas the clamp-switch probe is 44-bases long, and thus has an ideal end-to-end length > 10 nm, the measured height of the optimally target-responsive SAMs (described above) varied, at pH 6, within a small range of a few nanometers (see height profiles in Figure 2.6c). The latter is consistent with the fact that effective SAM stiffness (and, therefore, the AFM-measured height) depends on SAM density.[28,29] In particular, at very low densities, as in this case, DNA molecules can be easily tilted by a scanning AFM tip, thus leading to AFM-measured height values compatible with the axial width of the molecule instead of its end-to-end length. Figure 2.6g shows that, at pH 6, the hybridization with the 10-base-long target leads to a significant change of the height distribution, as a distinct, and ~25% higher component emerges with respect to a back ground distribution having a height peak at ~ 4 nm (see also a representative patch and its corresponding line profiles in Figure 2.6a-c). At pH 8 the AFM-measured height of the ssDNA SAM is ~ 3 nm higher than at pH 6, and after target hybridization the measured height values are ~ 10% lower as shown in Figure 2.6h (see also a representative patch and its corresponding line profiles in Figure 2.6d-f).
It is likely that, at pH 8, ssDNAs are more stretched than at pH 6, due to inherent electrostatic repulsion between phosphate groups along backbones, thus resulting in thicker SAMs. Thus, the small percentage height decrease, measured at pH 8 after hybridization with a target ~ 70% shorter than the surface-bound probe, is consistent with a small portion of the molecule becoming stiffer and shorter. On the contrary, at pH 6, a background distribution is unaltered after hybridization, and is compatible with the expected strong disturbance of the AFM tip on a more flexible chain. However, after hybridization, the frequent detection of ~25% higher SAMs, suggests that a longer portion of the molecule becomes stiffer. AFM results are, therefore, consistent with the interpretation that target hybridization leads to the formation of distinct motifs at pH 6 and 8, respectively a triplex and a duplex.

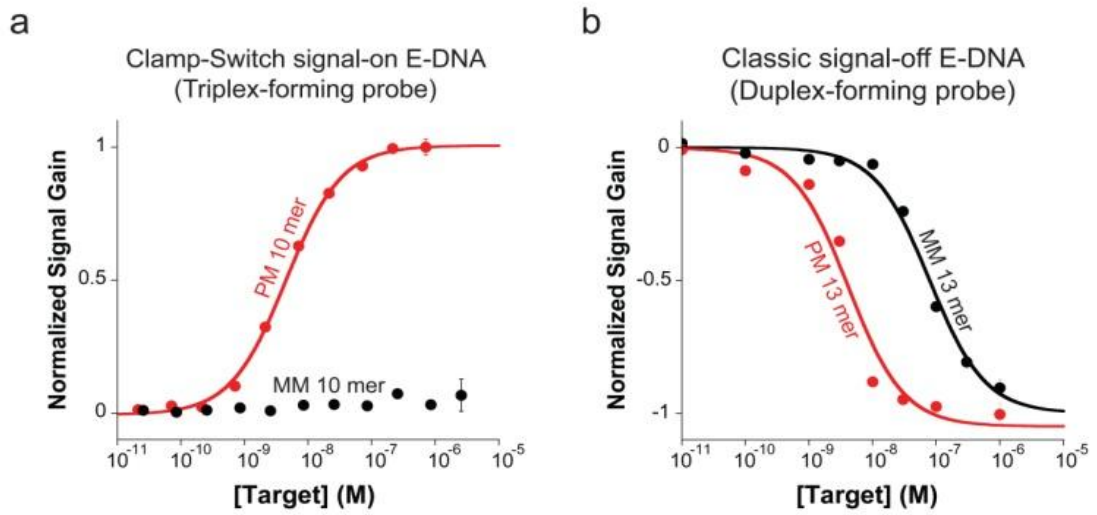

Figure 2.7. (a) The E-DNA clamp-switch sensor is highly specific. I demonstrate this by interrogating the sensor with a perfect match and a 1-base mismatch target (both 10-mer). The affinity of the mismatch target is at least 2000-fold poorer than that of the perfect match target, thus demonstrating that the sequence-specific Hoogsteen base pairs in the clamp-switch offer an additional specificity check that increases the probe specificity compared to an equivalent E-DNA sensor based solely on Watson-Crick interactions. (b) As a further demonstration of this I show here the binding curves obtained with a perfect match and a 1-base mismatch using a classic E-DNA sensor based on a linear DNA probe. This sensor (signal-off) shows a separation between the perfect-match and mismatch affinity of only ~ 20-fold. These binding curves were obtained by adding increasing concentration of a perfectly matched target and a 1-base mismatch target (10-mer for the clamp-switch and 13-mer for the linear probe) in a 2 mL 10 mM Tris buffer, 10 mM $MgCl_2$, 100 mM NaCl.

Beyond improving affinity, the E-DNA clamp-switch sensor also enhances specificity. To explore this I have tested our E-DNA clamp-switch against a perfectly matched and a single-base mismatched target (10-base). Experimental limitations didn't allow me to determine the K_D for the single-base mismatch target. In fact, even at very high concentrations (i.e. 10^5 M, 4 orders of magnitude higher than the K_D for a perfectly matched probe) I was not able to observe any significant signal change in the presence of the single-base mismatch target (Figure 2.7a). The E-DNA clamp-switch sensor thus provides a discrimination factor (ratio of the affinity constants, $K_D^{mismatch}/K_D^{perfect\ match}$) at least higher than 2000-fold ($K_D^{perfect\ match}$ = 4.5 nM). As a comparison, a classic E-DNA sensor based on a simple linear hybridization probe shows only 20-fold discrimination efficiency. While the single-base mismatch, as expected, gave a poorer

affinity ($K_D^{mismatch}$ = 79 nM) than that achieved with a perfect-match target ($K_D^{perfect\ match}$ = 3.7 nM), the discrimination efficiency is much smaller than that obtained with the clamp-switch sensor (Figure 2.7b). Due to experimental limitations (i.e. the linear probe does not bind with sufficient high affinity a 10-base target, see Figure 2.5b) the specificity of the E-DNA clamp-switch sensor was determined using a shorter target (10-base) than that employed with the E-DNA sensor using a linear probe (13-base). Simulations with the nearest–neighbor model,[30-32] however, confirmed that the small difference in target length is not the reason for the large difference in specificity we observed. Also in this case, the enhanced specificity of the E-DNA clamp-switch sensor is consistent with previous observations using similar DNA probes in solution.[4]

2.3 Conclusions

In this work, we have characterized a novel signal-on electrochemical sensor based on the use of a clamp-like DNA-based probe. We have demonstrated that by using such clamp-switch probe that binds a target through two distinct and sequential events, which leads to the formation of a triplex DNA structure, we can improve both the affinity and specificity of recognition compared to a classic Watson−Crick hybridization probe.
By turning this sensitive, specific architecture into an electrochemical probe, we have demonstrated that the signalon E-DNA sensor studied here provides a robust signal gain of up to 400%. Moreover, we were able to measure with nanomolar affinity a specific target as short as 10 bases. Finally, as a result of the extraordinary efficient molecular "double-check" provided by the concomitant Watson−Crick and Hoogsteen base pairings involved in target recognition, our signal-on E-DNA sensor proves incredibly specific toward single-base mismatches because it provides an excellent, unexpected, and unprecedented (over 2000-fold) discrimination efficiency. A drawback of our approach might be represented by the fact that triplex forming sequences are usually limited to homopurine or homopyrimidine tracks. Although this can limit the possible number of measurable targets, we also note that such sequences are common enough that it is straightforward to find unique sites with sequences of 16−20 bases in human or pathogen genomes.[33,34] Given the above attributes, the use of clamp-switch, triplex-based, electrochemical DNA probes holds great promise for the highly sensitive and sequence-specific detection of very short nucleic acids.

3.4 Materials and Methods

Materials. Reagent-grade chemicals, including (top-oligo(ethylene glycol), HS–$(CH_2)_{11}$–OEG_6–OH) TOEG6 (from Prochimia, Poland), 6-mercapto-1-hexanol, Tris[hydroxymethyl]aminomethane hydrochloride, tris-(2-carboxyethyl) phosphine hydrochloride, sulfuric acid, potassium phosphate monobasic, dibasic, ethanol and sodium chloride (all from Sigma-Aldrich, St. Louis, Missouri) were used without further purification. The clamp-switch and the linear probe were obtained from Biosearch Technologies (Novato, CA) and employed without further purification. The clamp-switch probe sequence is as follows:

5'-HS-$(CH_2)_6$-TATTTTCTTTTCCCCCCAGTTATTATTCCCCCCTTTTCTTTTGT-MB-3'. The probe is modified at the 5'-end with a thiohexyl moiety and at the 3'-end with a methylene blue (MB) redox label. The linear probe sequence is as follows: 5'-HS-$(CH_2)_6$-CGTCAA TCTTCTATTTCTCCACACTGCT-MB-3'. The probe is modified at the 5'-end with a thiohexylmoiety and at the 3'-end with a MB redox label.

Target DNA sequences. For the clamp-switch probe we have employed the following target DNA sequences of varying lengths and structures, all of which were obtained via commercial synthesis (Sigma-Aldrich):

PM13 mer (13-base target)	5'-GGAAAAGAAAATA-3'
PM12 mer (12-base target)	5'-GAAAAGAAAATA-3'
PM11 mer (11-base target)	5'-AAAAGAAAATA-3'
PM 10 mer (10-base target)	5'-AAAGAAAATA-3'
MM 10 mer (10-base mismatch target)	5'-AAAGCAAATA-3'

The target sequences for the linear probe were as follows:
Linear PM-13 (13-base target, 5'-GGAGAAATAGAAG-3') and linear MM-13 (13-base mismatch target, 5'-GGACAAATAGAAG-3').
In the above sequences the underlined bases identify the mismatched bases.

Sensor fabrication The sensors were fabricated using standard approaches.[8] Briefly, E-DNA sensors were fabricated on rod gold disk electrodes (3.0 mm diameter, BAS, West Lafayette, IN). The disk electrodes were prepared by polishing with diamond and

alumina (BAS), followed by sonication in water, and electrochemical cleaning (a series of oxidation and reduction cycles in 0.5 M H_2SO_4, 0.01 M KCl/0.1 M H_2SO_4 and 0.05 M H_2SO_4). Effective electrode areas were determined from the charge associated with the gold oxide reduction peak obtained after the cleaning process. The thiol-containing oligonucleotides we have employed are supplied as a mixed disulfide with 6-mercapto-1-hexanol in order to minimize the risk of oxidation. Thus the first step in sensor fabrication is the reduction of the probe DNA (100 μM) for one hour in a solution of 0.4 mM Tris(2-carboxyethyl)phosphine hydrochloride (TCEP) in 100 mM NaCl/10 mM potassium phosphate pH 7. The so-reduced relevant probe DNA was immobilized onto the freshly cleaned electrodes by incubating for 5 min in a solution of 1 M NaCl/10 mM potassium phosphate buffer, pH 7. Different probe densities were obtained by controlling the concentration of probe DNA employed during the fabrication process ranging from 10 nM to 500 nM. Following probe immobilization the electrode surface was rinsed with distilled, de-ionized water, passivated with 1 mM 6-mercaptohexanol in 1 M NaCl/10 mM potassium phosphate buffer, pH 7, overnight and rinsed with deionized water before measurement.

Electrochemical Measurements. The sensors produced as described above were tested at room temperature using an Autolabpotentiostat (EcoChemie, Utrecht, The Netherlands). Square wave voltammetry (SWV) was recorded from -0.1 V to -0.45 V versus an external Ag/AgCl reference electrode and a platinum counter electrode and amplitude of 25 mV with a frequencies of 100 Hz (unless otherwise states). The sensors were first allowed to equilibrate for about 20 minutes in a buffer solution (10 mM Tris[hydroxymethyl]aminomethane hydrochloride (TRIS) + 100 mM NaCl + 10 mM $MgCl_2$). Once the sensor's signal was stable the desired target concentration was added to the solution and the resulting signal decrease or increase was evaluated in real time by interrogating the electrode at regular intervals.

Calculation of Probe Surface Density. Probe surface density (i.e., the number of electroactive probe DNA moles per unit area of the electrode surface, N_{tot}) was determined using a previously established relationship with ACV peak current[11] described in Eq. 1:

$$I\ (\ ) = 2 \qquad \frac{\sinh\ (\qquad /\ )}{h\ (\qquad /\ ) + 1} \quad (1)$$

Where $I_{avg}(E_0)$ is the average AC peak current in a voltammogram, n is the number of electrons transferred per redox event (with our MB label n = 2), F is the Faraday current, R is the universal gas constant, T is the temperature, E_{ac} is the amplitude, and f is the frequency of the applied AC voltage perturbation. Perfect transfer efficiency was assumed (i.e., that all of the redox moieties participate in electron transfer); errors in this assumption would lead us to underestimate probe density. Experimentally, four frequency values were used (5, 10, 50, and 100 Hz), and the average current peak was calculated so as to give the value of N_{tot}.[12,13]

AFM methods

Solutions. For all Atomic Force Microscopy (AFM) experiments, DNA stocks preparation and monolayer were formed in a phosphate buffer solution (PBS, 10mM phosphate, 1M NaCl, 1mM $MgCl_2$, pH 7 in MilliQ water (resistivity ≥ 18.2 MΩ·cm). DNA oligos (see the sequences above) were purchased from IDT, suspended in PBS to a final concentration of 100 μM, and stored at -20˚C. AFM imaging and target incubation were carried out in a TRIS solution (10 mM TRIS, 100 mM NaCl, 10 mM $MgCl_2$), prepared with MilliQ water, and adjusted to pH values of 5, 6, or 8. All solutions were filtered with a sterile 0.2 μm syringe filter (VWR, Italy).

Sample preparation. Ultra-flat gold surfaces were prepared following a modified procedure from ref.[14] Briefly, A 100 nm thick film of gold was electron-beam deposited over a freshly cleaved mica surface sheet (Mica New York, clear ruby muscovite). Gold-on-mica chips of 5x5 nm^2 were glued on slightly smaller silicon chips by using an epoxy resist (SU-8 100, MicroChem, MA, USA), and cured at 130˚ C for at least 24 h. The obtained samples were stored in ambient conditions without any further precaution. Self-assembled monolayers were allowed to form over freshly cleaved gold surfaces in a solution containing 30 nM ssDNA probe in PBS buffer for 5 minutes, followed by 5-minutes-long washing in fresh PBS. DNA-modified surfaces were backfilled with the TOEG6 monolayer for gold-surface stabilization with a 15-minutes-long incubation in a 100 μM TOEG6 solution in PBS:EtOH=3:1, followed by washing in PBS. Samples were fixed in the AFM liquid cell with a cyclic olefin copolymer (TOPAS, TOPAS Advanced Polymers GmbH, Germany) on a glass support.

AFM analysis. All AFM measurements were performed in liquid on an Asylum Research MFP-3D Stand-Alone AFM. Monolayer heights were measured relative to an

internal reference provided by TOEG6 patches generated within the DNA monolayerbynanografting.[15] Several 2×2 μm^2 squared features were produced in a 10 μM TOEG6 solution in PBS buffer with relatively stiff cantilevers (NSC36/noAl by MikroMasch, nominal spring constant k = 1.0 N/m) by applying 100–150 nN. The action of the loading tip lets surface-bound DNA molecules be exchanged with TOEG6 molecules present in solution. Nanostructures were AFM imaged in AC-Mode at low forces, at all experimental stages, and with the same cantilever that was utilized for nanografting.

The step-height of the DNA monolayer with respect to each TOEG6 patch was obtained from 6 different height profiles, each being the average of 5 adjacent line profiles. Absolute DNA height values were derived from the measured values by adding the average height of the TOEG6 monolayer (3.1 nm) and subtracting the average length of the thiol linker (1 nm)[16]: $H_{abs} = H_{rel} + H_{TOEG} - H_{linker} = H_{rel} + 2.1$ nm.

2.5 References

(1) Vallée-Bélisle, A.; Bonham, A. J.; Reich, N. O.; Ricci, F.; Plaxco, K. W. *J. Am. Chem. Soc.* 2011, 133, 13836.

(2) Bonham, A. J.; Hsieh, K.; Ferguson, B. S.; Vallée-Bélisle, A.; Ricci, F.; Soh, H. T.; Plaxco, K. W. *J. Am. Chem. Soc.* 2012, 134, 3346.

(3) Cho, E. J.; Lee, J. W.; Ellington, A. D. *Annu. Rev. Anal. Chem.* 2009, 2, 241.

(4) Idili, A.; Plaxco, K. W.; Vallée-Bélisle, A.; Ricci, F. *ACS Nano* 2013, 7, 10863.

(5) Li, D.; Song, S.; Fan, C. *Acc. Chem. Res.* 2010, 43, 631.

(6) Fan, C.; Plaxco, K. W.; Heeger, A. J. *Proc. Natl. Acad. Sci. U.S.A.* 2003, 100, 9134.

(7) Kang, D.; Vallée-Bélisle, A.; Porchetta, A.; Plaxco, K. W.; Ricci, F. *Angew. Chem., Int. Ed.* 2012, 51, 6717.

(8) Lubin, A. A.; Plaxco, K. W. *Acc. Chem. Res.* 2010, 43, 496.

(9) Ricci, F.; Lai, R. Y.; Plaxco, K. W. *Chem. Commun.* 2007, 36, 3768.

(10) Xiao, Y.; Lai, R. Y.; Plaxco, K. W. *Nat.Protoc.* 2007, 2, 2875.

(11) Hoogsteen, K. *Acta Crystallogr.* 1959, 12, 822.

(12) Hoogsteen, K. *Acta Crystallogr.* 1963, 16, 907.

(13) Kandimalla, E. R.; Agrawal, S. *Gene* 1994, 149, 115.

(14) Kandimalla, E. R.; Agrawal, S. *Nucleic Acids Res.* 1995, 23, 1068.

(15) Kandimalla, E. R.; Manning, A.; Agrawal, S. *J. Biomol. Struct. Dyn.* 1996, 14, 79.

(16) Xodo, L. E.; Manzini, G.; Quadrifoglio, F. *Nucleic Acids Res.* 1990, 18, 3557.

(17) Lee, I. B.; Lee, J. Y.; Lee, N. K.; Hong, S. C. *Curr. Appl. Phys.* 2012, 12, 1027.

(18) Giovannangeli, C.; Thuong, N. T.; Helene, C. *Proc. Natl. Acad. Sci. U.S.A.* 1993, 90, 10013.

(19) Trkulja, I.; Biner, S. M.; Langenegger, S. M.; Häner, R. *ChemBioChem* 2007, 8, 25.

(20) Fatthalla, M. I.; Pedersen, E. B. *Helv. Chim. Acta* 2012, 95, 1538.

(21) Jeuken, L. J. C.; McEvoy, J. P.; Armstrong, F. A. *J. Phys. Chem. B* 2002, 106, 2304.

(22) Komorsky-Lovric, S.; Lovric, M. *Anal. Chim. Acta* 1995, 305, 248.

(23) White, R. J.; Plaxco, K. W. *Anal. Chem.* 2010, 82, 73.

(24) Esteban Fernández de Ávila, B.; Watkins, H. M.; Pingarrón, J. M.; Plaxco, K. W.; Palleschi, G.; Ricci, F. *Anal. Chem.* 2013, 85, 6593.

(25) Patterson, A.; Caprio, F.; Vallée-Bélisle, A.; Moscone, D.; Plaxco, K. W.; Palleschi, G.; Ricci, F. *Anal. Chem.* 2010, 82, 9109.

(26) Ricci, F.; Zari, N.; Caprio, F.; Recine, S.; Amine, A.; Moscone, D.; Palleschi, G.; Plaxco, K. W. *Bioelectrochemistry* 2009, 76, 208.

(27) Liu, G. Y.; Xu, S.; Qian, Y. *Acc. Chem. Res.* 2000, 33, 457.

(28) Mirmomtaz, E.; Castronovo, M.; Grunwald, C.; Bano, F.; Scaini, D.; Ensafi, A. A.; Scoles, G.; Casalis, L. *Nano Lett.* 2008, 8, 4134.

(29) Bosco, A.; Bano, F.; Parisse, P.; Casalis, L.; De Simone, A.; Micheletti, C. *Nanoscale* 2012, 4, 1734.

(30) Santalucia, J., Jr. *Proc. Natl. Acad. Sci. U.S.A.* 1998, 95, 1460.

(31) Santalucia, J., Jr.; Hicks, D. *Annu. Rev. Biophys. Biomol. Struct.* 2004, 33, 415.

(32) Owczarzy, R.; Tataurov, A. V.; Wu, Y.; Manthey, J. A.; Mc Quisten, K. A.; Almabrazi, H. G.; Pedersen, K. F.; Lin, Y.; Garretson, J.; Mc Entaggart, N. O.; Sailor, C. A.; Dawson, R. B.; Peek, A. S. *Nucleic Acids Res.* 2008, 36, 163.

(33) Goni, J. R.; de la Cruz, X.; Orozco, M. *Nucleic Acids Res.* 2004, 32, 354.

(34) Duca, M.; Vekhoff, P.; Oussedik, K.; Halby, L.; Arimondo, P. B. *Nucleic Acids Res.* 2008, 36, 5123.

(35) O'Connor, S. D.; Olsen, G. T.; Creager, S. E. *J. Electroanal. Chem.* 1999, 466, 197.

(36) Creager, S. E.; Wooster, T. T. *Anal. Chem.* 1998, 70, 4257.

(37) Sumner, J. J.; Weber, K. S.; Hockett, L. A.; Creager, S. E. *J. Phys. Chem. B* 2000, 104, 7449.

(38) Gupta, P.; Loos, K.; Korniakov, A.; Spagnoli, C.; Cowman, M.; Ulman, *A. Angew. Chem., Int. Ed.* 2004, 43, 520.

(39) Liu, G. Y.; Xu, S.; Qian, Y. *Acc. Chem. Res.* 2000, 33, 457.

(40) Castronovo, M.; Lucesoli, A.; Parisse, P.; Kurnikova, A.; Malhotra, A.; Grassi, M.; Grassi, G.; Scaggiante, B.; Casalis, L.; Scoles, G. *Nat. Commun.* 2011, 2, 297.

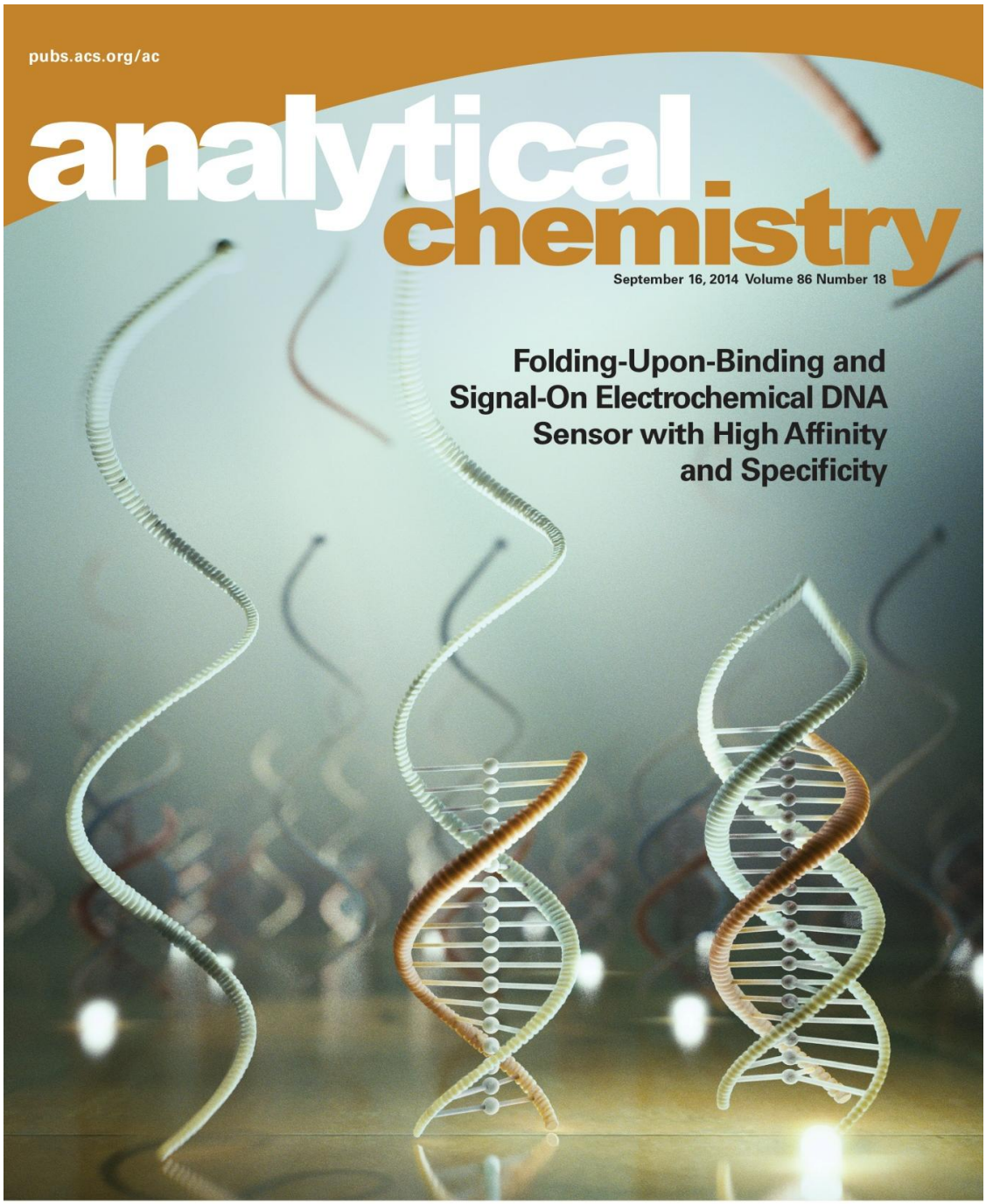
pubs.acs.org/ac
analytical chemistry
September 16, 2014 Volume 86 Number 18
Folding-Upon-Binding and Signal-On Electrochemical DNA Sensor with High Affinity and Specificity
ACS Publications
Most Trusted. Most Cited. Most Read.
www.acs.org

Chapter 3 - Rational design of pH-controlled DNA strand displacement

3.1 Introduction

DNA nanotechnology uses DNA (or nucleic acids) as a versatile material to rationally engineer tools and molecular devices that can find a multitude of different applications (e.g. in-vivo imaging, clinical diagnostics, drug-delivery, etc.).[1,2] An exciting development of this field, namely structural DNA nanotechnology, is characterized by the use of DNA to build complex nanometre-scale structures, often referred to as DNA origami or DNA tiles. [2-5] With its simple base-pairing code and its nanoscale dimension, in fact, DNA appears as the perfect building block to assemble and engineer complex molecular architectures with unique accuracy and precision. Similarly, the possibility to quantitatively predict and simulate DNA thermodynamics interactions, has allowed to expand the horizons of DNA nanotechnology into the construction of programmable and autonomous DNA-based nanodevices that can be engineered to have different functions. [1-9]

In order to create these complex nanostructures with enough precision and to engineer functional DNA nanodevices it is crucial to strictly control the thermodynamics and the kinetics with which DNA strands interact and hybridize with each other. A beautiful example of such possibility is represented by the toehold-mediated (or toehold-exchange) DNA strand displacement, a process through which two strands hybridize with each other displacing one (or more) pre-hybridized strands.[10-12] Such process, pioneered by Yurke and later expanded by Zhang, Winfree and Yurke himself, has been systematically applied to engineer functional DNA nanodevices. These include molecular motors,[6-13] tweezers,[14,15] autonomous nanomachines,[16,17] circuits,[18,19] and catalytic amplifiers.[20] Because it can allow a specific kinetic control of several reaction pathways, DNA strand displacement has also found applications in the construction of DNA-based nanostructures and origami.[21,22]

Despite the advantages represented by strand-displacement to build and engineer complex and functional DNA structures in a controlled way, additional features might help in improving the programmability of this process. For example, we note that, using the conventional approach, once the invading strand (i.e. the strand that activates strand-

displacement) is added to the reaction mixture, it is difficult to implement an additional external control to further regulate the process. That is, the strand-displacement reaction performs equally well in different environments (pH, temperature, etc). While this property can be an advantage for some applications,[23] it can be a limitation for others, as in some cases it could be preferable to exogenously control the entire displacement process. In this context, despite in recent years the DNA strand displacement process has seen a widespread application, only few examples have been reported that allow to activate strand displacement with small molecules[24,25] (i.e. Hg(II) metal ions and adenosine) or at acidic pHs using i-motif,[26] G-quadruplex[26] and triplex-forming strands.[27] More recently, light-controlled strand displacement reactions were also demonstrated using photoregulated oligonucleotides. [28-31]

3.2 Results and discussion

Motivated by the above arguments, I have rationally designed here two programmable toehold-based DNA strand displacement strategies that can be triggered and controlled by a simple pH change. I did so by taking advantage of the well-characterized pH sensitivity of the parallel Hoogsteen (T,C)-motif in triplex DNA.[32-34] The sequence-specific formation of a CGC parallel triplet through the formation of Hoogsteen interactions, in fact, requires the protonation of the N3 of cytosine in the third strand in order to form (average pK_a of protonated cytosines in triplex structure is ≈ 6.5). [35] For this reason, DNA strands containing cytosines can only form a triplex structure at acidic pHs. In contrast to previous examples, the versatility of our approach allows to activate/inhibit the displacement process at both basic and acidic pHs. More specifically, I designed two complementary strategies, for which DNA-strand displacement is activated either at basic pHs (strategy #1) (Figure 3.1) or at acidic/neutral pHs (strategy #2) (Figure 3.12). In the first strategy (OH^--activated strand displacement), a clamp-like, triplex-forming DNA prevents strand displacement at acidic pHs (conditions at which triplex formation is favoured) (Figure 3.1) while at basic pHs (when Hoogsteen interactions are destabilized) a classic strand-displacement reaction is observed. In the second strategy (H^+-activated strand displacement), in contrast, the invading strand (IS) contains a clamp-like triplex forming portion. Only

under pH conditions (acid/neutral) at which Hoogsteen interactions can form and lead to a triplex complex we observe the strand displacement process (Figure 3.12).

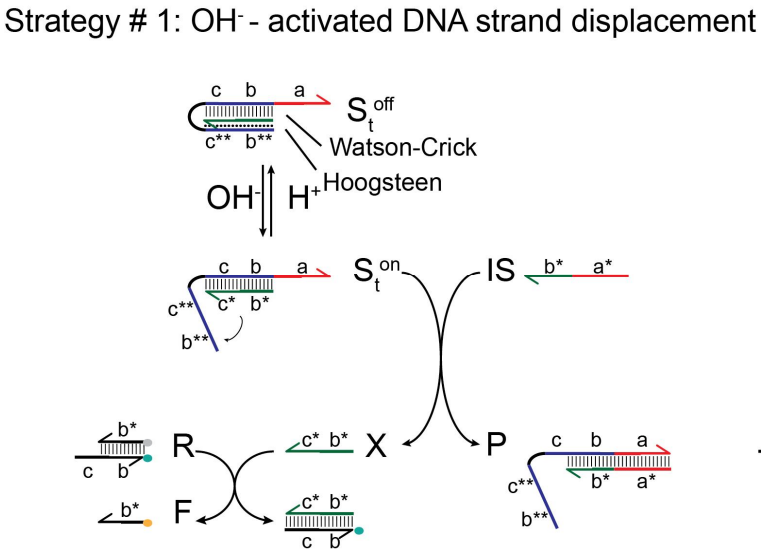

Figure 3.1. OH^--activated strand-displacement strategy. In the first strategy I have designed a DNA strand displacement that is activated at basic pHs. To do this, I have used a clamp-like DNA strand that, under acidic pHs, forms a triplex inactive complex (S_t^{off}) with the strand to be released (X). The additional Hoogsteen interactions in this triplex structures provide an increased stabilization to the complex that prevents strand displacement upon Invading Strand (IS) addition. At basic pHs, the destabilization of the Hoogsteen interactions leads to an active complex (S_t^{on}) characterized by a simple duplex conformation. Because this structure is not stabilized anymore by Hoogsteen interactions, it can undergo displacement through a classic toehold-exchange mechanism. In this study the progress of strand displacement is always followed using an optically labelled reporter complex (R) that stoichiometrically reacts with the released strand (X) to produce an unquenched fluorophore-labelled single strand DNA molecule (F). In this thesis, domains are represented by letters. Starred letters (*) represent domains complementary to the domains denoted by unstarred letters and forming classic Watson-Crick base pairings. Double starred letters (**) represent triplex-forming domains that form Hoogsteen interactions with duplex formed by the domains denoted by starred (*) and unstarred letters.

As a first control experiment, I checked the effect of the pH on the FRET pair used in the reporter complex (R), as well as on the reaction between R and the released strand (X). As confirmed by the binding curves, either the FRET pair (Figure 3.2) or the

reaction between R and X (Figure 3.3) are not sensitive to pH in the pH range I have investigated.

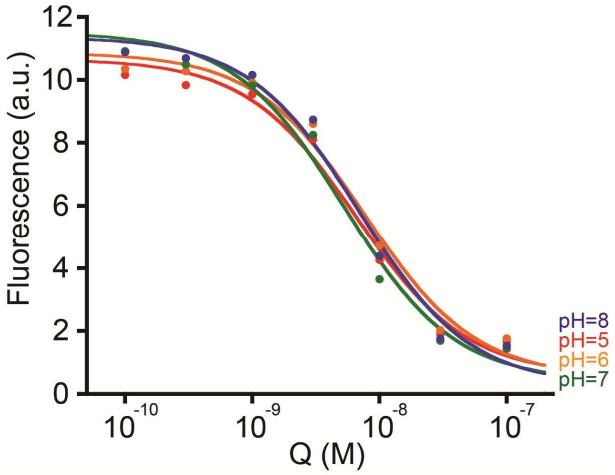

Figure 3.2. Study of pH effect on the FRET couple signal. Binding curves between F and Q (Figure 3.1 and Materials and methods for sequences) at different pH values demonstrate that the fluorescence of the reporter used in this work does not depend on pH and that the F/Q affinity is the same at all pHs investigated. Binding curves shown here were obtained by adding increasing concentrations of Q (cb) to a solution of F (b*) (10 nM) in a 0.01 M Tris buffer + 0.01 M $MgCl_2$, at 25° C.

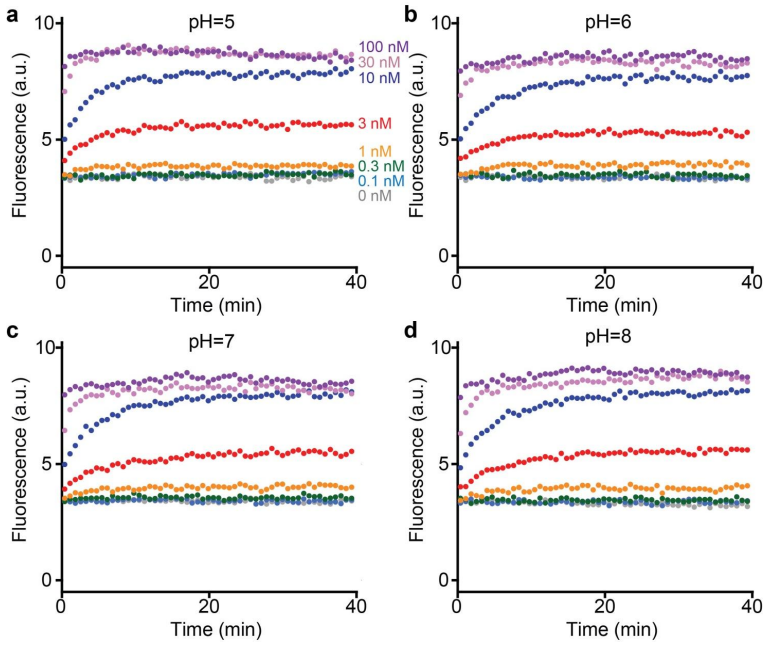

Figure 3.3. Study of the pH effect of the reaction between R and X. To study the effect of pH on the reaction between R and X I have added different concentrations of X (from 0.1 nM to 100 nM) to a solution of R (10 nM) in a 0.01 M Tris buffer + 0.01 M $MgCl_2$ at 25° C at

different pHs. (a) pH=5. (b) pH=6. (c) pH=7 (d) pH=8. The results confirm that the reaction between R and X is not affected by pH in the range I have investigated.

Both strategies rely on the use of pH-dependent clamp-like conformational switches (Figure 3.1, 3.12) that lead to triplex formation.[32,33] In the first strategy triplex formation is utilized to lock the strand that would be otherwise released in the presence of the IS.
As a first characterization of the first strategy, I have thus studied the pH-dependent stability of a clamp-like triplex complex. To do this I have initially studied the pH-dependent stability of the triplex complex (S_t^{off}) in strategy #1 (Figure 3.4a).

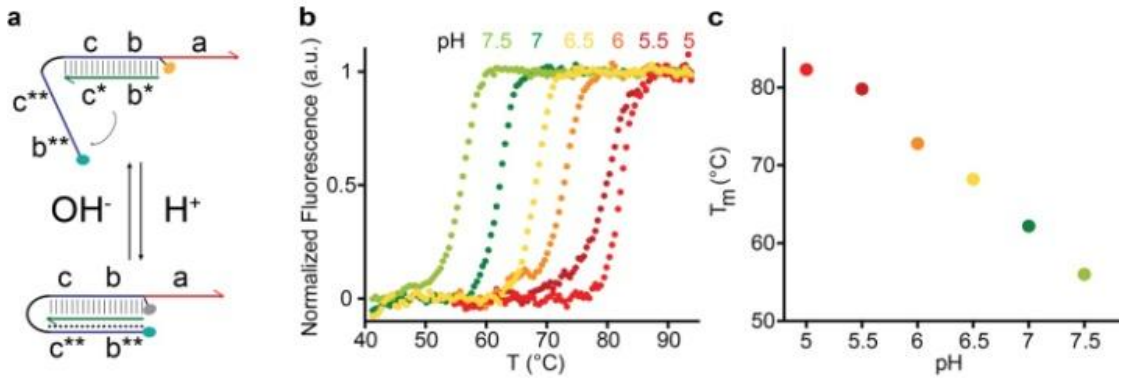

Figure 3.4. pH-dependent clamp-like triplex DNA formation. (a) Folding/unfolding of the triplex complex of strategy #1 (see Figure 3.1) is monitored here through a pH-insensitive FRET pair located in an internal position (Cy3) and at the 5'-end (Cy5) of the clamp-like strand. (b) Shown are the melting denaturation curves of the complex S_t (20 nM) obtained at different pH values in a 0.01 M Tris buffer solution + 0.01 M $MgCl_2$. (c) At a pH at which triplex formation is favoured (pH = 5), the melting temperature of the complex is 82.3° C. As the acidity of the solution is progressively reduced to reach pH 7.5, at which triplex formation is unfavoured, the complex is progressively destabilized until it reaches a melting temperature of 56.0° C.

More specifically I have used a dual labelled clamp-like triplex forming strand and, after hybridization to a target DNA oligo, I have performed thermal denaturation of the so-formed complex at different pHs (Figure 3.4b). As expected, under acidic pHs, a condition at which triplex formation is favoured,[32,33] the overall stability of the complex is improved. For example, at a pH low enough to allow triplex formation (pH = 5), the denaturation of the complex occurs at very high temperatures (i.e. T_m = 82.3° C). In contrast, under pH values at which triplex formation is unfavoured (pH = 7.5), the

denaturation of the complex occurs at a much lower temperature (T_m=56.0° C) (Figure 3.4c).

I also note that at acidic pH the possible alternative i-motif [36] that the triplex forming strand (in Figure 1, $c^{**}b^{**}$) could form does not affect the pH-dependence of my system. These results demonstrate that the clamp-like triplex formation based on Hoogsteen interactions offers highly efficient and tunable pH regulation, which could be suitable toward the realization of pH-dependent DNA-based molecular devices.

As mentioned above, triplex formation allows to rationally control the kinetic of the displacement process by simply changing the solution pH. For example, for strategy #1 (OH^--activated strand displacement), at pH 8 (a pH at which triplex formation is unfavoured), strand displacement proceeds with a fast kinetic upon IS addition (Figure 3.5a, left). At pH 5, in contrast, which is acidic enough for the clamp-like strand to form a triplex, inactive complex (S_t^{off}) (see Figure 3.4a), the addition of the IS does not result in any significant signal change (Figure 3.5a, right), suggesting that no displacement occurs. Such pH-dependent strand displacement process is observed over a wide range of IS concentrations.

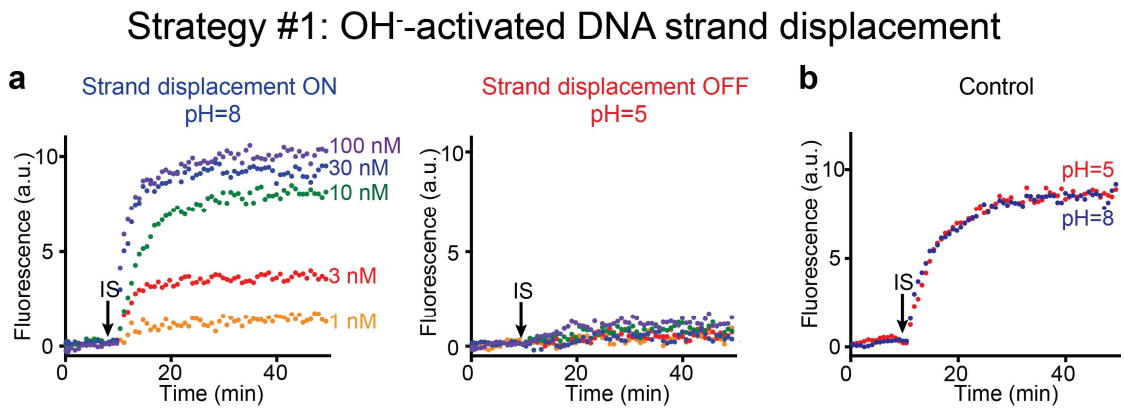

Figure 3.5. OH^-- activated toehold-based DNA strand displacement. (a) In the first strategy I dissect here, strand displacement is only observed at basic pHs (a, *right*) while under acidic pHs (a, *left*) triplex formation leads to a very stable complex (S_t^{off}, Figure 3.1) that prevents strand displacement. Such pH-dependence is observed over a wide range of IS concentrations (from 1 nM to 100 nM). (b) A control toehold-based DNA strand displacement that uses the same sequences except for the fact that it lacks the terminal triplex-forming portion (b** and c**) is, as expected, independent to pH. Here, I used an IS with a toehold portion (a* in Figure 3.1) of 15 bases and an invading portion (b* in Figure 3.1) of 10 bases. Strand displacement is followed by fluorescence measurements obtained in a solution of complex S (10 nM) in the presence of

reporter R (30 nM) after the addition of the IS at a concentration of 30 nM in a 0.01 M Tris buffer + 0.01 M $MgCl_2$, at 25° C.

A conventional strand displacement toehold-exchange process (thus based on a complex that cannot form a triplex structure) is independent to pH and occurs with very similar kinetics in the entire pH range I have investigated (Figure 3.5b) and over a wide range of IS concentrations (Figure 3.6).[12] Of note, this duplex-only control complex (used here for a comparison) has the same sequence of that used in the OH^--activated strand displacement process except that it lacks the domains b** and c**, i.e. the portions able to form the triplex (see Figure 3.1 and Materials).

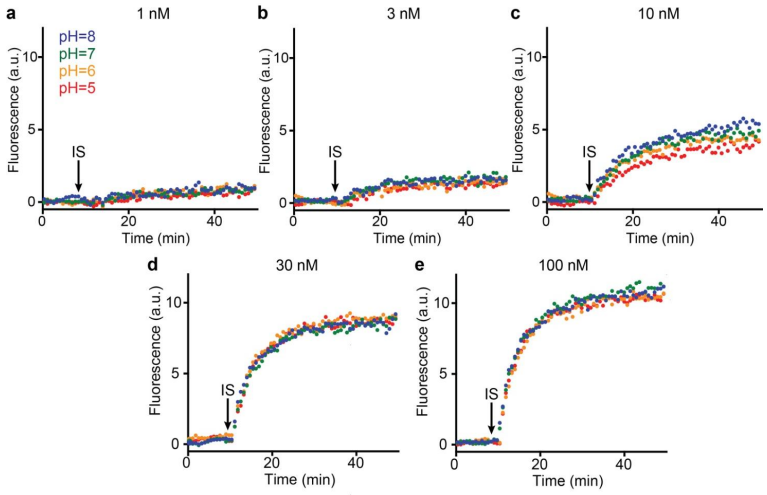

Figure 3.6. Study of the pH effect on the control DNA strand displacement of strategy #1. To demonstrate that a conventional strand displacement process (thus based on a complex that cannot form a triplex structure) is independent to pH, I have performed a control experiment using a complex S that is not able to form a triplex (control strand, S_{duplex}, see Materials). Strand displacement reactions of this control using different concentrations of IS show no pH dependence over the entire pH range investigated (from pH 5 to pH 8). (a) IS (1 nM). (b) IS (3 nM). (c) IS (10 nM). (d) IS (30 nM). (e) IS (100 nM). Here strand displacement is followed by fluorescence measurements obtained in a solution of S_{duplex} (10 nM) in the presence of R (30 nM) after the addition of different concentration of IS (see each panel) in a 0.01 M Tris buffer + 0.01 M $MgCl_2$, at 25° C. Here I used an IS with a toehold length of 15 bases and an invading portion of 10 bases (IS10).

In order to obtain a further confirmation I performed electrophoresis experiments (PAGE) in native conditions. As shown in Figure 3.8, these experiments confirm such pH-dependency (Figure 3.7). At pH 8 I only observe the band corresponding to the product of strand displacement (P). In contrast at pH 5 I can see both bands

corresponding to complex S_t and product P demonstrating that strand displacement is inhibited. I note, however, that despite with fluorescence experiments I observed a complete inhibition of strand displacement at pH 5 (see Figure 3.6a), the PAGE experiments I have performed do not show complete inhibition and I still observe a partial formation of the product P even at acidic pHs. This could be probably ascribed to the fact that gel is formed under basic conditions and the strand displacement reaction could partially occur during the gel run. Attempts to decrease the running time did not give satisfying results because did not allow to separate well enough the bands of complex S_t and product P.

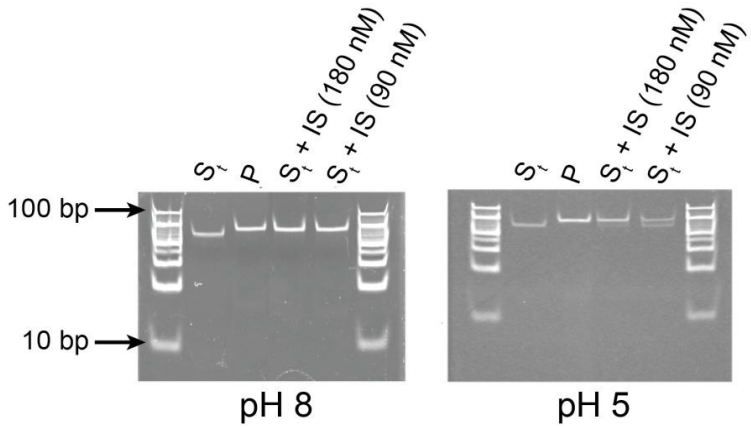

Figure 3.7. OH^--activated strand displacement strategy studied by PAGE electrophoresis.

Because triplex stability can be tuned at different pHs (see Figure 3.5), a gradual inhibition/activation of the strand displacement process can be achieved by gradually changing the solution's pH (Figure 3.8).

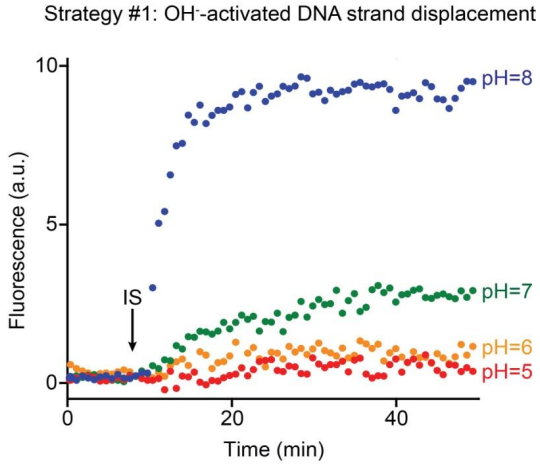

Figure 3.8. pH-activation of the OH^--activated DNA strand displacement (strategy #1). I can rationally tune the activation/inhibition of the strand displacement process by simply changing

the pH of the solution at which strand-displacement occurs. Here strand displacement is followed by fluorescence measurements obtained in a solution of complex S (10 nM) in the presence of reporter R (30 nM) after the addition of the IS at a concentration of 30 nM in a 0.01 M Tris buffer + 0.01 M $MgCl_2$, at 25° C. Here I used an IS with a toehold length of 15 bases and an invading portion of 10 bases (IS10).

As expected, intermediate kinetics are observed under pH conditions at which triplex/duplex equilibrium is more balanced (around pH 7). Again, such tunable behaviour is observed over a wide concentration range of IS (i.e. from 1 nM to 100 nM) (Figure 3. 9).

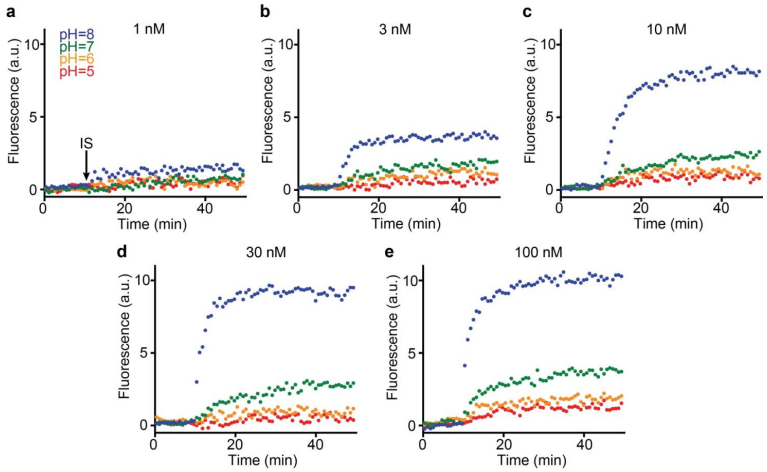

Figure 3.9. pH-activation of the OH-activated DNA strand displacement (strategy #1).The tunability of activation/inhibition of the strand displacement process shown in Figure 3.8 (above) is observed over a wide concentration range of IS. (a) 1 nM. (b) 3 nM. (c) 10 nM. (d) 30 nM. (e) 100 nM. Here strand displacement is followed by fluorescence measurements obtained in a solution of complex S (10 nM) in the presence of R (30 nM) after the addition of IS at different concentrations (see each panel) in a 0.01 M Tris buffer + 0.01 M $MgCl_2$, at 25° C. Here I used an IS with a toehold length of 15 bases and an invading portion of 10 bases (IS10).

Different degree of inhibition can also be achieved varying the IS length (Figure 3.10, 3.11). For example, by changing the pH of the solution from pH 8 to pH 5 we can observe only a partial inhibition of the displacement reaction using an IS containing an invading domain of 12 bases (Figure 3.10).

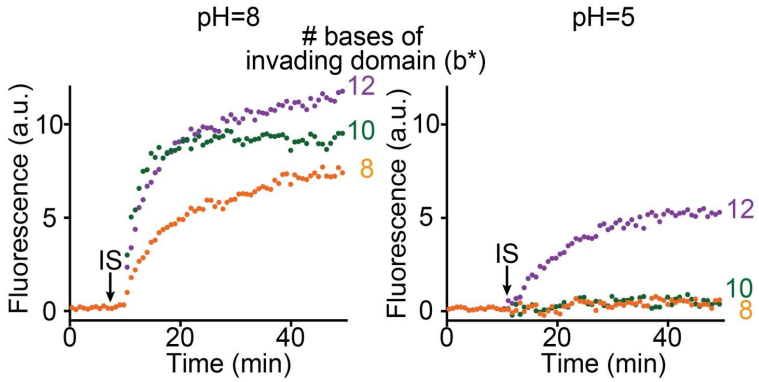

Figure 3.10. Effect of the length of the invading domain (b*) in the IS on the pH-dependence of the strand displacement process (strategy #1). I can rationally tune the pH-dependence of the strand displacement process by changing the length of the invading domain (b*) in the IS. For example, at pH 5 (*right*) I observe only a gradual inhibition of the displacement process with an IS containing a 12-base invading domain (purple curve). In contrast, shorter invading domains (10-base and 8-base) show a complete inhibition of the displacement process under the same acidic conditions (green and orange curves). (*left*) The same IS give similar strand-displacement kinetics at basic pHs (pH=8).

With the same pH change I observe a complete inhibition of the displacement process when I use shorter invading domains (i.e. 10 bases and 8 bases) (Figure 3.10). A similar trend is observed at different pH values and with different concentration of IS (Figure 3.11).

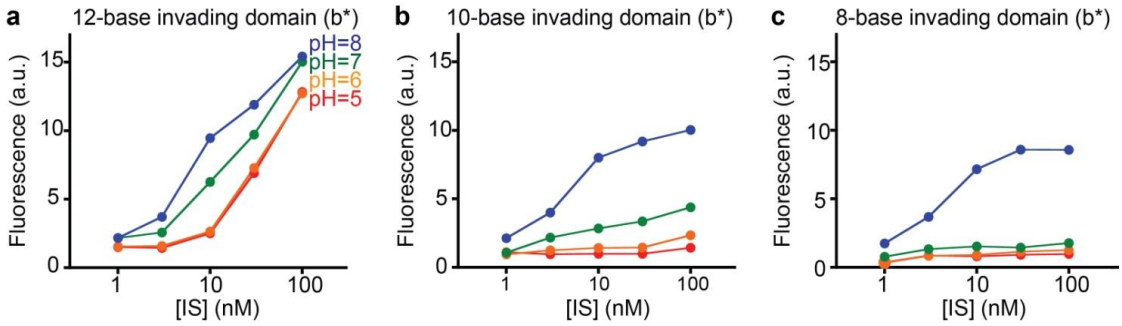

Figure 3.11. Effect of the length of the invading domain (b*) in the IS on the pH-dependence of the strand displacement process (strategy #1). The pH-dependence of the strand displacement process can be rationally tuned by changing the length of the invading domain (b*) in IS. (a) 12-base invading domain. (b) 10-base invading domain. (c) 8-base invading domain. This trend is observed over a wide range of IS concentration. Here strand displacement is followed by fluorescence measurements obtained in a solution of complex S (10 nM) in the presence of R (30 nM) after the addition of different concentrations of IS bearing invading domains (b*) of different lengths (12, 10, 8 bases) but with the same toehold-binding domain's length (15 bases)

(see Materials for details). Experiments were performed in a 0.01 M Tris buffer + 0.01 M $MgCl_2$ at 25° C.

In the second strategy (H^+-activated DNA strand displacement) I present here, pH-dependent triplex formation triggers strand displacement. Of note, in this case, contrarily to the first strategy described above, the triplex forming portion is within the IS (Figure 3.12).

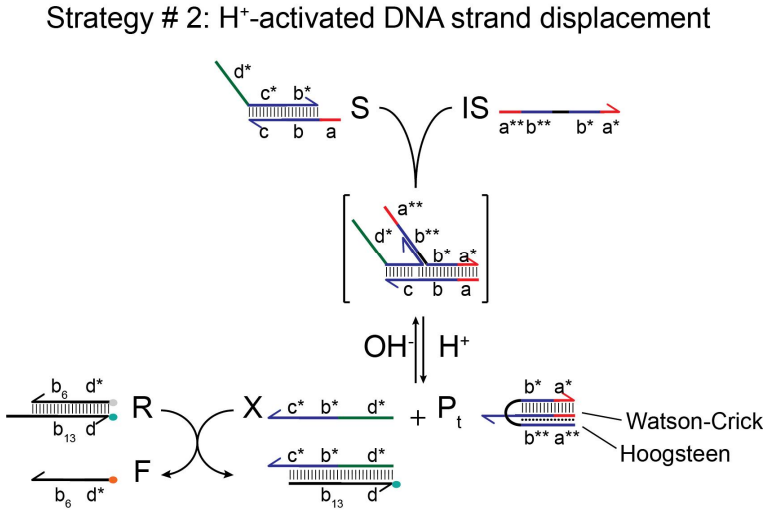

Figure 3.12. H^+-activated strand-displacement strategy. In the second strategy I dissect in this work I have designed a toehold-based DNA strand displacement process that is activated at acidic/neutral pHs (H^+-activated strand-displacement). To do this, I have designed an IS comprised of a triplex-competent DNA sequence that can bind through a clamp-like mechanism a strand in the complex S. Under basic conditions, this IS can only form Watson-Crick interactions and, due to the content and length of the toehold (a*) and invading (b*) portion, strand displacement process is unfavoured. In contrast, at acidic pHs, triplex formation through Hoogsteen interactions provides an additional energetic contribution that allows strand displacement to occur. In this study the progress of strand displacement is always followed using an optically labelled reporter complex (R) that stoichiometrically reacts with the released strand (X) to produce an unquenched fluorophore-labelled single strand DNA molecule (F). In this thesis, domains are represented by letters. Starred letters (*) represent domains complementary to the domains denoted by unstarred letters and forming classic Watson-Crick base pairings. Double starred letters (**) represent triplex-forming domains that form Hoogsteen interactions with duplex formed by the domains denoted by starred (*) and unstarred letters.

As highlighted above, also the second strategy relies on the use of pH-dependent clamp-like conformational switches (Figure 3.12) that lead to triplex formation. [32,33] In contrast with the first strategy, in the second strategy clamp-like triplex formation triggers strand displacement. Also for the second strategy as first characterization, I have studied the pH-dependent stability of a clamp-like triplex complex. To do this I have studied the pH-dependent stability of the triplex complex in strategy #2 (Figure 3.13a). More specifically I have used a dual labelled clamp-like triplex forming strand and, after hybridization to a target DNA oligo, I have performed thermal denaturation of the so-formed complex at different pHs (Figure 3.13b). As expected, also for the second strategy, I obtained a pH-dependence similar to the one observed with the triplex forming sequences of strategy #1 (Figure 3.4b,b).

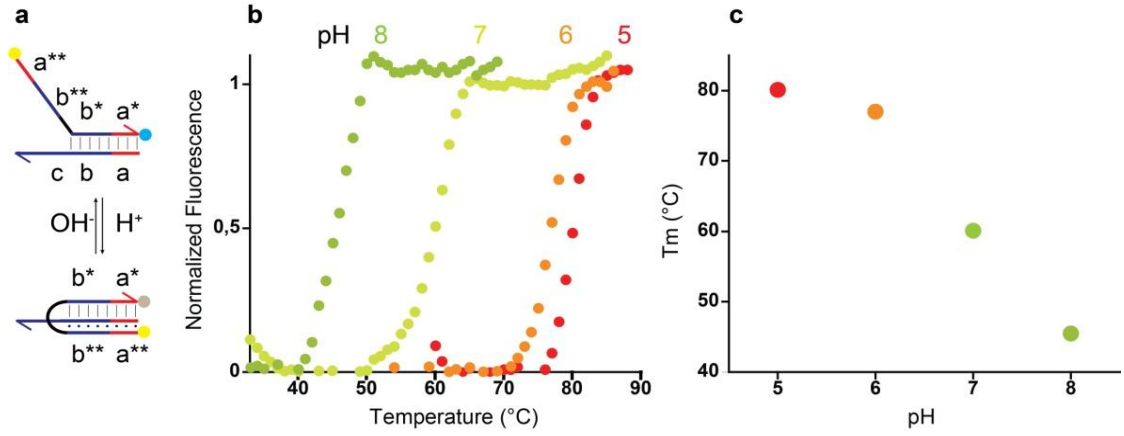

Figure 3.13. pH-dependent clamp-like triplex DNA formation using the triplex complex (P_t) of strategy #2 (see Figure 1b). (a) The triplex formation here is monitored through a pH-insensitive FRET pair located at the 3'-end (Cy3) and at the 5'-end (Cy5) of the clamp-like strand. (b) Shown are the melting denaturation curves of the complex P_t (20 nM) obtained at different pH values in a 0.01 M Tris buffer solution + 0.01 M $MgCl_2$. (c) At a pH at which triplex formation is favoured (pH = 5), the melting temperature of the complex is 80.1° C. As the acidity of the solution is progressively reduced to reach pH 8.0, at which triplex formation is unfavoured, the complex is progressively destabilized until it reaches a melting temperature of 45.5° C.

As highlighted above, also in the second strategy, triplex formation allows to rationally control the kinetic of the displacement process by simply changing the solution pH.

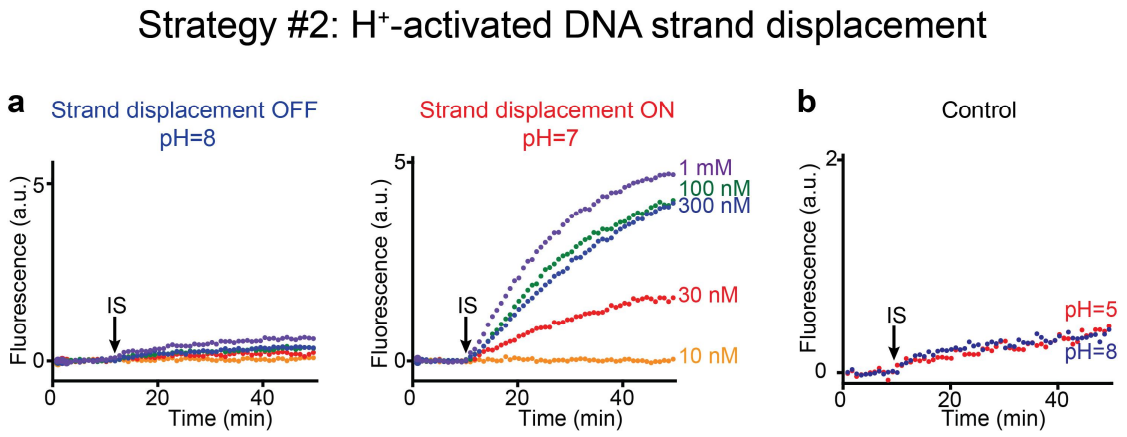

Figure 3.14. H^+-activated toehold-based DNA strand displacement. (a) In the second strategy the addition of the IS under basic conditions (pH 8) does not result in any significant strand displacement reaction (a, *left*). Strand displacement reaction is triggered at acidic pHs, due to the formation of a triplex complex (c, *right*). Also in this case, such pH dependence is observed over a wide range of IS concentrations (from 10 nM in to 1 μM). (b) A control IS with the same toehold and invading domains as the one used above but lacking the triplex forming portion (a** and b**) does not lead to any displacement reaction over the entire pH range we have investigated. Strand displacement is followed by fluorescence measurements obtained in a solution of complex S (10 nM) in the presence of reporter R (30 nM) after the addition of the IS at a concentration of 30 nM in a 0.01 M Tris buffer + 0.01 M $MgCl_2$, at 25° C.

At pH 8 (triplex destabilizing condition), the addition of the IS does not result in any significant fluorescence signal increase (Figure 3.14a, left). In contrast, at pH 7 (a pH low enough to form already a triplex complex), the addition of the IS successfully leads to the strand displacement reaction (Figure 3.14a, right). In this H^+-activated strategy, a pH change of just one unit (from pH 8 to pH 7) is sufficient to activate/inhibit the strand displacement process. Similarly to what I have achieved with the OH^--activated strategy, also in this case the pH-dependent behaviour is observed over a wide range of IS concentration (from 30 nM to 1 μM, see Figure 3.15).

A control experiment obtained using an IS with the same sequence used above except that it lacks the domains a** and b**, i.e. the portion necessary to form the triplex (see Figure 3.12 and Materials) shows that the displacement process is independent to pH, as expected. More specifically, I did not observe any significant displacement signal over the entire pH range investigated (from 5 to 8) (Figure 3.14b) and over the same IS concentration range (from 30 nM to 1 μM) (Figure 3.16).

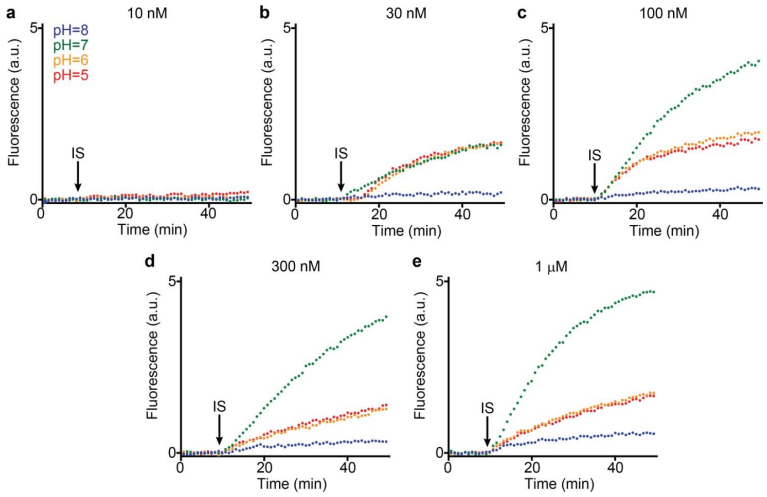

Figure 3.15. pH-activation of the H+-activated DNA strand displacement (strategy #2). The tunability of activation/inhibition of the strand displacement process shown in Figure 3.9 is also observed for strategy #2 over a wide concentration range of IS. (a) 10 nM. (b) 30 nM. (c) 100 nM. (d) 300 nM. (e) 1 μM. Here strand displacement is followed by fluorescence measurements obtained in a solution of complex S (10 nM) in the presence of R (30 nM) after the addition of the IS at different concentrations (see each panel) in a 0.01 M Tris buffer + 0.01 M $MgCl_2$, at 25° C.

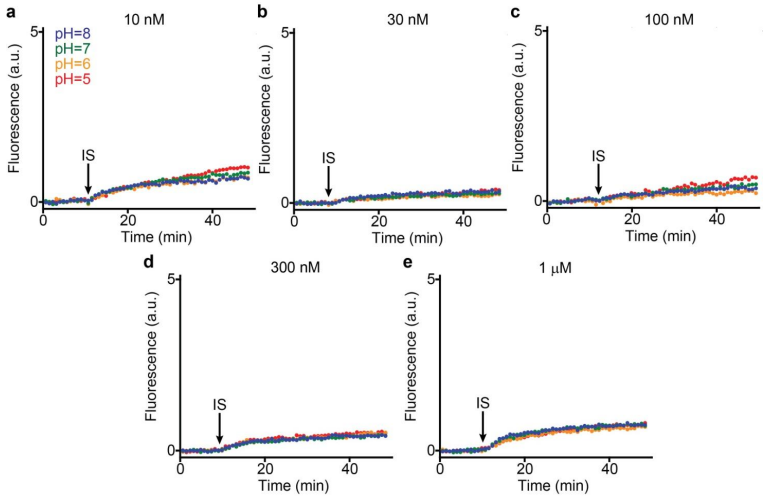

Figure 3.16. Study of the pH effect on the control DNA strand displacement of strategy #2. As a control experiment for strategy #2 we have used an IS that is not able to form a triplex (duplex-forming IS control, see Materials). Strand displacement reactions of this control using different concentrations of duplex-forming IS control show no pH dependence over the entire pH range we have investigated (from pH 5 to pH 8). (a) IS (10 nM). (b) IS (30 nM). (c) IS (100 nM). (d) IS (300 nM). (e) IS (1 μM). Here strand displacement is followed by fluorescence measurements obtained in a solution of S (10 nM) in the presence of R (30 nM) after the

addition of different concentration of duplex-forming IS control (see each panel) in a 0.01 M Tris buffer + 0.01 M $MgCl_2$, at 25° C.

Interestingly, while the pH-independent analogue of strategy #1 is always in an ON-state (i.e. strand displacement occurs with the same efficiency at both acidic and basic pH values) (Figure 3.5b, 3.6), the pH-independent analogue of strategy #2 is always in the OFF state and no strand displacement occurs at both acidic and basic pH values (Figure 3.14b, 3.16).

Both the strategies I have dissected here allow an external control over the strand displacement process. I further demonstrate this by adding the IS under initial inhibiting conditions (Figure 3.17) for both strategies. The addition of the IS under these conditions does not lead to any significant strand displacement (Figure 3.17, red curves). Upon addition of either OH^- (Figure 3.17a) or H^+ (Figure 3.17b), I was able to activate both processes and I observed an immediate increase of the fluorescence signals associated to the strand displacement reactions (Figure 3.17, blue curves). A similar feature has been observed over a wide IS concentration range (Figure 3.18).

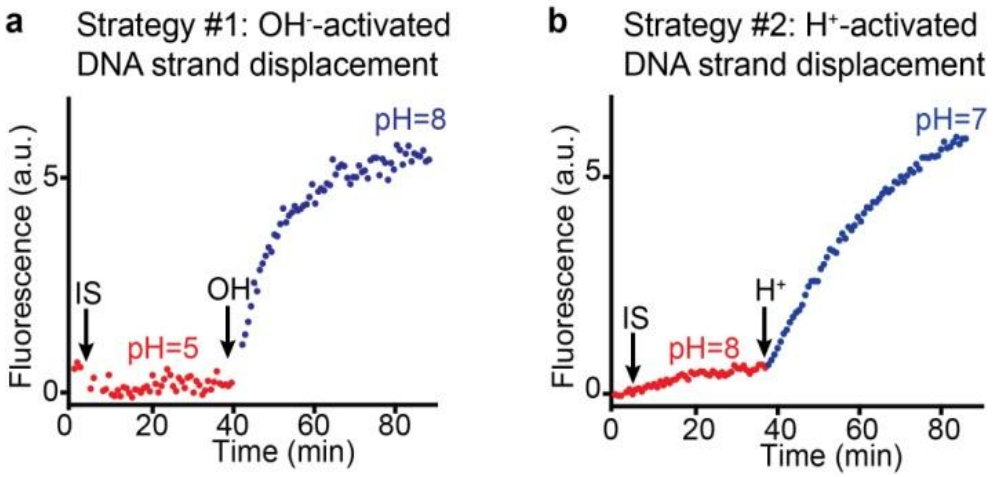

Figure 3.17. Toehold-based DNA strand displacement in the triplex-DNA based strategies I propose here can be triggered by changing the solution's pH. Under inhibiting conditions the addition of the IS does not result in any displacement reaction (red lines). Upon addition of (a) Na_2CO_3 (to reach a pH of 8) or (b) NaH_2PO_4 (to reach a neutral pH) strand displacement is triggered and I observe a fast signal increase (blue lines). Experiments were performed in a 0.01 M Tris buffer + 0.01 M $MgCl_2$, at 25° C.

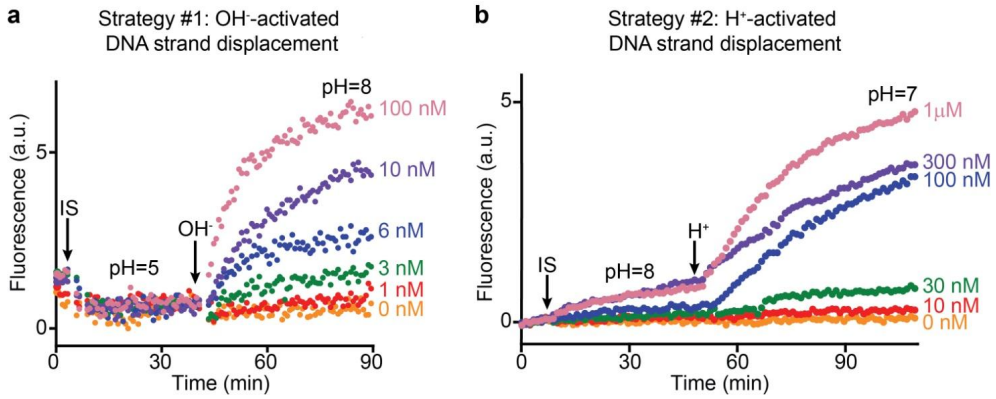

Figure 3.18. pH-activation of strand displacement reaction. DNA strand displacement in the triplex-DNA based strategies I propose here can be simply activated by changing the solution's pH. (a) For the OH^--activated strand displacement strategy (strategy #1), under acidic conditions the addition of the IS does not result in any significant strand displacement (pH = 5). Upon addition of Na_2CO_3 (to reach a pH of 8) a fast kinetic of strand displacement is observed over a wide range of IS concentrations (from 1 nM to 100 nM). I used here an IS with a toehold length of 15 bases and an invading domain of 8 bases. (b) A similar activation is achieved with the H^+-activated strategy (strategy #2) by changing the solution's pH from a value of 8 to a value of 7 (adding NaH_2PO_4). Here strand displacement is followed by fluorescence in a solution of complex S (10nM) in the presence of R (30nM) after the addition of the IS (concentrations ranging from 10 nM to 1 μM). Here I used an IS with a toehold length of 6 bases and an invading domain of 9 bases. Experiments were performed in a 0.01 M Tris buffer + 0.01 M $MgCl_2$ at 25° C.

3.3 Conclusions

Here I have rationally designed triplex-based DNA strand displacement reactions that can be triggered/activated at both basic and acidic pHs. I did so by taking advantage of the pH-dependence of parallel Hoogsteen interactions. In the first strategy (OH^--activated), I have designed a clamp-like strand that can bind-and-lock the strand to be released into a very stable triplex complex, thus inhibiting strand displacement under conditions at which such triplex structure is favoured (acidic pHs). In the second strategy, on the contrary, I have designed a clamp-like, triplex-competent, IS that can wrap a portion of the preformed, strand to release-containing complex, through the formation of both Watson-Crick and Hoogsteen interactions. Because of the increased stabilization provided by the action of extra Hoogsteen interactions (that are highly

favoured at acidic pHs), this results in a more effective displacement of the strand to release compared to a reaction where only Watson-Crick base pairings take place.
I note that alternative DNA or RNA base pairings (Hoogsteen, sugar edges, etc.) and secondary DNA structures (i-motif, G-quadruplex, etc) are likely more amenable to exogenous control (pH, Mg^{2+}, etc) than the classic Watson-Crick base pairings. This might open the future to new and exciting possibilities in the field of functional DNA nanotechnology. Compared with other pH-dependent DNA secondary structures (e.g. the i-motif [36, 37]), the use of triplex DNA might allow a better control and a tunable pH-dependency over a wide pH range.[33]
The possibility to activate/inhibit the toehold-exchange DNA strand displacement process through a simple change of the solution's pH appears particularly interesting for several reasons. Since strand displacement has been used to assemble dynamic and static DNA-based nanostructures[11,38] the strategies presented in this work could be adopted to introduce additional control over the formation and functionality of similar DNA nanoarchitectures. For example, our approach would permit in principle to regulate DNA-based origami formation or DNA-based nanodevices' activity exclusively through pH changes. In addition, since pH dysregulation is often associated to different diseases (e.g. many cancers are characterized by an inverted pH gradient between the inside and the outside of cells [39]), it could be useful to activate the functionality of drug-releasing DNA-based nanomachines only at specific pH values.

3.4 Materials and Methods

Materials. Reagent-grade chemicals, including tris-(2-carboxyethyl) phosphine hydrochloride, sodium chloride, magnesium chloride, ethanol and acetone (all from Sigma-Aldrich, St Louis, Missouri) were used without further purifications. HPLC purified oligonucleotides modified with a Cy3 or Cy5 were purchased from IBA (Gottingen, Germany) and employed without further purification. The following oligos modified and non-modified were used (in brackets the domains of each strand):

1) Strategy #1: OH^--activated strand-displacement (see Figure 1a for details on the notation of the sequences).

Clamp-like triplex forming strand (strand forming complex S_t) (b** c** c b a) (a 5-base loop, italic bases, is present between domains c** and c):

5'- TTCCTTTCTCCT TCTTTT *AACTA* TTTTCT TCCTCTTTCCTT GTTACATTGCACACT -3'

Released strand: X (b* c*): 5'- AAGGAAAGAGGA AGAAAA -3'

Invading strands:

IS12 (12-base invading domain) (a*15 b*12):

5'- AGTGTGCAATGTAAC AAGGAAAGAGGA -3'

IS 10 (a*15 b*10): 5'- AGTGTGCAATGTAAC AAGGAAAGAG -3'

IS 8 (a*15 b*8): 5'- AGTGTGCAATGTAAC AAGGAAAG -3'

Control strand (strand forming complex S_{Duplex}) (c b a) (a 5-base domain identical to the 5-base loop of the clamp-like triplex forming strand, see above, is present before domain c.):

5'- *AACTA* TTTTCT TCCTCTTTCCTT GTTACATTGCACACT -3'

Reporters:

F (b*): 5'- (Cy3) AAGGAAAGAGGA -3'

Q (c b): 5'- TTTTCT TCCTCTTTCCTT (Cy5) -3'

Labelled clamp-like triplex forming strand (strand forming complex S_t): (b** c** c b a)

5'-(Cy5)- TTCCTTTCTCCT TCTTTT *AACTA* TTTTCT TCCTCTTTCCTT (Cy3) GTTACATTGCACACT -3'

2) Strategy #2: H^+-activated strand-displacement (see Figure 1b for details on the notation of the sequences).

Released strand: X (d* c* b*):

5’- CAACATACATTATATT CTTCAATTAAA **CTTTCTCTC** -3’

Complex S-forming strand (a b c):

5’- AGGGAGAAG **GAGAGAAAG** TTTAATTGAAG -3’

Clamp-like triplex-forming invading strand, IS (a** b** b* a*) (a 5-base loop, italic bases, is present between domains b** and b*):

5’- CTCTTC **CTCTCTTTC** *GTTTC* **CTTTCTCTC** CTTCTC -3’

Duplex-forming invading strand control (b* a*): 5’- **CTTTCTCTC** CTTCTC -3’

Reporters:

F (d* b_6*): 5’- (Cy3)- CAACATACATTATATT **CTTCAA** -3

R (b_{13} d): 5’- **AGTTTAATTGAAG** AATATAATGTATGTTG -(Cy5)-3’

Labelled clamp-like triplex forming strand (strand forming complex P_f) (a* b* b** a**):

5’-(Cy5) CTCTTC **CTCTCTTTC** *GTTTC* **CTTTCTCTC** CTTCTC (Cy3) - 3’

In the sequences above underlined, italics and bold bases have been used to identify in a clearer way the different domains of each strand.

Buffer conditions. DNA oligonucleotides were suspended to a final concentration of 100 μM and stored in 0.01 M Tris + 0.01 M $MgCl_2$, pH 7, at -20° C. In all experiments we used solutions of Tris buffer 0.01 M + 0.01 M $MgCl_2$ with the pH adjusted with the addition of HCl or NaOH. All experiments were performed at 25° C.

Substrate preparation. All the complexes (R, S_t and S) used in the experiments were prepared mixing the oligos necessary for the formation of the complex at equimolar concentration (1 μM) in TRIS buffer 0.01 M + 0.01 M $MgCl_2$ pH 7 and letting them to react at room temperature overnight.

Fluorescence measurements. All fluorescence measurements were obtained using a Cary Eclipse Fluorimeter (Varian) with excitation at 548 nM (± 5 nm) and emission at 563 nM (± 5 nm). Strand displacement experiments were performed using a concentration of R of 30 nM and 10 nM of substrate (S_t or S). The IS was added at the selected concentration (from 0.1 nM to 100 nM for strategy # 1, from 10 nM to 1μM for strategy # 2) after 10 minutes to allow a stable baseline. The signal increase of Cy3 was followed for 40 minutes after IS addition.

Melting curves analysis. Fluorescence melting curves were obtained in a Real Time PCR Stratagene MX3005P (Agilent Technologies), using a total reaction volume of 200 µL. Melting curves was recorded for S_t complex (at 0.05 µM), diluted in TRIS buffer 0.01 M + 0.01 M $MgCl_2$ at different pHs. The experiments were performed by heating from 25° C to 95° C at a rate of 2° $C^{-1}s$. The reported melting curves have been normalized through the use of the interpolation model.[40] Melting temperatures (T_m) have been obtained using the same model from the intersection of the calculated median and the experimental melting curve.

Native PAGE experiments. Formation of control DNA complexes (S_t and P) was achieved by mixing at equimolar concentrations DNA strands forming S_t and P in TRIS buffer 0.01 M + 0.01 M $MgCl_2$ at pH 7 and incubated overnight at RT. Different concentrations of invading strand (IS8) were added to the so formed complex S_t. The strand displacement reaction was allowed to proceed at RT for 30 minutes and then the solution was loaded onto the native PAGE. At pH 8 I only observe the band corresponding to the product of strand displacement (P). Here native PAGE containing 18% polyacrylamide (29:1 acrylamide/bisacrylamide) was run on a Mini-PROTEAN Tetra cell electrophoresis unit (Bio-Rad) at RT (90 V). TAE/Mg^{2+} buffer [40 mM Tris base, 20 mM acetic acid, 1 mM EDTA and 2 mM $MgCl_2$] was used both as the running buffer and the buffer in the gel. After electrophoresis, the gels were stained with Ethidium Bromide (Sigma) and scanned with a Gel Doc XR+ (Bio-Rad).

3.5 References

(1) Krishnan, Y.; Bathe, M. *Synth. Cell Biol.* 2012, 22, 624.

(2) Lu, C.H.; Willner, B.; Willner, I. *ACS Nano* 2013, 7, 8320.

(3) Douglas, S. M.; Bachelet, I.; Church, G. M. *Science* 2012, 335, 831.

(4) Winfree, E.; Liu, F.; Wenzler, L. A.; Seeman, N. C. *Nature* 1998, 394, 539.

(5) Rothemund, P. W. K. *Nature* 2006, 440, 297.

(6) Ke, Y.; Voigt, N. V.; Gothelf, K. V.; Shih, W. M. *J. Am. Chem. Soc.* 2011, 134, 1770.

(7) Turberfield, A. J.; Mitchell, J. C.; Yurke, B.; Mills Jr., A. P.; Blakey, M. I.; Simmel, F. C. *Phys. Rev. Lett.* 2003, 90, 118102/1.

(8) Bath, J.; Turberfield, A. J. *Nat. Nanot.* 2007, 2, 275.

(9) Mao, C. *Nat Nanot.* 2008, *3*, 75; d) Krishnan, Y.; Simmel, F. C. *Angew. Chem. - Int. Ed.* 2011, 50, 3124.

(10) Seelig, G.; Soloveichik, D.; Zhang, D. Y.; Winfree, E. *Science* 2006, 314, 1585;

(11) Zhang, D. Y.; Seelig, G. *Nat Chem* 2011, 3, 103.

(12) Zhang, D. Y.; Winfree, E. *J. Am. Chem. Soc.* 2009, 131, 17303.

(13) Wickham, S. F. J.; Bath, J.; Katsuda, Y.; Endo, M.; Hidaka, K.; Sugiyama, H.; Turberfield, A. J. *Nat. Nanot.* 2012, 7, 169.

(14) Han, X.; Zhou, Z.; Yang, F.; Deng, Z. *J. Am. Chem. Soc.* 2008, 130, 14414.

(15) Liu, M.; Fu, J.; Hejesen, C.; Yang, Y.; Woodbury, N. W.; Gothelf, K.; Liu, Y.; Yan, H. *Nat Commun* 2013, *4*.

(16) Yang, Y.; Liu, G.; Liu, H.; Li, D.; Fan, C.; Liu, D. *Nano Lett.* 2010, *10*, 1393.

(17) Zhu, C.; Wen, Y.; Li, D.; Wang, L.; Song, S.; Fan, C.; Willner, I. *Chem. – Eur. J.* 2009, 15, 11898.

(18) Elbaz, J.; Lioubashevski, O.; Wang, F.; Remacle, F.; Levine, R. D.; Willner, I. *Nat. Nanot.* 2010, 5, 417.

(19) Genot, A. J.; Bath, J.; Turberfield, A. J. *J. Am. Chem. Soc.* 2011, 133, 20080.

(20) Sun, Y.-H.; Kong, R.-M.; Lu, D.-Q.; Zhang, X.-B.; Meng, H.-M.; Tan, W.; Shen, G.-L.; Yu, R.-Q. *Chem. Commun.* 2011, 47, 3840.

(21) Chen, H.; Weng, T.-W.; Riccitelli, M. M.; Cui, Y.; Irudayaraj, J.; Choi, J. H. *J. Am. Chem. Soc.* 2014, 136, 6995.

(22) Wang, F.; Lu, C.-H.; Willner, I. *Chem. Rev.* 2014, 114, 2881.

(23) Zhang, D. Y.; Chen, S. X.; Yin, P. *Nat. Chem.* 2012, 4, 208.

(24) Xu, X.; Yang, X. *Chem. Commun.* 2014, 50, 805.

(25) Ding, W.; Deng, W.; Zhu, H.; Liang, H. *Chem. Commun.* 2013, 49, 9953.

(26) Tang, W.; Wang, H.; Wang, D.; Zhao, Y.; Li, N.; Liu, F. *J. Am. Chem. Soc.* 2013, 135, 13628.

(27) Liu, Z.; Mao, C. *Chem. Commun.* 2014, 50, 8239.

(28) Jester, S.-S.; Famulok, M. *Acc. Chem. Res.* 2014, 47, 1700.

(29) Kamiya, Y.; Asanuma, H. *Acc. Chem. Res.* 2014, 47, 1663;

(30) Lohmann, F.; Ackermann, D.; Famulok, M. *J. Am. Chem. Soc.* 2012, 134, 11884.

(31) d) Lohmann, F.; Weigandt, J.; Valero, J.; Famulok, M. *Angew. Chem. Int. Ed.* 2014, 126, 10540.

(32) Idili, A.; Plaxco, K. W.; Vallée-Bélisle, A.; Ricci, F. *ACS Nano* 2013, 7, 10863.

(33) Idili, A.; Vallée-Bélisle, A.; Ricci, F. *J. Am. Chem. Soc.* 2014, 136, 5836.

(34) Ohmichi, T.; Kawamoto, Y.; Wu, P.; Miyoshi, D.; Karimata, H.; Sugimoto, N. *Biochemistry* 2005, 44, 7125.

(35) Soto, A. M.; Loo, J.; Marky, L. A. *J. Am. Chem. Soc.* 2002, *124*, 14355.

(36) Li, T.; Ackermann, D.; Hall, A.M.; Famulok, M.*J. Am. Chem. Soc.* 2012, *134*, 3508. Li, T.; Famulok, M. *J. Am. Chem. Soc.* 2013, 135, 1593.

(37) Modi, S.; Nizak, C.; Surana, S.; Halder, S.; Krishnan, Y. *Nat. Nanotechnol.* 2013, 8, 459.

(38) Baker, B. A.; Mahmoudabadi, G.; Milam, V. T. *Soft Matter* 2013, 9, 11160.

(39) Harguindey, S.; Orive, G.; Luis Pedraz, J.; Paradiso, A.; Reshkin, S. J. *BBA - Rev. Cancer* 2005, 1756, 1.

(40) Mergny J.-L.; Lacroix, L. *Oligonucleotides* 2003, 13, 515.

Chapter 4 – Controlling DNA Nanotubes self-assembly with pH

4.1 Introduction

DNA nanotechnology uses DNA as a versatile engineering material in a wide range of field, such as drug delivery, [1] cell biology, [2] imaging[3] and smart therapeutics. [4] Structural DNA nanotechnology, an exciting development of this field, pioneered by Seeman[5], pursuit to build complex materials with nanoscale features.[4,6-14] DNA appears as the perfect building block to assemble and engineer complex molecular architectures, due to the predictability and the programmability of Watson-Crick base pairings, to the stability and the high persistence length of the double strand (dsDNA), as well as the automated synthesis and the decrease of its costs.

DNA tile based-self assembly is one of the most used approaches to build complex architectures. In this strategy, rigid building blocks, called tiles, constitute the assembly units. A wide number of different tiles have been designed, double-crossover tile, [8] triple crossover,[15,16] quadruple crossovers,[17] as well as more complex tiles, such as 4×4 cross-tiles,[18-21] 3-, 5- and 6-point star tiles, [22-26] six-helix bundle.[27] The tiles are characterized by the presence of single-stranded overhangs, called sticky-ends, that allow controlled self-assembly of the tiles into complex molecular nanostructures with variable shapes and size.[8-28] DNA tile self-assembly has been used not only to build complex static molecular nanostructures, but also to develop DNA tile actuators,[29] to organize nanoparticles,[30-32] for nanoscale organization of ligands and proteins,[33-35] and for prototypical computation.[36-41]

Among these structures, an interesting example is represented by DNA nanotubes. Because of their remarkable size (reaching over microns in length) and particular features, nanotubes hold great promise for a range of applications, i.e., from nanofabrication to biophysical studies. [42] In particular, DNA nanotubes have been reported as a detergent-resistant alignment medium for NMR-based protein structure determination,[43] as templates for conductive nanowires, [11] and as tools for loading and releasing molecular cargo[44] or to deliver small molecules into cells. [45,46] Achieving strict control of thermodynamics and kinetics of DNA nanotubes self-assembly, would greatly contribute to fulfil their potentiality. In this context, despite in recent years DNA nanotubes have seen a widespread application, only few examples have been reported

that allow activation of DNA nanotubes self-assembly at room temperature, and with external control. The application of small molecule (DNA-porphyrin[47]), gold nanoparticles,[48] long enzymatically produced backbone[49] and strand displacement reaction[50] have been demonstrated as valuable inputs to control the self-assembly process of DNA nanotubes.

4.2 Results and discussion

With the abovementioned motivations, in this chapter I show how I achieved the design and development of a DNA tile self-assembly process that integrates a pH-controlled DNA strand displacement circuitry, which I partially developed along with the activities discussed in the previous chapter (chapter three).[51] By taking advantage of such an approach, DNA nanotubes self-assembly can be controlled by means of pH changes. I did so by taking advantage of the well characterized pH sensitivity of the parallel Hoogsteen (T,C)-motif in triplex DNA. [52-54] In fact, in order to obtain the formation of the sequence-specific formation of a CGC parallel triplet, the protonation of the N3 of cytosine in the third strand is needed (average pK_a of cytosines in triplex structure is ≈ 6.5).[55] As a result, triplex structures containing CGC triplets are stabilized only at acidic pHs. More specifically, I integrated a pH-dependent strand displacement circuitry into a classical DNA tile self-assembly scheme (Figure 4.1a). The upstream strand displacement circuitry is activated only at neutral/basic pHs, thus releasing in solution a strand, termed deprotector (D), that by reacting with specific protected tile (Figure 4.1b, right), causes DNA nanotubes formation. The whole strand displacement circuitry is regulated by the pH. To do so, I engineered a pH-dependent substrate (Figure 4.1a violet strand) that, at acid pHs, prevents the strand displacement reaction, thanks to the formation of Hoogsteen interactions. Under these conditions, nanotubes formation is inhibited. Only at basic pHs (when Hoogsteen interactions are destabilized), the efficiency of the strand displacement circuitry is restored and nanotubes formation occurs efficiently. In this work, I used as tile a DAE-E double-crossover tile composed of five different strands (Figure 4.1b, left): the three in the centre contribute to structural rigidity, while the outer two contain sticky ends that permit the self-association of the tiles.[50]

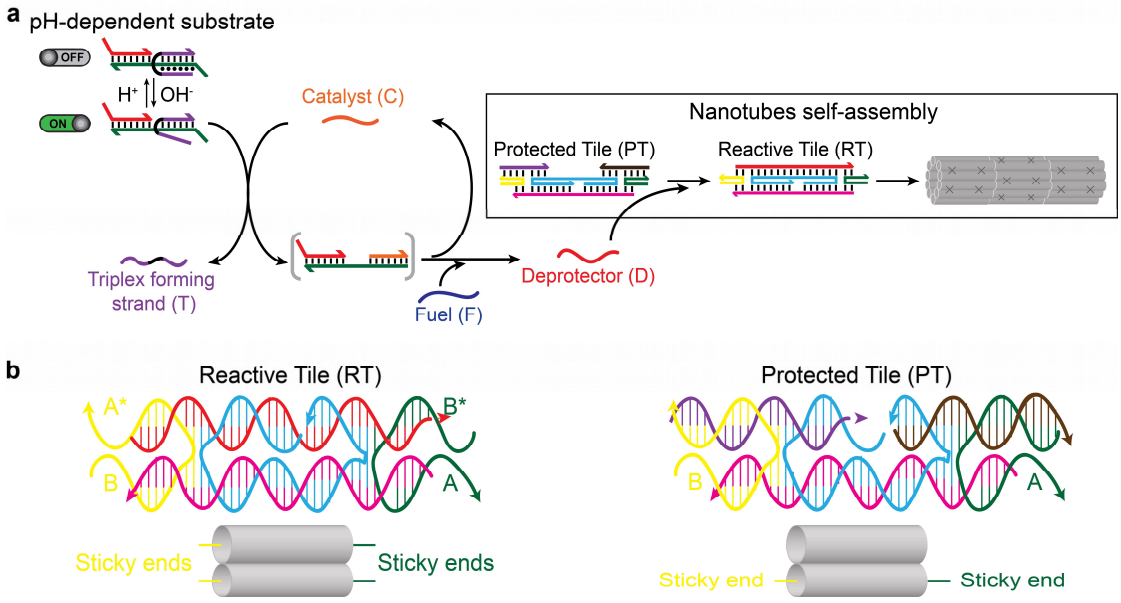

Figure 4.1. pH-controlled DNA nanotubes self-assembly strategy. (a) pH-dependent upstream catalytic strand displacement. Catalyst (C) binds the pH-dependent substrate thanks to the toehold-domain presents in this complex. The presence in the pH-dependent substrate of a clamp-like DNA strand forms a triplex complex that is inactive at acidic pHs. The additional Hoogsteen interactions prevent strand displacement upon C addition. On the contrary, at basic pHs, the destabilization of Hoogsteen interactions activate the complex. The association between C and the pH-dependent, activated substrate, releases the triplex forming strand (T), which in turn exposes a toehold-domain in the complex centre. The gain of accessibility of such toehold domain allows the fuel (F) to bind to the complex. This further association releases C and another single strand, termed deprotector (D). In this way, the turn over of C allows the same molecule to bind another copy of the pH-dependent complex, thus leading to multiple turnover events. In contrast, the strand D permanently associates with the protected tile (PT) through a strand displacement reaction that displaces the protectors, and leads to a reactive tile (RT). This mechanism allows several RT to self-assemble into nanotubes. (b) (*left*) RT is made of five synthetic DNA strands that hybridize into a rigid rectangular core characterized by two double helices with a single-stranded five-base overhang (sticky end) at each corner (A, A*, B, B*). The presence of these sticky ends allow the self-assembly of RT into nanotubes. (*right*) In the PT, two of the four sticky ends (A* and B*) are protected with two complementary strands, thus leading to stable, monomeric tiles that cannot form nanotubes.

This strategy relies on the use of pH-dependent clamp-like conformational switches (Figure 4.1a, 4.14) that lead to triplex formation. [51-53] In particular, triplex formation is

utilized to prevent the reaction between C and the pH-dependent substrate, by locking the strand that would be otherwise released in the presence of C. As a first characterization, I have studied the pH-dependent stability of the clamp-like triplex complex in the pH-dependent substrate. To do so, I have used a pH-dependent substrate, in which the triplex forming strand (T) is dual labelled (Figure 4.2, left). After hybridization, I have performed a pH-titration curve of the so-formed complex at different pHs (Figure 4.2b). As expected, under acidic pHs, a condition at which triplex formation is favoured, a low fluorescence signal is observed. By increasing the pH solution the fluorescence signal increases because of the destabilization of Hoogsteen interactions at basic pHs (Figure 4.2, right).

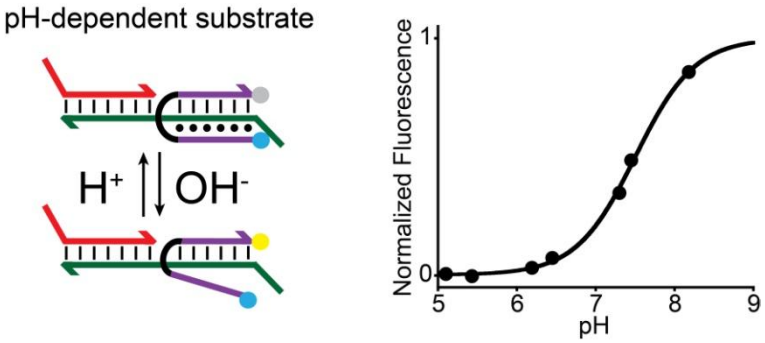

Figure 4.2. pH-dependent clamp-like triplex DNA formation in the pH-DS (see Figure 4.1a). (a) The triplex formation is monitored through a pH-insensitive FRET pair, located at the 3'-end (Cy3) and at the 5'-end (Cy5) of the clamp-like strand presents in the pH-dependent substrate. (b) Shown is the pH-titration curve of the pH-sensitive clamp-like DNA strand in the pH-dependent substrate (at 10 nM concentration) performed in TAE 1x + 15 mM $MgCl_2$ at 25° C.

Triplex formation in the upstream strand displacement reaction allows to rationally control the kinetic of the displacement circuitry by simply changing the solution's pH. In order to demonstrate this, I have first characterized the pH-dependent strand displacement circuitry (Figure 4.3a), by using an external, optically labelled reporter (R), that stoichiometrically reacts with the deprotector strand (D). At pH 5, which is acidic enough for the clamp-like strand to form a triplex, inactive complex (see Figure 4.3a), the addition of the catalyst (C) does not result in any significant signal change (Figure 4.3b, left), suggesting that the circuitry is blocked (off state). On the contrary, at pH 8 (a pH at which triplex formation is unfavoured), strand displacement successfully proceeds with a fast kinetic upon C addition (Figure 4.3b, right). In these conditions the circuitry is active (on state).

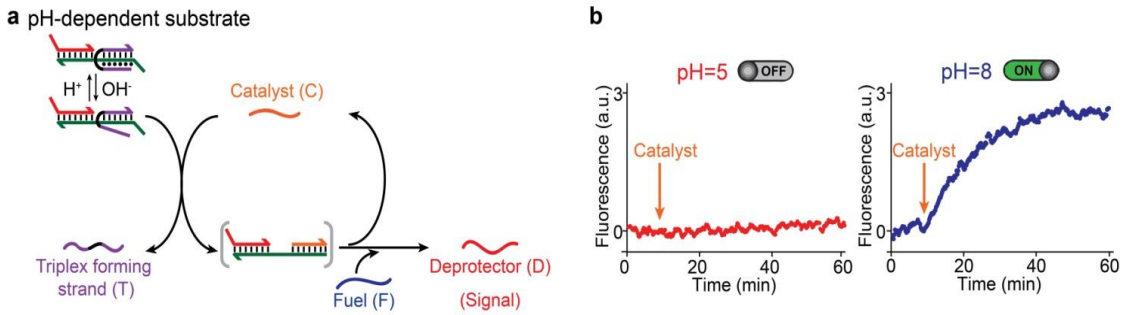

Figure 4.3. OH^--activated DNA strand displacement circuitry. (**a**) The clamp-like triplex strand prevents the strand displacement reaction at acidic pH, thanks to the additional energetic contribution of Hoogsteen interaction. On the contrary at basic pH the destabilization of Hoogsteen interaction leads to an active complex, characterized by a simple duplex conformation. In this condition, C can bind to pH-dependent substrate, thus exposing a previously shielded toehold domain in the complex centre and realising a by-product. The formation of a new toehold domain allow the binding between F and the complex, that releases two single strands, C and D. C can react with other molecules of pH-dependent substrate, engaging in a multiple turnover events, D reacts with an external reporter (R). R is labelled with a FRET pair (see Material) and stoichiometrically reacts with the released strand D. (**b**) The fluorescence kinetics show that at pH 5, after the addition of C the fluorescence signal does not change over 1h. This demonstrates that the formation of the triplex structure in the pH-dependent substrate prevents strand displacement upon C addition. At pH 8 and after C addition, an increase of the fluorescence signal is observed. This demonstrates that the destabilization of Hoogsteen interactions at basic pH allows strand displacement upon C addition. Strand displacement is followed by fluorescence measurements obtained in a solution of complex pH-dependent substrate (10 nM) and F (20 nM) in the presence of reporter R (30 nM) after the addition of the C at a concentration of 30 nM in a TAE 1x buffer + 15 mM $MgCl_2$, at 25° C.

To explore the possibility of modulating the kinetic thus establishing different levels of activation by changing the pH of the solution rather than varying the catalyst concentration, I performed the same experiment at other pHs (Figure 4.4). The addition of the catalyst, does not produce a significant fluorescence signal change at acidic pHs (Figure 4.4, top). At neutral/basic pHs, instead, an increase of fluorescence is observed upon catalyst addition (Figure 4.4, bottom). Of note, the kinetic profiles observed at these two pH values are different. In fact, if we compare the kinetic profiles obtained by using the same amount of catalyst, we systematically observe a faster kinetic at pH 8. This result suggests that it should be possible to control the kinetic of DNA tile self-

assembly not only by varying the amount of catalyst in solution (as described by others), but also by changing the solution pH.

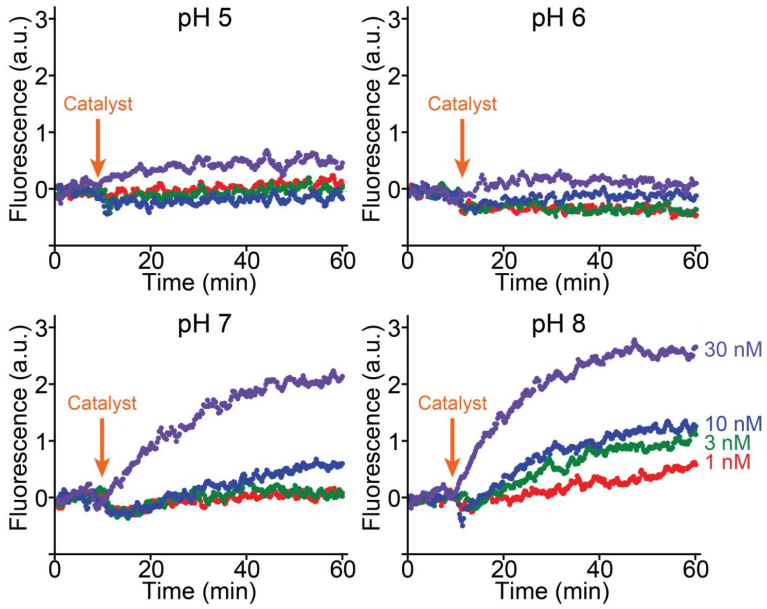

Figure 4.4 pH-tunability of the DNA strand displacement circuitry. Upon C addition (from 1nM to 30 nM) no significant fluorescence signal change at pH 5 and 6 is observed, thus demonstrating that the formation of sequence specific Hoogsteen interaction at acidic pHs strongly stabilize the pH-dependent substrate. The destabilization of Hoogsteen interactions allows strand displacement to occur upon C addition (from 1nM to 30 nM) either at pH 7 or at pH 8. However, the kinetic profiles at such pHs, show a different kinetic of the strand displacement process, thus demonstrating a faster kinetic at pH 8. This behaviour is observed for all the different concentration of C (from 1 nM to 30 nM). Strand displacement is followed by measuring the fluorescence of a solution of complex pH-dependent substrate (10 nM) and F (20 nM) in the presence of reporter R (30 nM), and after the addition of the C at a concentration of 30 nM in a TAE 1x buffer + 15 mM $MgCl_2$, at 25° C.

Towards achieving a reliable control of the molecular circuitry, I have designed a pH-independent substrate in which T has been substituted with a strand that has a random tail, not able to form a triplex structure (Figure 4.5a). In this way, I obtained a conventional strand displacement circuitry that is independent to pH (Figure 4.5b). Since it is the formation of the triplex structure that switches the circuitry from the on-state to the off-state, the absence of the triplex in the control $_1$ complex steadily sets the strand displacement circuitry in the on-state (Figure 4.5b).

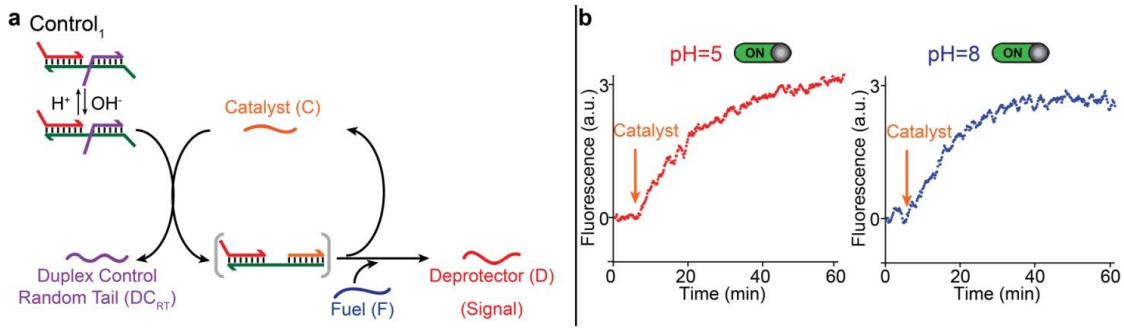

Figure 4.5. pH-independent substrate strand displacement circuitry (Control $_1$). (a) S presents a strand with a random tail (S_{DC_RT}). This random tail does not allow triplex formation. In this condition, C can bind S_{DC_RT}, thus exposing a previously shielded toehold domain in the complex centre, and realising a by-product. The formation of a new toehold domain allows the association between F and the complex, which releases the single strands termed C and D. C can react with other molecules of S_{DC_RT}, thus engaging in multiple turnover events, whereas D can react with an external reporter (R). R is labelled with a FRET pair (see Material) and stoichiometrically reacts with the released strand D. (b) The fluorescence kinetics shows that either at pH 5 or at pH 8 and after the addition of C, an increase of the fluorescence is observed. Strand displacement is followed by fluorescence measurements obtained in a solution of complex S_{DC_RT} (10 nM) and F (20 nM), in the presence of reporter R (30 nM), and after the addition of the C at a concentration of 30 nM in a TAE 1x buffer + 15 mM $MgCl_2$ at 25° C.

The pH-independent substrate is steady upon pH changes and performs with very similar kinetics in the entire pH range explored, and over a wide range of catalyst concentrations (Figure 4.6).

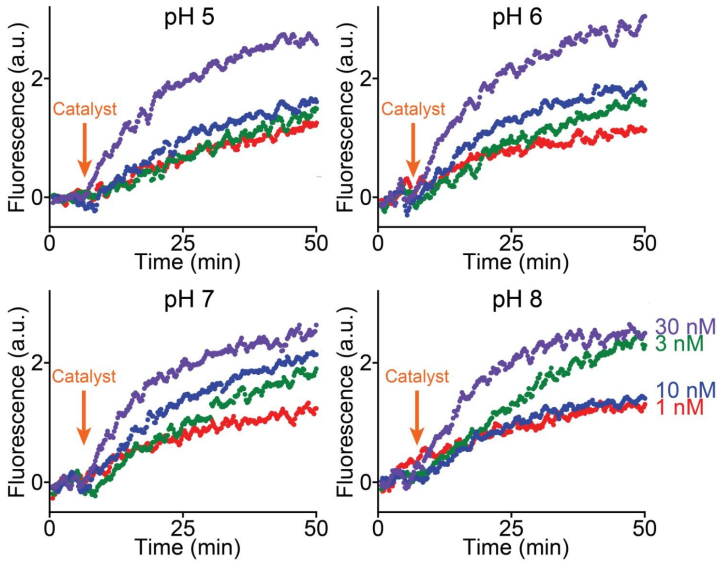

Figure 4.6. pH-independent substrate strand displacement circuitry (Control$_1$). The fluorescence signal upon C addition (from 1 nM to 30 nM) lead to a fluorescence increase at all the pHs

investigated (pH 5, 6, 7, 8). Moreover, the kinetic profiles have the same behaviour at all the pHs, by comparing kinetic profile registered at the same concentration of added C. Strand displacement is followed by fluorescence measurements obtained in a solution of complex S_{DC_RT} (10 nM) and F (20 nM) in the presence of reporter R (30 nM) after the addition of the C at a concentration of 30 nM in TAE 1x buffer + 15 mM $MgCl_2$, at 25° C.

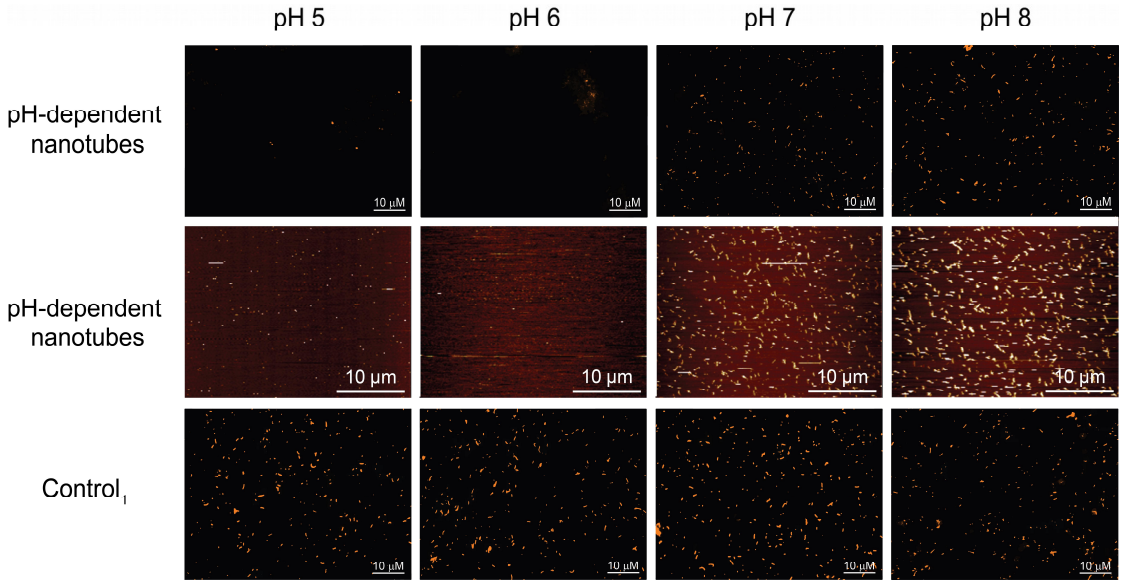

Figure 4.7. Optical fluorescence microscopy and atomic force microscopy (AFM) of the integrated reaction network. The first two rows is a set of images related to the integrated reaction network, in which the upstream strand displacement reaction is pH-sensitive (first row fluorescence microscope images, second row AFM images). At acidic pHs (pH 5, 6) no DNA nanotubes are observed within the time-frame of the experiment. At neutral/basic pHs (pH 7, 8), DNA nanotubes formation is observed. The latter row shows images obtained with the control (i.e. the initial complex is unable to form a triplex structure) for all the pHs investigated (pH 5, 6, 7, 8). At all pHs DNA nanotubes formation is observed. All the experiments were performed with the same concentration of reagents: PT (200 nM), F (440 nM), pH dependent substrate / S_{DC_RT} (220 nM) and C (20 nM), in TAE 1x buffer + 15 mM $MgCl_2$ at 25° C. For all the fluorescence microscope experiments, a cy3-modified version of the tile central strand (t4, see Materials) was used.

After preliminary characterization, I have merged the two systems. Fluorescence microscope images (Figure 4.7, first row) show that nanotubes formation occurs only at neutral/basic pHs, while no nanotubes form over the reaction time at pH 5 and pH 6. AFM images (Figure 4.7, second row) confirmed the results obtained.
Repeating the experiment with the pH-independent substrate leads to nanotubes formation in the entire pH range investigated (Figure 4.7, bottom row). To perform an

independent experimental control, I performed the strand displacement (both pH-dependent and pH-independent) reaction in the presence of a protected tile, and in the absence of the catalyst. Fluorescence microscope images (Figure 4.8) show that nanotubes do not form both for the pH-dependent reaction and for the control, at all the pHs investigated.

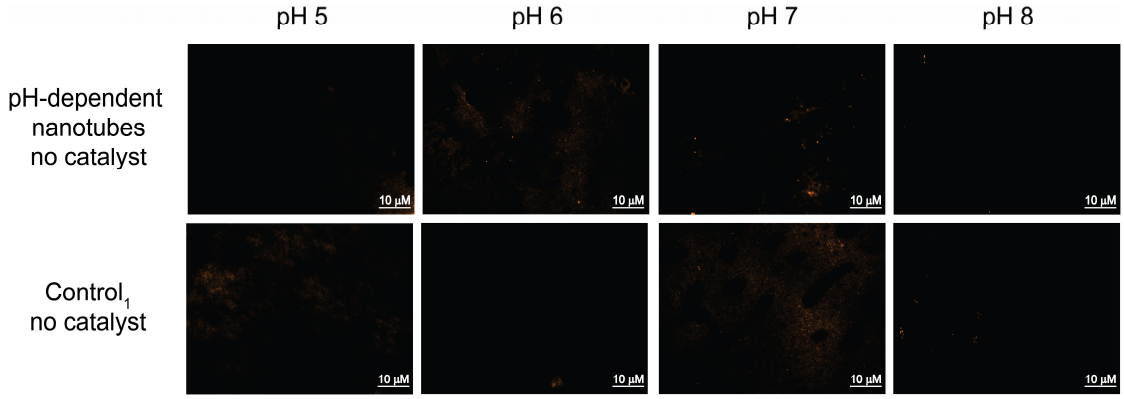

Figure 4.8. Fluorescence microscopy images of the integrated reaction network without catalyst. The first row is a collection of images related to the integrated reaction network, in which the upstream strand displacement reaction is pH-sensitive. No DNA nanotubes are observed at all the pHs investigated (pH 5, 6, 7, 8). The second row are shows images obtained with the control (the initial complex is not able to form triplex structure) at all the pHs investigated (pH 5, 6, 7, 8). As before, in this case no nanotubes formation is observed without catalyst over the entire reaction time. All the experiments were performed with the same concentration of reagents: PT (200 nM), F (440 nM), pH dependent substrate / S_{DC_RT} (220 nM), in TAE 1x buffer + 15 mM $MgCl_2$, at 25° C. For all the fluorescence microscope experiments, a cy3-modified version of the tile central strand (t4, see Material) was used.

A direct test of nanotube formation was carried out by triggering the DNA tiles self-assembly in the entire range of pH investigated without involving the previsously described, pH-dependent circuitry (Figure 4.9). To perform this control (Control$_1$) I therefore added the deprotector to a mixture reaction that contained the protected tile (Figure 4.9a). Fluorescence microscopy demonstrates the formation of nanotubes in a pH-independent fashion (Figure 4.9b).

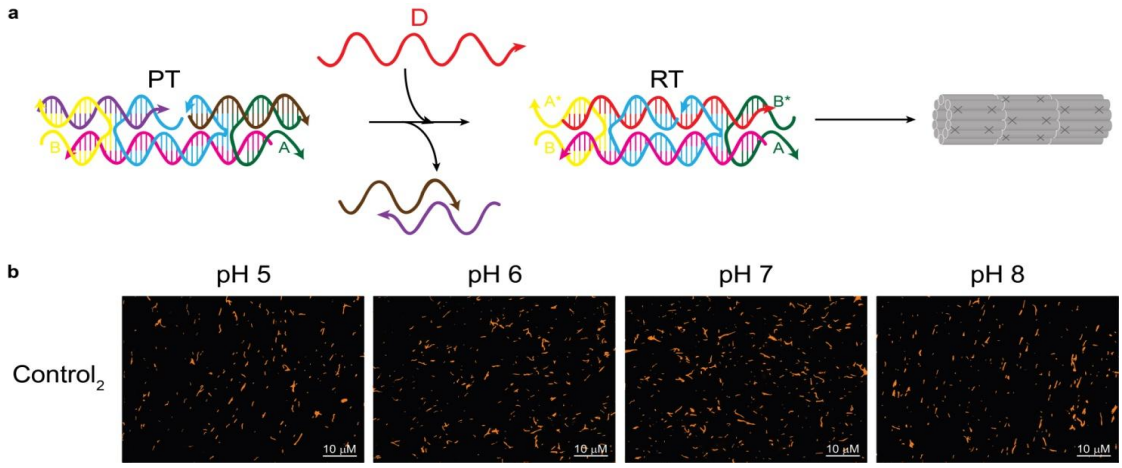

Figure 4.9. Direct nanotubes formation (Control$_2$). (a) D reacts with PT by displacing the two protectors strands and thus exposing the other two sticky ends. Strand displacement leads in turn to the formation of readily reactive tiles that isothermally form DNA nanotubes. (b) Fluorescence microscopy of the reaction between PT and D shows that DNA nanotubes form at all the pHs investigated (pH 5, 6, 7, 8). Experiments were performed by using a concentration 200 nM (PT) and a concentration of 220 nM (D) in TAE 1x buffer + 15 mM $MgCl_2$, at 25° C. For all the experiments with fluorescence microscopy, a cy3-modified version of the strand in the tile centre (t4, see Material) was used.

4.3 Conclusions

In this chapter I demonstrated that I was able to integrate two different systems, pH-dependent strand displacement circuitry and DNA tile self-assembly, thus obtaining a pH-control of nanotubes self-assembly at room temperature. Moreover, by taking advantage of pH-tuneable Hoogsteen interactions, I can control the kinetic of DNA tile self-assembly by simply changing the solution pH, rather than by varying the amount of C employed (as done by others). [50] The results obtained in this work open the door to interesting opportunity in the field of structural DNA nanotechnology. One of the most promising potential applications of such DNA nanotubes is related to their analogy with the roles of nanotubes and nanofilaments in living cells, [42] and thus they could be used as controllable models for such complex structures. Another intriguing potential application is the use of DNA nanotubes as smart drug-delivery system. [45,46] By taking into account that very often nature achieves spatiotemporal control of supramolecular self-assembly by implementing a variety of molecular mechanisms, I believe that having the ability to increase the number of parameters that concur to fine-tune the assembly and disassembly of DNA nanostructures is of great importance. The feasible

use of pH to reach such goal is extremely interesting and promising, and in particular because of the pivotal role of pH in healthy and pathological tissues.

4.4 Materials and Methods

Reagent-grade chemicals, including tris-base, glacial acid acetic, sodium chloride, magnesium chloride, ethylenediaminetetraacetic acid, ethanol and acetone (all from Sigma-Aldrich, St Louis, Missouri) were used without further purifications. HPLC purified oligonucleotides were purchased from IBA (Gottingen, Germany) and employed without further purification. The following oligos modified and non-modified were used:

Protected tile (ccc, ddd):
t1: 5'-ATACCATAGATCCTGATAGC-3'
t2: 5'-AGCAACCTGAAACCAGAATT-3'
t3: 5'-GAATTCTACTCGTGGATCTATGGTAT-3'
t4: 5'-AGAATTGCGTCGTGGTTGCTAGGTCTCGCTATCACCGATGTG-3'
t4_cy3:
5'-AGAATTGCGTCGTGGTTGCTAGGTCTCGCTATCACCGATGTG-(cy3)-3'
t5: 5'-AATTCTGGTTTCACCTTAACGATACC-3'
t6: 5'-CGTTAAGGACGACGCAATTCTCACATCGGACGAGTAG-3'
pH-modulated strand displacement circuitry.
Fuel (F): 5'-AGCAACCTGAAACCACCCTCTTTTCTTTCCC-3'
Catalyst (C): 5'-TTTTCTTTCCCTCACCATG-3'
Deprotector (D):
5'-ATAGATCCTGATAGCGAGACCTAGCAACCTGAAACCA-3'
Substrate (S):
5'-CATGGTGAGGGAAAGAAAAGAGGGTGGTTTCAGGTTGCTAGGTCTC-3'
Clamp-like triplex forming strand (T):
5'-CCCTTTCTTTTCTCCC-GTTTG-CCCTCTTTTCTTTCCC-3'
Random tail control strand (DC_RT):
5'-ATCTTAACGTACTGATTA-ATTCC-CCCTCTTTTCTTTCCC-3'
Reporter:
R1: 5'-(cy3)-ATAGATCCTGATAGCGAGAC-3'
R2: 5'- TTGCTAGGTCTCGCTATCAGGATCTATR-(cy5)-3'
Labelled clamp-like triplex forming strand (strand forming complex T):
5'-(cy5)-CCCTTTCTTTTCTCCC-GTTTG-CCCTCTTTTCTTTCCC-(cy3)-3'

Buffer conditions. DNA oligonucleotides were suspended to a final concentration of 100 μM and stored in 0.01 M TRIS + 0.01 M MgCl2, pH 7, at -20° C. In all experiments we used solutions of TAE 1x + 15 mM $MgCl_2$ with the pH adjusted with the addition of HCl or NaOH. All experiments were performed at 25° C.

Protected tile annealing. The protected tile was prepared with nominally correct stoichiometry at 5 μM and annealed with a Bio-Rad Mastercycler Gradient thermocycler. The solution was brought down from 95° C to 20° C at a constant rate over a course of 6 h.

Substrate preparation. All the complexes (R, pH-DS and S_{DC_RT}) used in the experiments were prepared mixing the oligos necessary for the formation of the complex at equimolar concentration (1 μM) for the kinetics experiment or (10 μM) for the integrated experiment in TAE buffer 1x + 15 mM $MgCl_2$ pH 7 and were let to react overnight at room temperature.

Fluorescence measurements. All fluorescence measurements were obtained using a Cary Eclipse Fluorimeter (Varian) with excitation at 548 nM (± 5 nm) and emission at 563 nM (± 5 nm). Strand displacement experiments were performed using a concentration of R of 30 nM, F of 20nM and 10 nM of initial complex (pH-DS or S_{DC_RT}). The C was added at the selected concentration (from 1 nM to 100 nM) after 10 minutes to allow a stable baseline. The signal increase of Cy3 was followed for 1h after C addition.

Integrated experiment. This experiment was performed by adding (PT) 200 nM to a mixture reaction of (pH-DS or S_{DC_RT}, the latter for $Control_1$) (220 nM), F (440 nM), C was added or not, depending on the type of experiment, at a concentration of 20 nM in TAE buffer 1x + 15 mM $MgCl_2$ at room temperature. Reaction time, 24 h.

Atomic force microscopy. All AFM topographic measurements were performed in AC mode using MFP-3D Stand-Alone AFM (Asylum research Santa Barbara,CA, USA). 20 μl of each sample (different concentration depending on the type of experiment) of sample were deposited onto freshly cleaved mica substrate. The self assembly formation

step lasted for 20 minutes for all pHs. Afterwards, 100 µl of DNA-free TAE/Mg buffer (TAE 1x with 12.5mM Magnesium acetate tetrahydrate, pH 5, 6, 7, 8, with respect to the original pH of the sample) was introduced onto the sample, so as to have enough solution that covers the home-made liquid cell. The imaging parameters were as follow:
AFM mode:AC mode in liquid
Cantilever type: BL-AC40TS-C2 (a bioLever Mini Silicon tip on nitride lever)
Resonant frequency:110kHZ (as specified by the manufacturer (Olympus,Japan))
Spring constant : 0.09 N/m (as specified by the manfacturer)
Scan rate:1Hz
After AFM topographic measurements, the images acquired were analysed using Igor Pro 6.37, followed by a quantitative histogram representative of the thickness of DNA nanotubes. (For further details see AFM Methods section in Chapter 2).

Fluorescence microscopy. For fluorescence image microscopy imaging only, the central strand of the tile (t3, see sequence above) was labelled at 3' with a cy3 fluorophore. I used a Axio Scope A1 ZEISS microscope. The emitted photons were collected by a 63 x, air objective (ZEISS) and a monochrome CCD camera (Axiocam 503 mono - ZEISS). The images were analyzed using ZEN 2 lite (ZEISS) software. A 2 µL drop of 50 nM of the sample was deposited between a clean microscope slide and a coverslip.

4.5 References

(1) Perrault, S. D.; Shih. W. M.; *ACS Nano* 2014, 8, 5132.

(2) Shaw, A.; *et. al.* *Nature Methods* 2014, 11, 841.

(3) Choi, H. M. T.; Beck, V. A.; Pierce, N. A. *ACS Nano* 2014, 8, 4284.

(4) Douglas, S. M.; Bachelet, I.; Church, G. M. *Science* 2012, 335, 831.

(5) Seeman, N. C. *J. Theor. Biol.* 1982, 99, 237.

(6) Krishnan, Y.; Bathe, M. *Synth. Cell Biol.* 2012, 22, 624.

(7) Lu, C. H.; Willner, B.; Willner, I. *ACS Nano* 2013, 7, 8320.

(8) Winfree, E.; Liu, F.; Wenzler, L. A.; Seeman, N. C. *Nature* 1998, 394, 539.

(9) Rothemund, P. W. K. *Nature* 2006, 440, 297.

(10) Turberfield, A. J.; Mitchell, J. C.; Yurke, B.; Mills, A. P., Jr.; Blakey, M. I.; Simmel, F. C. *Phys. Rev. Lett.* 2003, 90, 118102/1.

(11) Bath, J.; Turberfield, A. J. *Nat. Nanotechnol.* 2007, 2, 275.

(12) Mao, C. *Nat. Nanotechnol.* 2008, 3, 75.

(13) Krishnan, Y.; Simmel, F. C. *Angew. Chem., Int. Ed.* 2011, 50, 3124.

(14) Seeman, N. C. *Mol Biotechnol* 2007, 37, 246.

(15) LaBean, T. H; Yan, H.; Kopatsch, J.; Liu, F. R.; Winfree, E.; Reif, J. H.; Seeman, N. C. *J. Am. Chem. Soc.* 2000, 122, 1848.

(16) Li, H. Y.; Park, S. H.; Reif, J. H.; LaBean, T. H.; Yan, H. *J. Am. Chem. Soc.* 2004, 126 418.

(17) Reishus, D.; Shaw, B.; Brun, Y.; Chelyapov, N.; Adleman, L. *J. Am. Chem. Soc.* 2005,127 17590.

(18) Yan, H.; Park, S. H.; Finkelstein, G.; Reif, J. H.; LaBean, T. H. *Science* 2003, 301, 1882.

(19) Lund, K.; Liu, Y.; Lindsay, S.; Yan, H. *J. Am. Chem. Soc.* 2005, 127, 17606.

(20) Park, S. H.; Finkelstein, G.; LaBean, T. H. *J. Am. Chem. Soc.* 2008, 130 40.

(21) Park. S. H.; Pistol, C.; Ahn, S. J.; Reif, J .H.; Lebeck, A. R.; Dwyer, C.; LaBean, T. H. *Angew. Chem., Int. Edn.* 2006, 45, 735.

(22) He, Y.; Tian, Y.; Chen, Y.; Deng, Z. X.; Ribbe, A. E.; Mao, C. D. *Angew. Chem., Int. Ed.* 2005, 44, 6694.

(23) He, Y.; Tian, Y.; Ribbe, A. E.; Mao, C. D. *J. Am. Chem. Soc.* 2006,128, 15978.

(24) He, Y.; Ye, T.; Su, M.; Zhang, C.; Ribbe, A. E.; Jiang, W.; Mao, C. D. *Nature* 2008, 452 198.

(25) Zhang, C.; Su, M.; He, Y.; Zhao, X.; Fang, P. A.; Ribbe, A. E., Jiang, W.; Mao., C. D. Proc. *Natl Acad. Sci. USA* 2008, 105, 10665.

(26) Mathieu, F.; Liao, S.; Mao, C.; Kopatsch, J.; Wang, T.; Seeman, N. C. *Nano Lett.* 2005, *5*, 661.

(27) Hamblin, G. D.; Carneiro, K. M. M.; Fakhoury, J. F.; Bujold, K. E.; Sleiman, H. F. *J. Am. Chem. Soc.* 2012, 134, 2888.

(28) Lo, P. K.; Altvater, F.; Sleiman, H. F. *J. Am. Chem. Soc.* 2010, *132*, 10212.

(29) Sharma, J.; Ke, Y.; Lin, C.; Chhabra, R.; Wang, Q.; Nangreave, J.; Liu, Y.; Yan H. *Angew. Chem., Int. Ed.* 2008, 47, 5157.

(30) Zhang, J.; Liu, Y.; Ke, Y.; Yan, H. *Nano Lett.* 2006, 6, 248.

(31) Roy, S.; Olesiak, M.; Shang, S.; Caruthers, M. H. *J. Am. Chem. Soc.* 2013, 135, 6234.

(32) Park, S. H.; Yin, P.; Liu, Y.; Reif, J. H.; LaBean, T. H.; Yan, H. *Nano Lett.* 2005, 5, 729.

(33) Liu, Y.; Lin, C.; Li, H.; Yan, H. *Angew. Chem. Int . Ed.* 2005, 44, 4333.

(34) Lin, C.; Katilius, E.; Liu, Y.; Zhang, J.; Yan, H. *Angew. Chem. Int. Ed.* 2006, 45, 5296.

(35) Li, H.; Park, S. H.; Reif, J. H.; LaBean, T. H.; Yan, H. *J. Am. Chem. Soc.* 2004, 126, 418.

(36) Winfree, E.; Eng, T.; Rozenberg, G. *LNCS* 2001, 2054, 63.

(37) Seeman, N. C. *AnnuRev Biophys Biomol Struct* 1998, 27, 225.

(38) Reif, J. H. *Science* 2002, 296, 478.

(39) Rozenberg, G.; Spaink, H. *Theor Comput Sci* 2003, 292, 653.

(40) Mao, C.; LaBean, T. H.; Reif J. H.; Seeman, N. C. *Nature* 2000, 407, 493.

(41) Yan, H.; Feng, L.; LaBean, T. H.; Reif, J. H. *J. Am. Chem. Soc.* 2003, 125, 14246.

(42) Rothemund, P. W. K.; Ekani-Nkodo, A.; Papadakis, N.; Kumar, A.; Kuchnir Fygenson, D.; Winfree, E. *J. Am. Chem. Soc.*2004, 126, 16344.

(43) Douglas, S. M.; Chou, J. J.; Shih, W. M. *Proc Natl Acad Sci U.S.A* 2007, 104, 6644.

(44) Liu, D.; Park, S. H.; Reif, J. H.; LaBean, T. H. *Proc Natl Acad Sci U.S.A*. 2004, 101, 717

(45) Ko, S. H.; Liu, H.; Chen, Y.; Mao, C. *Biomacromolecules* 2008, 9, 3039.

(46) Sellner, S.; Kocabey, S.; Nekolla, K.; Krombach, F.; Liedl, T.; Rehberg, M. *Biomaterials* 2015, 53, e453.

(47) Endo, M.; Seeman, N. C.; Majima, T. *Angew. Chem. Int. Ed.* 2005, 44, 6074.

(48) Sharma, J.; Chhabra, R.; Cheng, A.; Brownell, J.; Liu, Y.; Yan, H. *Science* 2009, 323, 5910

(49) Hamblin, G. D.; Hariri, A. A.; Carneiro, K. M. M., Lau, K. L.; Cosa, G.; Sleiman, H. F. *ACS Nano* 2013, 7, 3022

(50) Zhang, D. Y.; Hariadi, R. F.; Choi, H. M. T.; Winfree, E. *Nat Comm* 2013, 4, 1965.

(51) Amodio, A.; Zhao, B.; Pochetta, A.; Idili, A.; Castronovo, M.; Fan, C.; Ricci, F. *J. Am. Chem. Soc.* 2014, 136, 16469.

(52) Idili, A.; Plaxco, K. W.; Vallée-Bélisle, A.; Ricci, F. *ACS Nano* 2013, 7, 10863.

(53) Idili, A.; Vallée-Bélisle, A.; Ricci, F. *J. Am. Chem. Soc.* 2014, 136, 5836.

(54) Ohmichi, T.; Kawamoto, Y.; Wu, P.; Miyoshi, D.; Karimata, H.; Sugimoto, N. *Biochemistry* 2005, 44, 7125.

(55) Soto, A. M.; Loo, J.; Marky, L. A. *J. Am. Chem. Soc.* 2002, 124, 14355.

Chapter 5 – Conclusions

With the work presented in this PhD thesis I have demonstrated that the fundamental features of the triplex DNA motif can be applied to achieve different relevant and unprecedented results in the field of nucleic acid nanotechnology.

In particular, in chapter two, I have shown how to engineer a clamp-switch probe to develop and optimize an electrochemical biosensor with improved affinity and specificity. The impressive results obtained in terms of discrimination efficiency hold great promise for the development of new structure-switching biosensors, for example for the detection of single nucleotide polymorphisms.

In chapter three the formation of Hoogsteen interactions inherent the triplex DNA motif has allowed the enrichment of the classical strand displacement reaction, one of the most versatile tool in dynamic DNA nanotechnology, with an external control variable that has a profound significance in living systems, the pH. In particular, I developed two strategies in which strand displacement reaction can be triggered, and finely regulated at basic (strategy #1) or acidic/neutral pHs (strategy #2). The results obtained will be adopted to introduce a reliable, external control over the formation and function of DNA nanoarchitectures such as, for instance, switches for *in vivo* imaging.

In chapter four, I have demonstrated the possibility to use a pH-dependent strand displacement reaction to trigger and regulate the self-assembly of DNA nanotubes. The results obtained could have important implications towards development of model systems that mimic the properties of nanotubes and nanofilaments that are present in living cells, and/or to develop new smart drug-delivery system.

In view of the essential role of pH in the cellular pathways of both in healthy and pathological tissues, the results presented in this thesis, demonstrate that triplex DNA is greatly valuable as a new entry in the toolbox of DNA nanotechnology. In fact, although the recent, progressive developments in this research area, much remains to achieve for enabling the construction of robust and controllable DNA-based nanomachines, and improving their functionality to permit challenging applications such as targeted drug-release, biomolecular imaging, and theranostic approaches.